NOAA Technical Report ERL 253-APCL 25

U.S. DEPARTMENT OF COMMERCE
NATIONAL OCEANIC AND ATMOSPHERIC ADMINISTRATION
Environmental Research Laboratories

Observations of the Vertical Transport of Water Vapor, Ozone, and Aerosols by Thunderstorms

PETER M. KUHN
WALTER D. KOMHYR
THOMAS B. HARRIS
PAUL A. ALLEE
W.E. MARLATT

BOULDER, COLO.
FEBRUARY 1973

MENTAL RESEARCH LABORATORIES

of the Environmental Research Laboratories is to study the oceans, inland
d upper atmosphere, the space environment, and the earth, in search of the
to provide more useful services in improving man's prospects for survival
physical environment. Laboratories contributing to these studies are:

Earth Sciences Laboratories (ESL): Seismology, geomagnetism, geodesy, and related earth sciences; earthquake processes, internal structure and shape of the earth and distribution of the earth's mass.

Atlantic Oceanographic and Meteorological Laboratories (AOML): Geology and geophysics of ocean basins, oceanic processes, sea-air interactions, hurricane research and weather modification (Miami, Florida).

Pacific Oceanographic Laboratories (POL): Oceanography with emphasis on the geology and geophysics of the Pacific Basin and margins; oceanic processes and dynamics; tsunami generation, propagation, modification, detection, and monitoring (Seattle, Washington).

Atmospheric Physics and Chemistry Laboratory (APCL): Processes of cloud and precipitation physics; chemical composition and nucleating substances in the lower atmosphere; and laboratory and field experiments toward developing feasible methods of weather modification.

Air Resources Laboratories (ARL): Diffusion, transport, and dissipation of atmospheric contaminants; development of methods for prediction and control of atmospheric pollution; geophysical monitoring for climatic change (Silver Spring, Maryland).

Geophysical Fluid Dynamics Laboratory (GFDL): Dynamics and physics of geophysical fluid systems; development of a theoretical basis, through mathematical modeling and computer simulation, for the behavior and properties of the atmosphere and the oceans (Princeton, New Jersey).

National Severe Storms Laboratory (NSSL): Tornadoes, squall lines, thunderstorms, and other severe local convective phenomena directed toward improved methods of prediction and detection (Norman, Oklahoma).

Space Environment Laboratory (SEL): Solar-terrestrial physics, service and technique development in the areas of environmental monitoring and forecasting.

Aeronomy Laboratory (AL): Theoretical, laboratory, rocket, and satellite studies of the physical and chemical processes controlling the ionosphere and exosphere of the earth and other planets, and of the dynamics of their interactions with high altitude meteorology.

Wave Propagation Laboratory (WPL): Development of new methods for remote sensing of the geophysical environment with special emphasis on optical, microwave and acoustic sensing systems.

Marine Minerals Technology Center (MMTC): Research into aspects of undersea mining of hard minerals: development of tools and techniques to characterize and monitor the marine mine environment; prediction of the possible effects of marine mining on the environment; development of fundamental mining technology (Tiburon, California).

Weather Modification Program Office (WMPO): Plans and directs ERL weather modification activities, operates ERL aircraft fleet, research in cumulus cloud modification.

NATIONAL OCEANIC AND ATMOSPHERIC ADMINISTRATION

BOULDER, COLORADO 80302

U.S. DEPARTMENT OF COMMERCE
Frederick B. Dent, Secretary

NATIONAL OCEANIC AND ATMOSPHERIC ADMINISTRATION
Robert M. White, Administrator
ENVIRONMENTAL RESEARCH LABORATORIES
Wilmot N. Hess, Director

NOAA TECHNICAL REPORT ERL 253-APCL 25

Observations of the Vertical Transport of Water Vapor, Ozone, and Aerosols by Thunderstorms

PETER M. KUHN
WALTER D. KOMHYR
THOMAS B. HARRIS
PAUL A. ALLEE
W.E. MARLATT

Prepared for the Office of the Assistant Secretary
for Systems, Development, and Technology,
Department of Transportation
Contract No. DOT-AS-20001

BOULDER, COLO.
February 1973

For sale by the Superintendent of Documents, U. S. Government Printing Office, Washington, D. C. 20402

DISCLAIMER

The Environmental Research Laboratories do not approve, recommend, or endorse any proprietary product or proprietary material mentioned in this publication. No reference shall be made to the Environmental Research Laboratories or to this publication furnished by the Environmental Research Laboratories in any advertising or sales promotion which would indicate or imply that the Environmental Research Laboratories approve, recommend, or endorse any proprietary product or proprietary material mentioned herein, or which has as its purpose an intent to cause directly or indirectly the advertised product to be used or purchased because of this Environmental Research Laboratories publication.

CONTENTS

PREFACE

Considerable interest has developed in the past few years to learn more of the natural fluctuations in the stratosphere with respect to the vertical transport of water vapor by thunderstorms, the mixing process at the tropopause, and the aerosol component of the upper troposphere and lower stratosphere. Solutions to problems in radiation transfer, circulation, and cloud physics must be solved before a study of manmade pollutants can be intelligently analyzed.

A first study, a 4-day field project, was conducted in an area bounded by San Francisco, Calif., on the west, La Crosse, Wis., on the east, and Santa Fe, N. Mex., on the south. It was a joint effort including the National Oceanic and Atmospheric Administration (NOAA) Atmospheric Physics and Chemistry Laboratory and Air Resources Laboratories, the National Aeronautics and Space Administration (NASA) Ames Research Center, and Colorado State University. The project was sponsored by the Department of Transportation, Office of the Assistant Secretary for Systems, Development, and Technology.

This Technical Report is divided into four sections, each contributed by the experimenters involved. The sections and contributors are as follows:

1. Infrared radiometric observations of stratospheric injection of water vapor by thunderstorms, Peter M. Kuhn;
2. Upper troposphere ozone and carbon dioxide measurements in the vicinity of thunderstorms, Walter D. Komhyr and Thomas B. Harris;
3. Aitken and ice nuclei concentration observations around thunderstorms, Paul A. Allee; and
4. Vertical transport of water vapor and aerosols, William E. Marlatt.

The aircraft furnished by the NASA Ames Research Center was a Convair (CV) 990, capable of flying to altitudes of 45,000 feet (13.7 km) which, in most instances, is into the lower stratosphere. This flying laboratory, having both speed and range, has been adapted to experimentation of this type and has repeatedly proven an effective platform by virtue of its in-cabin environment.

OBSERVATIONS OF THE VERTICAL TRANSPORT OF WATER VAPOR, OZONE, AND AEROSOLS BY THUNDERSTORMS

Peter M. Kuhn[1], Walter D. Komhyr[2], Thomas B. Harris[2], Paul A. Allee[1], and W. E. Marlatt[3]

The purpose of this field study was to determine the amount of water vapor and particulate matter transported into the stratosphere by thunderstorms in the Plains as well as to investigate the increases in ozone concentration beneath the tropopause in areas of thunderstorm activity. Carbon dioxide measurements were also made to augment information on the mixing process. Measurements of water vapor show an average stratospheric water vapor mass of 9.8×10^{-4} g cm^{-2} to which a typical thunderstorm added 11.2×10^{-4} g cm^{-2} at an altitude of 41,500 feet. Small increases in ozone were observed in areas of thunderstorm activities, corresponding to about a 2-percent change in ozone in a vertical column of the atmosphere above 33,000-feet altitude. The ozone data were, however, inadequate to distinguish between downward transport of ozone from the stratosphere and possible production of ozone by electrical discharges in the clouds. A combination of an ozone high and a carbon dioxide low that occurred during the final flight, not in an area of thunderstorm activity, was interpreted as significant evidence for mixing of stratospheric air into the troposphere. Aitken nuclei counts observed in areas of thunderstorm activity were remarkably high. Maximum concentration measured around the La Crosse, Wis., storm at 40,000 feet of altitude was 7,000 nuclei/cm^3, while typical values around the Grover, Colo., storm at about 42,000 feet of altitude were approximately 20,000 nuclei/cm^3.

1. INFRARED RADIOMETRIC OBSERVATIONS OF STRATOSPHERIC INJECTION OF WATER VAPOR BY THUNDERSTORMS

1.1 Introduction

During the period July 12-15, 1971, an intense study was initiated for measuring water vapor injection into the stratosphere by Plains thunderstorms, ozone and carbon dioxide to determine circulation and mixing processes across the tropospause, and aerosol and trace gasses to investigate the cloud physics in the study area.

---

[1]NOAA Atmospheric Physics and Chemistry Laboratory, Boulder, Colo.
[2]NOAA Air Resources Laboratories, Boulder, Colo.
[3]Colorado State University, Fort Collins, Colo.

This section will be devoted to water vapor measurements, instrumentation, and calculations used to infer water vapor mass. Subsequent sections will deal with the above listed observations.

1.2 Radiometric Instrumentation

An in-line chopper bolometer radiometer was modified by installation of filter optics to operate over the 17.5- to 26.32-μm portion of the rotational water vapor spectral band. This radiometer, with a 0.14^{o} total-included angular field of view, provided the "bottom"-sounding instrumentation to infer radiometrically the total mass of water vapor (g cm^{-2}) above the jet aircraft laboratory. The radiometer for optics consists of a 4-inch (10.20-cm) Cassegrainian telescope directed to the zenith through the hull of the jet. The in-line chopper bolometer radiometer used exhibits a noise equivalent change in radiance (N.E.ΔN) of 2.00×10^{-6} w cm^{-2} sr^{-1} in the spectral interval of measurement. At approximately a 13.0-km altitude and for a typical July temperature sounding for Denver, Colo., this measurement corresponds to an rms error in the radiometrically inferred columnar water vapor mass above 13.0 km of 1.0×10^{-4} g cm^{-2}. The standard error (the rms error divided by the square root of the number of observations of the same target) is approximately one-tenth of the rms error. A second infrared channel, operating in the 10.0- to 12.0-μm band, provides a constant check on the presence of any cloud particles in the path that would negate the water vapor channel measurements. Table 1 summarizes the performance characteristics of the radiometer used.

Table 1. Water Vapor Radiometer Performance Characteristics

Spectral band, filter system	17.5 to 26.3 μm
Field of view	0.14^{o}
Detectivity (radiation)	2.00×10^{-6} w cm^{-2} sr^{-1}
Bandwidth	~0.1 Hz
Detectivity (water vapor)	1.0×10^{-4} g cm^{-2} at 13 km
Detector	Hyperimmersed thermistor bolometer

Infrared inference techniques were used to avoid the difficulty of obtaining satisfactory, uncontaminated water vapor mass samples from aircraft with frost-point or wet-chemical instrumentation. (Barclay et al., 1960; Mastenbrook, 1968; and Mastenbrook, 1971a). It was possible to modify the existing onboard (the NASA CV-990) radiometer to operate over the 17.5- to 26.32-μm portion of the rotational water vapor spectral band as a bottom sounder. Bottom-sounding measurements as opposed to satellite top-sounding measurements require careful system purging by dry nitrogen (Kuhn, 1970). This is necessary because the mass of the water vapor measured above the aircraft is very small, approximately 10^{-4} of the mass above the earth's surface, and contamination of the aircraft cabin must be eliminated. Houghton and Seeley (1960) made limited aircraft observations of water vapor over the United Kingdom and, more recently, McKinnon and Morewood (1970) made aircraft solar-absorption measurements of water vapor along a meridian from Albuquerque, N. Mex., to Fairbanks, Alaska. This measurement system, however, required difficult solar tracking.

1.3 Flight Field Program

High-altitude infrared measurements of the total mass of water vapor above flight level in the vicinity of thunderstorms, at and just below the base of the stratosphere, were made in July 1971 over the Central Plains. Observations reveal that the vertical drive of these huge storm cells results in the local injection of large amounts of water into the atmosphere.

To obtain the results desired, it was decided to flay a flight pattern similar to that of figure 1, but extending the downstream south-north legs gradually eastward. This pattern would give some indication of the easterly extent of the water vapor excess transported upward and swept eastward by thunderstorm systems. Obviously, the altitudes are determined by the height of the thunderstorm, tropopause, and interfering cirrus. The thunderstorm cell of July 15, 1971, shown in figure 9 and referred to subsequently, illustrates clearly the deformation in the westerly flow across the anvil top.

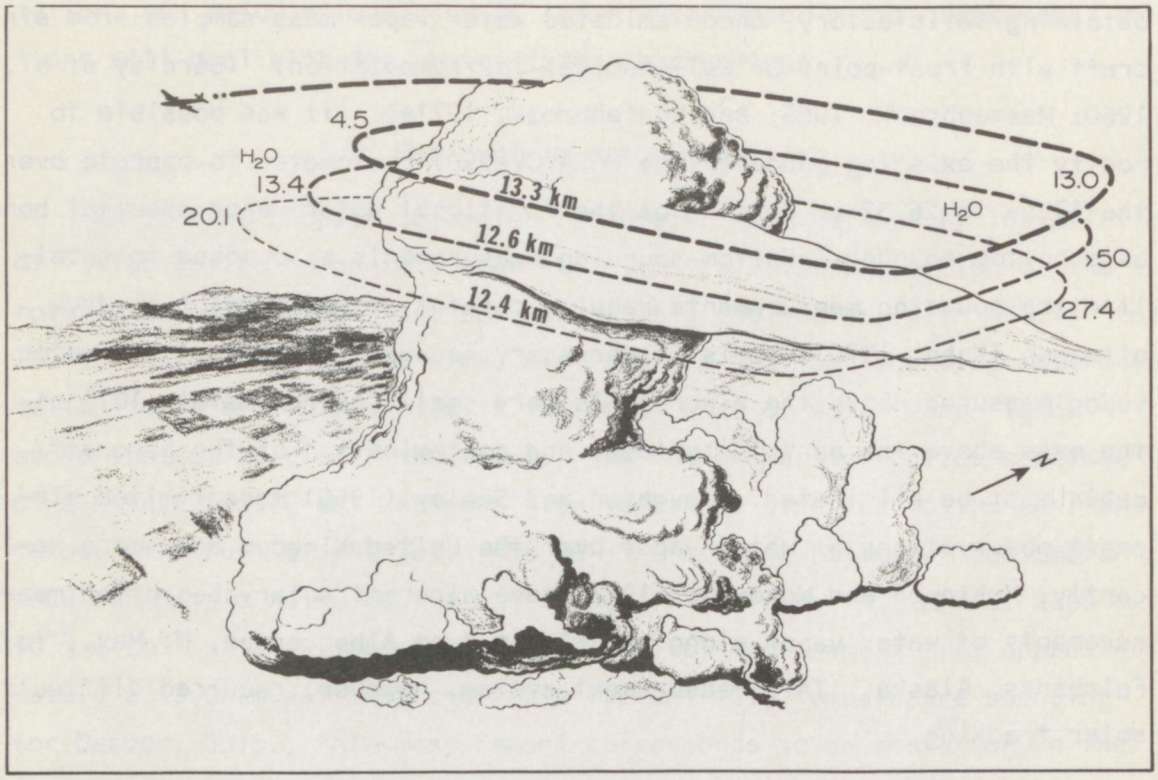

Figure 1. Thunderstorm flight pattern. Light figures indicate water vapor mass in g cm^{-2} × 10^4. Dark figures display flight altitudes.

At times, the boxed thunderstorm area would roughly cover a 3^o by 6^o rectangle (180 nm north-south by 360 nm east-west). This boxed area occurred and is discussed subsequently for the storm on July 13-14, 1971, between 2305-0025 UT (fig. 13).

1.4 Applied Theory for Data Analyses and Reduction

An inverse solution of the radiative transfer equation is used to infer the mass of water vapor above a reference plane in the atmosphere. The rapidly converging solution is obtained by iteration (Smith, 1970). Briefly, the downward radiance $N_c\downarrow$ is expressed mathematically as,

$$N_c\downarrow = -\int_{\nu_1}^{\nu} \int_{\tau=1}^{\tau} B(\nu,T(P))\, d\tau(P,u(H_2O))d\nu, \qquad (1.1)$$

where ν is the wavenumber, τ the transmissivity, B the Planck function, P the pressure, and $u(H_2O)$ the optical mass of water vapor. Having an upward temperature profile, we can calculate the downward radiance, $N_c\downarrow$, assuming an initial water vapor mass profile. This assumption is one of a constant mixing ratio profile, $\bar{s}(P)$, in g g^{-1}. A unique optical mass above the reference level is found by computer calculation so that the difference between the observed, $N_o\downarrow$, and calculated, $N_c\downarrow$, downward radiance, $|N_o\downarrow - N_c\downarrow|$, is minimized. This is accomplished by a conventional iterative method (Newton's) to obtain repeated $|N_o\downarrow - N_c\downarrow|$'s from successive approximations of $u(H_2O)$.

We summarize the iterative, radiometric inference of the water vapor mass in the following functional notations:

$$N_o\downarrow = N_o\downarrow (u), \tag{1.2}$$

$$N_c\downarrow = N_c\downarrow (\tau), \tag{1.3}$$

$$\tau = \tau(u), \tag{1.4}$$

$$u = u(\bar{s}) = \frac{1}{g} \bar{w}\, \Delta P, \tag{1.5}$$

$$\bar{s} = \bar{s} \quad |N_o\downarrow - N_c\downarrow| \leq \varepsilon \text{ (noise equivalent radiance, N.E.}\Delta N) \text{ .} \tag{1.6}$$

In Equations 1.2 through 1.6, g is the acceleration due to gravity, ε is the N.E.ΔN of the radiometer, and $\bar{w}$ is the mean water vapor mixing ratio.

Table 2 is a sample input and output to the pertinent computer program, "Total Water Vapor," on magnetic tape file in the NOAA Atmospheric Physics and Chemistry Laboratory at Boulder, Colo.

The input data indicate the frequencies in cm^{-1}, 430-590, and the frequency interval, $\Delta\nu$, 10 cm^{-1}; the "look" angle of the radiometer (in this case, 0^o); the type of filter; the geographical location and date; the direction of the approaching radiant power (radiance); the pressure-temperature sounding; and finally, the observed downward radiance (in

Table 2. Input and Output Data, "Total Water Vapor" Program

```
LIST OF INPUT CONTROL CARDS FOLLOWS

FREQUENCIES          430     590     10
ANGLES  0.
FILTER  SAIEDY,PHI=.50  NEW
STATION WALLOPS 16SEPT71
DOWNWARD BEGIN    .1            LEVELS        1
PT  DATA(3F8.0)
100.     -69.1
87.      -63.6
70.      -60.6
50.      -56.8
43.      -56.6
30.      -50.0
20.      -47.7
15.      -44.7
12.      -39.0
10.      -40.3
8.4      -40.1
7.5      -37.3
5.       -35.
2.       -10.
1.       4.
.6       7.
.3       -2.
.2       -250.
.1       -272.
PT  END
PROCESS .000012
STOP

END OF RUN


DOWNWARD RADIANT POWER FOR 19 LAYERS

STATION, WALLOPS      DATE, 16SEPT71

WAVE LENGTH REGION FROM  16.95 TO  23.26 MICRONS WITH FILTER = SAIEDY
     WAVE NUMBERS FROM 430.00 TO 590.00 BY    10.00  PHI=.50

     W O              RADIANCE          WATER VAPOR          DIFFERENCE
 3.000000-003     1.328590-005      3.068928-004      1.285901-006
 5.000000-003     1.773626-005      5.114880-004      5.736255-006
 9.000000-003     2.455489-005      9.206784-004      1.255489-005
 1.000000-003     7.860089-006      1.022976-004      4.139911-006
 2.000000-003     1.063869-005      2.045952-004      1.361311-006
 4.000000-003     1.562916-005      4.091904-004      3.629157-006
 2.500000-003     1.200010-005      2.557440-004      1.037388-010
```

the example, 12.0×10^{-6} w cm^{-2} sr^{-1}) to which a convergent calculation is required.

The bottom one-third of table 2, containing downward radiant power for 19 layers, illustrates the stepwise iteration required to reach convergence, listing the assumed water vapor mixing ratio, w_0 (cm g kg^{-1}), mean profile; the calculated radiances (w cm^{-2} sr^{-1}); the calculated water vapor mass *above* flight level (g cm^{-2}); and the differences between downward observed and calculated radiances ($N_o\downarrow$ and $N_c\downarrow$). These calculations are for the 100-mb flight level. The convergence criterion, ε, is 1×10^{-7} w cm^{-2} sr^{-1} by the noise equivalent radiance of the radiometer, N.E.ΔN.

1.5 Meteorological Discussion of the Results Obtained

Four isolated thunderstorm cell systems penetrating the tropopause were investigated. The difference between upstream and downstream water vapor mass is a measure of the thunderstorm vertical transport because the mean wind moves through, around, and above the visible turret, generally from west to east. It then appears logical to look for any addition of water vapor into the upper troposphere and lower stratosphere in a volume translated downstream from the turret itself. Because the vapor is presumably swept along in this mean wind field, this situation will insure measurement of any actual addition of water vapor to the stratosphere or upper troposphere persisting away from the cell. Recall that the rms error in the inferred total water vapor mass measurements is approximately 1.0×10^{-4} g cm^{-2}.

Data presentation in the figures consists of 1-minute intervals plotted on flight tracks around each of the four systems, with the time of the beginning and end of the track, the wind (angle and speed) vectors, and the amount of water vapor mass observed at each 1-minute interval (g $cm^{-2} \times 10^4$), the cloud location, and the longitude as ordinate and the latitude as abscissa. The four figures corresponding to the Grover, Colo., La Crosse, Wis., O'Neill, Nebr., and southwestern Colorado-New Mexico storms are, respectively, figures 10, 11, 12, and 13. The corresponding tables, giving aircraft time, latitude, longitude,

speed, pitch, roll, altitude, air temperature, wind direction and amplitude, voltage, and water vapor, are tables 3, 4, 5, and 6. The occurrence of cirrus overhead, as indicated by channel 2 (10.0-12.0 μm) of the radiometer, and any significant roll of the CV-990, are noted in a column to the right of the water vapor column. The four storms will be discussed individually, with frequent references made to table 7, Summary of Data on Vertical Transport of Water Vapor by Thunderstorms, which summarizes data from the abovementioned four figures and four tables in a simple resultant form. One should note that sampling occurred once per second, but the sample data are averaged and centered on the integral minute.

1.5.1 Grover, Colo., Storm of July 15, 1971

A typical reconnaissance of a single cell system was that of July 15, 1971, between 0000 and 0130 (fig. 10). The data for this storm are tabulated at 1-minute intervals in both figure 10 and table 3 and are summarized in table 7. The times (UT) given in table 3 are the data periods for which averages were obtained. This reconnaissance was conducted upstream and downstream of an isolated thunderstorm cell 90 nautical miles north-northeast of Denver, at altitudes of 12.4, 12.6, and 13.3 km. The cell top was at 14.8 km. The tropopause averaged approximately 13.3 km, but was not clearly bounded. Mastenbrook (1971b) emphasizes that true stratospheric air in the summer over West Central United States occurs principally above 16.0 km. The measurements for this reconnaissance are made in the transitional or mixing zone at the beginning of the stratosphere. In situ temperature and aerosol concentration measurements indicate that the CV-990 was just at the stratospheric base.

Figures 2 through 9 illustrate port side camera views with time around this cell system from 0043 to 0119 UT. East-west tracks are approximately 60 nautical miles long while north-south tracks are about 50 nautical miles long. The observations approximately spanned the cell system life cycle.

Table 7, summarizing the data of table 3 and the flight track of figure 10, clearly indicates an increase of 9.0×10^{-4} g cm^{-2} in the mass

Figure 2. Port side view of Grover, Colo., thunderstorm east-west leg, 43,000 feet, 0043 UT, July 15, 1971.

Figure 3. Port side view of Grover, Colo., thunderstorm east-west leg, 43,000 feet, 0044 UT, July 15, 1971.

Figure 4. Port side view of Grover, Colo., thunderstorm east-west leg, 43,000 feet, 0051 UT, July 15, 1971.

Figure 5. Port side view of Grover, Colo., thunderstorm east-west leg, 43,000 feet, 0052 UT, July 15, 1971.

Figure 6. Port side view of Grover, Colo., thunderstorm south-north leg, 43,000 feet, 0109 UT, July 15, 1971.

Figure 7. Port side view of Grover, Colo., thunderstorm south-north leg, 43,000 feet, 0114 UT, July 15, 1971.

Figure 8. Port side view of Grover, Colo., thunderstorm east-west leg, 43,000 feet, 0118 UT, July 15, 1971.

Figure 9. Port side view of Grover, Colo., thunderstorm east-west leg, 43,000 feet, 0119 UT, July 15, 1971.

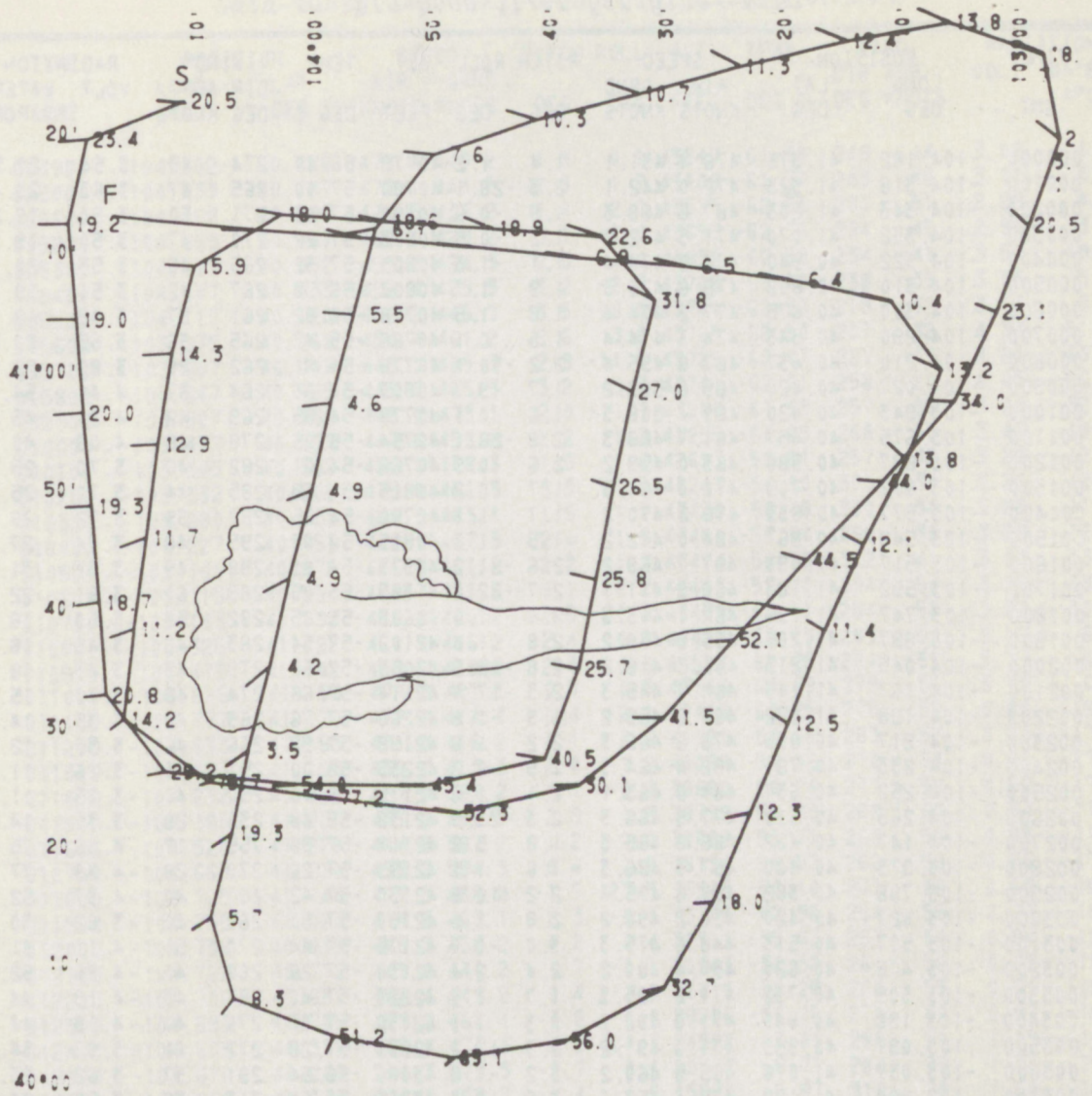

Figure 10. Flight tracks around Grover, Colo., thunderstorm, 0000-0114 UT, July 15, 1971. Short segment lines indicate wind direction (point into wind) and speed (1 cm = 100 kt), and the numerals indicate water vapor (in g cm^{-2} × 10^{4}). Latitude and longitude measurements in 10-minute intervals are to the left and top, respectively.

of water vapor above flight level and downstream in the wind field when compared to the upstream (of the Grover thunderstorm) fair weather background at flight level (43,500 ft). At the lowest circumnavigation level, 40,700 feet, the water vapor mass increase was 7.3 × 10^{-4} g cm^{-2}, ranging from 20.1 to 27.4 × 10^{-4} g cm^{-2}. In the three circumferential flight tracks, the mass of water vapor (g cm^{-2}) above the flight level was

Table 3. Aircraft Navigation, Meteorological, and Water Vapor Data--July 15, 1971, 0000-0137 UT

TIME	POSITION		SPEED		PITCH	ROLL	ALT.	TEMP.	WIND		RADIATION	
	LONG	LAT	AIR	GRND					DIR	AMP	VOLT	WATER
GMT	DEG	DEG	KNOTS	KNOTS	DEG	DEG	FEET	DEG C	DEG	KNOTS		VAPOR
000000	-104.182	41.375	476.4	431.1	1.4	1.2	40778	-56.40	274	49	3.54	20.5
000100	-104.318	41.323	472.0	442.1	2.3	-28.1	40790	-57.00	265	47	3.63	23.4
000200	-104.343	41.203	467.6	468.3	1.9	-0.6	40790	-57.06	271	50	3.50	19.2
000300	-104.332	41.070	471.3	472.2	1.2	-0.5	40803	-57.22	270	47	3.50	19.0
000400	-104.322	40.940	474.9	474.4	1.1	-1.3	40803	-57.32	265	48	3.53	20.0
000500	-104.310	40.808	475.6	475.3	1.9	1.7	40803	-56.98	267	42	3.51	19.3
000600	-104.300	40.675	477.2	474.4	1.8	1.5	40778	-56.82	261	37	3.49	18.7
000700	-104.290	40.543	474.3	474.4	1.5	0.1	40766	-55.47	265	36	3.55	20.8
000800	-104.210	40.437	467.8	495.4	2.2	-30.1	40778	-54.91	262	29	3.80	29.2*
000900	-104.027	40.420	465.6	503.2	1.7	-9.7	40803	-54.93	264	37	4.41	54.0**
001000	-103.843	40.420	463.4	508.3	1.6	0.1	40778	-54.85	269	42	4.21	45.4**
001100	-103.675	40.457	461.7	488.3	2.8	-28.1	40754	-55.05	278	48	4.09	40.5*
001200	-103.627	40.580	463.0	459.2	2.6	-0.9	40766	-54.61	282	46	3.70	25.7
001300	-103.602	40.705	470.0	464.3	1.7	0.2	40815	-54.69	285	44	3.70	25.8
001400	-103.577	40.833	478.2	470.2	1.7	1.1	40790	-54.25	287	39	3.72	26.5
001500	-103.548	40.967	484.0	472.2	1.5	1.3	40815	-54.09	295	46	3.74	27.0
001600	-103.517	41.093	487.7	469.2	2.6	-21.2	40973	-54.83	298	49	3.87	31.8
001700	-103.592	41.183	468.9	411.1	2.7	-22.6	41385	-55.75	289	60	3.61	22.6
001800	-103.747	41.195	462.1	413.3	2.8	1.0	41628	-55.85	292	52	3.50	18.9
001900	-103.897	41.205	455.9	409.2	2.8	1.4	42102	-57.54	283	46	3.49	18.6
002000	-104.045	41.215	460.3	418.2	2.8	-15.9	42053	-57.66	279	43	3.47	18.0
002100	-104.167	41.143	464.7	445.3	2.3	-17.4	42114	-57.68	274	48	3.40	15.9
002200	-104.198	41.022	464.9	458.2	1.9	-1.8	42260	-57.76	269	48	3.35	14.3
002300	-104.217	40.895	473.6	466.3	2.2	1.6	42199	-57.98	266	46	3.30	12.9
002400	-104.233	40.763	482.4	464.3	1.5	-0.2	42235	-58.00	251	45	3.26	11.7
002500	-104.252	40.637	481.0	463.1	2.1	1.6	42175	-58.46	250	41	3.25	11.2
002600	-104.265	40.510	477.3	466.3	2.3	-23.5	42138	-58.48	235	28	3.35	14.2
002700	-104.147	40.422	466.8	485.3	1.8	-5.6	42114	-57.98	255	17	4.86	75.7**
002800	-103.973	40.400	457.3	486.3	1.6	1.1	42199	-57.26	270	28	4.89	77.2*
002900	-103.798	40.382	457.6	495.4	2.2	-10.8	42150	-57.42	280	40	4.37	52.3**
003000	-103.627	40.420	456.2	490.2	2.8	1.8	42150	-57.50	269	40	3.82	30.1*
003100	-103.507	40.513	448.6	475.3	3.0	-0.7	42175	-57.44	270	51	4.11	41.5*
003200	-103.408	40.620	457.4	480.2	2.4	2.4	42138	-57.26	268	41	4.36	52.1*
003300	-103.305	40.732	471.2	485.3	1.7	0.5	42223	-57.40	287	43	4.19	44.5*
003400	-103.198	40.840	471.8	492.2	2.3	1.1	42138	-57.32	276	41	4.18	44.0*
003500	-103.097	40.953	471.3	491.2	2.3	-12.2	42235	-57.28	272	41	3.92	34.0*
003600	-103.037	41.078	465.5	460.2	3.2	-1.6	43000	-56.54	291	37	3.62	23.1
003700	-102.990	41.198	470.4	453.1	3.2	2.4	43365	-56.50	313	38	3.55	20.5
003800	-102.947	41.318	469.5	449.2	2.3	-13.2	43486	-56.76	308	46	3.62	23.1
003900	-102.967	41.435	463.2	417.2	2.4	-20.4	43389	-57.90	294	52	3.49	18.7
004000	-103.098	41.480	465.2	412.3	3.2	-14.5	43316	-58.10	292	57	3.33	13.8
004100	-103.245	41.455	464.4	419.2	2.5	-0.3	43328	-59.04	292	55	3.29	12.4
004200	-103.397	41.420	449.5	409.2	3.1	1.5	43778	-58.28	299	53	3.25	11.4
004300	-103.538	41.382	468.2	423.3	2.3	-0.3	43268	-60.13	287	54	3.23	10.7
004400	-103.685	41.347	462.5	418.2	2.7	2.0	43425	-60.19	287	52	3.21	10.3
004500	-103.832	41.298	465.6	432.1	2.7	-16.5	43195	-60.11	276	48	3.12	7.6
004600	-103.912	41.195	470.3	447.3	3.5	-6.3	43425	-60.19	259	49	3.08	6.7
004700	-103.943	41.075	455.9	449.2	2.1	0.9	43523	-60.47	273	49	3.04	5.5
004800	-103.975	40.952	464.5	452.1	1.7	1.5	43535	-61.13	263	46	3.01	4.6

• CI
* ROLL
** ROLL–CI

Table 3. Aircraft Navigation, Meteorological, and Water Vapor Data--July 15, 1971, 0000-0137 UT (continued)

TIME	POSITION		SPEED		PITCH	ROLL	ALT.	TEMP.	WIND		RADIATION	
	LONG	LAT	AIR	GRND					DIR	AMP	VOLT	WATER
GMT	DEG	DEG	KNOTS	KNOTS	DEG	DEG	FEET	DEG C	DEG	KNOTS		VAPOR
004900	-104.002	40.828	470.4	448.2	1.9	0.1	43547	-61.59	249	44	3.02	4.9
005000	-104.033	40.707	472.1	444.3	2.8	1.7	43608	-61.37	243	48	3.01	4.9
005100	-104.062	40.583	474.5	437.2	1.4	2.0	43535	-62.53	231	51	2.99	4.2
005200	-104.093	40.467	462.1	429.2	3.1	-1.9	43693	-62.76	234	45	2.96	3.5
005300	-104.117	40.352	453.6	424.3	2.5	-1.0	43838	-62.59	234	41	3.51	19.3•
005400	-104.147	40.233	452.4	425.3	3.2	-2.7	43705	-63.20	238	39	3.05	5.7
005500	-104.117	40.120	452.2	445.3	3.5	-19.0	43741	-62.96	219	32	3.14	8.3
005600	-103.975	40.068	450.4	461.2	2.6	3.6	43765	-62.53	207	32	4.34	51.2•
005700	-103.807	40.042	449.3	465.3	2.9	-11.5	43729	-62.47	227	19	4.61	63.1•
005800	-103.647	40.065	445.3	465.3	3.2	-9.3	43741	-62.21	258	20	4.45	56.0•
005900	-103.507	40.138	445.0	473.1	2.0	-11.7	43268	-61.99	257	36	3.89	32.7•
010000	-103.437	40.257	447.6	459.2	2.2	1.2	43255	-60.29	268	33	3.47	18.0
010100	-103.385	40.382	456.9	478.3	1.9	-1.4	42697	-59.51	257	42	3.28	12.4
010200	-103.332	40.505	475.8	466.3	3.9	-1.5	43243	-58.60	303	34	3.29	12.5
010300	-103.280	40.633	468.9	463.1	1.5	1.0	43425	-58.48	300	34	3.25	11.4
010400	-103.227	40.753	472.9	467.3	2.4	1.5	43401	-57.94	296	36	3.28	12.1
010500	-103.165	40.872	476.9	461.2	2.2	-1.7	43474	-58.18	312	41	3.33	13.8
010600	-103.115	40.997	461.7	441.2	3.1	-22.2	43413	-57.70	294	50	3.31	13.2
010700	-103.183	41.092	456.8	406.2	2.5	-20.0	43438	-60.11	284	52	3.22	10.4
010800	-103.325	41.122	461.1	406.2	2.4	0.8	43425	-60.19	283	53	3.07	6.4
010900	-103.475	41.142	459.0	408.2	2.4	-0.5	43523	-60.75	284	51	3.07	6.5
011000	-103.625	41.153	477.9	421.1	0.7	0.5	43146	-60.69	279	56	3.09	6.9
011100	-103.777	41.170	472.6	414.3	0.4	-2.1	42405	-60.25	275	58	0.80	-19.0
011200	-103.933	41.183	471.0	416.2	0.1	2.6	41191	-59.06	283	57	0.50	-17.1
011300	-104.083	41.195	468.0	413.3	2.0	1.2	40086	-56.82	270	54	0.51	-17.2
011400	-104.232	41.210	457.8	397.2	0.7	-0.7	39880	-56.24	277	59	0.52	-17.2
011500	-104.380	41.220	451.1	390.1	2.9	1.5	38799	-54.39	268	60	0.54	-17.5
011600	-104.520	41.228	444.5	387.2	1.2	-2.0	38896	-53.71	268	56	0.55	-17.5
011700	-104.660	41.220	453.2	394.3	0.4	1.5	38131	-53.57	262	59	0.56	-17.6
011800	-104.765	41.148	477.3	438.2	-1.5	-27.3	35945	-50.14	241	66	0.68	-18.4
011900	-104.755	41.023	474.5	463.1	-2.3	-0.3	33335	-42.98	254	55	0.77	-18.9
012000	-104.738	40.898	465.3	458.2	0.2	0.4	31319	-35.63	257	54	0.84	-19.2
012100	-104.722	40.772	449.8	440.2	0.7	-0.1	30943	-32.32	261	56	0.85	-19.2
012200	-104.708	40.650	452.4	449.2	0.4	-1.6	31015	-32.28	266	55	0.91	-19.4
012300	-104.693	40.525	459.2	462.1	-3.8	0.0	29206	-30.28	271	60	0.97	-19.5
012400	-104.675	40.392	465.4	477.3	-5.2	20.3	24592	-18.86	286	51	1.19	-19.6
012500	-104.670	40.262	506.3	475.3	-3.7	0.1	20548	-8.71	284	39	1.36	-19.2
012600	-104.668	40.135	506.6	465.3	-2.4	-4.6	15970	-0.87	310	28	1.54	-18.4
012700	-104.652	40.008	509.6	419.2	-6.5	4.4	13068	0.77	316	10	1.78	-16.6
012800	-104.653	39.902	202.7	352.3	0.7	-7.2	10688	9.46	221	15	2.15	-12.4
012900	-104.620	39.820	231.0	302.2	1.8	1.8	10761	9.68	290	3	2.19	-11.8
013000	-104.568	39.748	231.1	301.3	0.3	25.5	10373	11.01	286	11	2.24	-11.1
013100	-104.602	39.683	231.0	250.2	-2.7	14.1	9061	12.71	271	25	2.26	-10.7
013200	-104.668	39.693	212.5	213.1	0.1	1.6	7264	16.86	263	14	2.43	-7.9
013300	-104.707	39.738	524.4	189.2	-1.5	3.9	6718	18.15	243	19	2.46	-7.4
013400	-104.682	39.760	511.4	157.2	1.3	15.2	5625	18.41	231	26	2.48	-6.9
013500	-104.660	39.732	511.4	51.3	-1.7	0.3	5358	17.81	153	115	2.41	-8.2
013600	-104.652	39.722	511.3	14.2	-1.6	-0.3	5394	17.06	131	151	0.47	-16.9
013700	-104.652	39.725	511.4	18.3	-1.6	1.1	5394	16.28	330	146	0.25	-14.6

•CI

considerably larger--as far as 30 nautical miles downstream of the cell than upstream. Within the resolution accuracy of the radiometric inference system, the water vapor at 50 nautical miles downstream was again equivalent to the upstream mass at the end of the first traverse. The upstream values of water vapor mass (fig. 10 and table 3) are in general agreement with Mastenbrook (1968).

Considering only the Grover storm observations at the highest flight level (table 7), we infer a mean water vapor mixing ratio of 2.8 g g^{-1} (ppm) upstream of the cell and 8.3 g g^{-1} (ppm) downstream in the streamline flow. The former figure is certainly consistent with Mastenbrook (1968).

The core of the cell was displaced approximately 15 nautical miles eastward during the total observation period of 90 minutes. For all three traverses, the maximum downstream range at which excess water vapor in the column above the aircraft could be detected approximated 45 nautical miles. Based upon these observations, the residual time above the flight level for the excess thunderstorm water vapor is 90 minutes. This residual time depends upon the limits of the radiometer sensitivity. At 0105 UT, only background water vapor levels were detectable.

To establish further the validity of the radiometric inferences, saturation conditions are *calculated* and the presence or absence of cirrus is noted. Assuming that the entire mass of 27×10^{-4} g cm^{-2} of water vapor observed downstream and above the lower flight level of 12.4 km (table 7) was contained in the column between 12.4 and 14.8 km (the cell top), we would calculate a mean water vapor mixing ratio of 33 ppm. Saturation conditions over ice for this column at a measured temperature of $-60.0^{\circ}C$ would require a mixing ratio of 43 ppm. In agreement with this calculation, no cirrus was observed above the aircraft during the first traverse.

During the second traverse of the cell at 12.6 km, about 20 minutes later, the mixing ratio inferred from the optical mass of water vapor reached 52.0 ppm. This ratio results from cirrus, which remained above flight level during most of the traverse, and gives a "false" water vapor mass. The 10.0- to 12.0-μm channel clearly indicated the cirrus

above. The last traverse around the cell was at 13.3 km. If the entire mass of water vapor measured above the aircraft, 17.0×10^{-4} g cm^{-2}, were concentrated in the column between 13.3 km (the flight level) and 14.8 km (the cell top), saturation would just be reached. On this final traverse, occurrence of cirrus approximately one-half of the time is consistent with the calculation. Restricting the layer to 14.8 km (the visible cell top) precludes any assumptions that the water vapor extends above the cloud top in the lower stratosphere and is an extreme case for saturation.

1.5.2 La Crosse, Wis., Cell System of July 12, 1971

Data for this storm are tabulated at 1-minute intervals in both figure 11 and table 4 and summarized in table 7. Circumnavigation of the 49,000-foot thunderstorm system was made at two levels, 33,500 and 40,000 feet. During the lower flight track, cirrus occurred above the aircraft only once at 2221 UT. Cirrus was above the jet at 2245 UT during the high-level track. The average water vapor increase downwind of the storm was least at the higher flight level, but amounted to 27 percent of the upstream overburden. This flight covered a 90- by 90-nautical-mile box.

1.5.3 O'Neill, Nebr., Cell System of July 14, 1971

The data for this storm appear in both figure 12 and table 5 and are summarized in table 7. The anvil shield from the parent storm extended for nearly 140 nautical miles. This cloud shield necessitated a very long, narrow flight pattern, commencing on a westerly course flown entirely at 35,200 feet. Between 2223 and 2230 UT, cirrus was present above the aircraft, having swept south-southeastward in relatively strong 35,000-foot winds from 285°. The water vapor increase downwind of the storm between longitudes $96^{\circ}00'$ and $97^{\circ}00'$ was least in this storm system due to its diffuse and dissipating stage, but the increase still amounted to 11 percent.

Climbout for this storm commenced at 2306 UT to the east of the old cell. During climbout, we have a classic example of a steady decrease in the water vapor mass above the jet from longitudes $96^{\circ}30'$ to $99^{\circ}30'$

occurring as we passed upstream of the subsiding cell. Averages for the mass are listed in table 7. The results are similar to those of the La Crosse, Wis., system described in subsection 1.5.2 above.

1.5.4 Southwestern Colorado-New Mexico Cell Arrays of July 14, 1971

Data for this extensive storm traverse are given in figure 13 and table 6, with the summary appearing in table 7. The flight track around this very large group of merging storm cells (located to the southwest of Denver and reaching into southwestern Colorado) was 360 nautical miles, east-west, by approximately 150 miles, north-south. The main storm system center was at latitude $36^{o}30'$ and longitude $105^{o}00'$.

The entire mission was flown at 42,300 feet for the average water vapor mass increase observations. The upstream leg was actually northwest of the main system, while the downstream leg was north of the system. The percent of water vapor mass increase is the largest for any system investigated, reaching 2.11 times the fair weather background mass.

We can now consider a vertical transport mechanism in thunderstorms to increase the water vapor mass by 10×10^{-4} g cm^{-2} in a column above the downstream flight level of 40,700 feet (12.4 km) calculated for the Grover storm, subsection 1.5.1 above (fig. 1). This total turbulent vertical transport, Tr, assumed to continue for approximately 20 minutes, is given by

$$Tr = \rho w \bar{s} t = 7.3 \times 10^{-4} \text{ g cm}^{-2}, \qquad (1.7)$$

where ρ is density (g cm^{-2}), 1.8×10^{-4}; w is the mean vertical velocity (cm sec^{-1}) and $\bar{s}$ is the mixing ratio in ppm (g g^{-1}), 23.0; and t is time (sec), 1.2×10^{3}. Solving for w in equation (1.7), we obtain 1.5 m sec^{-1} for the upward vertical velocity of the Grover storm cell over the 20-minute period. This result is consistent with previous thunderstorm research (Byers and Braham, 1949) for an average cell. The RHI radar indicated a top growth rate of approximately 1.6 km in 20 minutes.

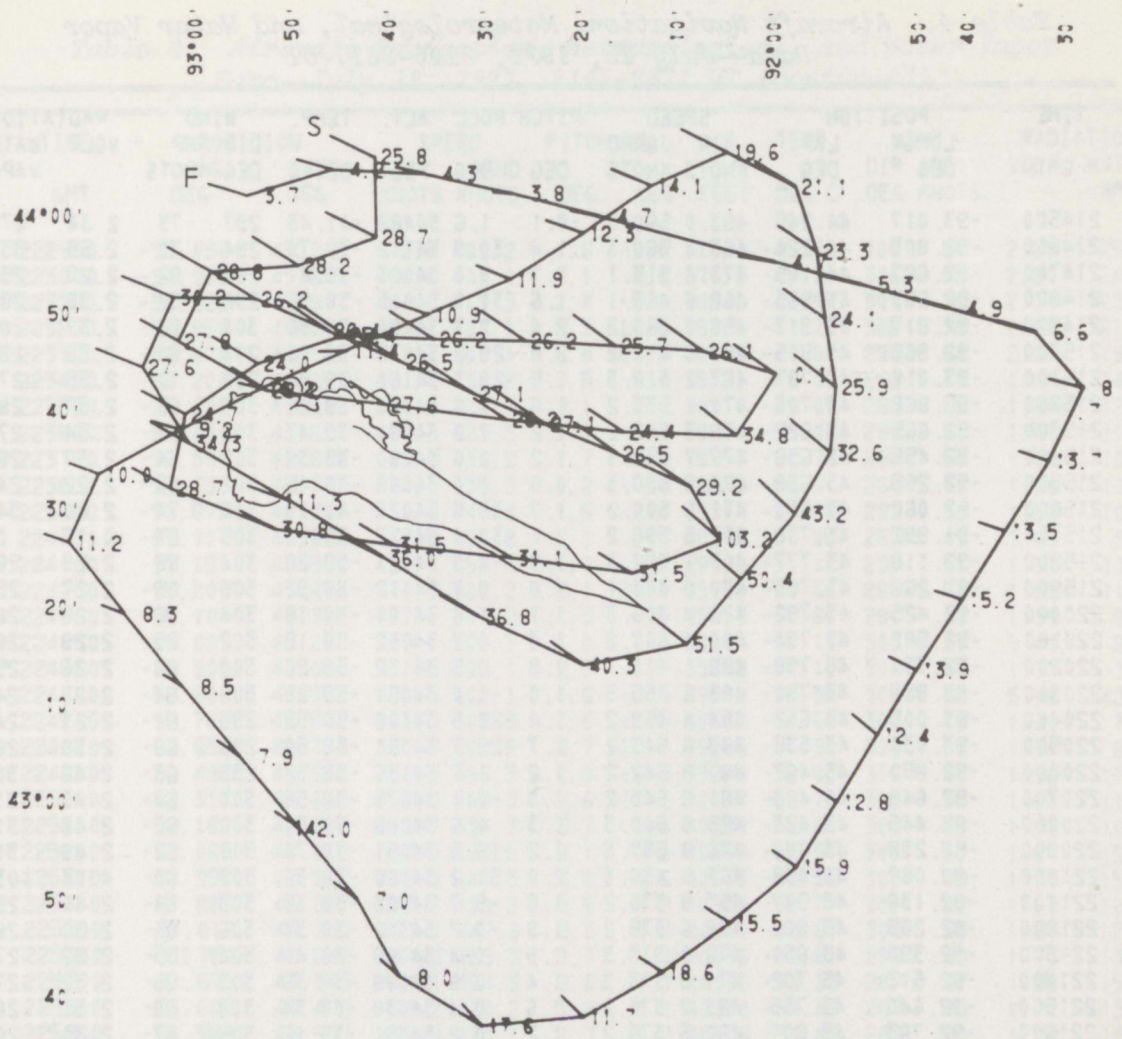

Figure 11. Flight tracks around La Crosse, Wis., thunderstorm, 2147-2310 UT, July 12, 1971. Short segment lines indicate wind direction (point into wind) and speed (1 cm = 100 kt), and the numerals indicate water vapor (in g cm^{-2} × 10^{4}). Latitude and longitude measurements in 10-minute intervals are to the left and top, respectively.

1.6 Conclusion

In conclusion, we have found that average stratospheric and upper tropospheric water vapor injection by Plains thunderstorms above a mean flight level of 41,500 feet is 11.2 × 10^{-4} g cm^{-2} above the undisturbed atmospheric background water vapor mass of 9.8 × 10^{-4} g cm^{-2}. This result was possible only with the use of a high-performance jet aircraft to obtain the data.

Table 4. Aircraft Navigation, Meteorological, and Water Vapor Data--July 12, 1971, 2145-2311 UT

TIME	POSITION		SPEED		PITCH	ROLL	ALT.	TEMP.	WIND		RADIATION	
GMT	LONG DEG	LAT DEG	AIR KNOTS	GRND KNOTS	DEG	DEG	FEET	DEG C	DIR DEG	AMP KNOTS	VOLT	WATER VAPOR
214500	-93.017	44.245	493.0	560.3	-0.1	1.6	34488	-41.43	297	73	2 34	27.5
214600	-92.803	44.220	483.4	560.3	1.4	30.9	34112	-39.79	294	73	2.55	33.3
214700	-92.687	44.105	471.4	515.1	1.7	9.0	34063	-39.47	295	82	2.27	25.8
214800	-92.683	43.965	468.6	463.1	1.6	31.9	34015	-38.96	296	92	2.38	28.7
214900	-92.817	43.917	458.7	389.2	2.4	2.7	34100	-38.96	302	86	2.37	28.2
215000	-92.965	43.905	464.5	417.2	2.8	-29.2	34075	-39.06	298	80	2.39	28.8
215100	-93.018	43.787	467.2	518.3	1.5	-29.7	34160	-38.96	298	70	2.35	27.8
215200	-92.868	43.703	471.1	533.2	1.6	-7.6	34173	-38.86	303	65	2.37	28.2
215300	-92.665	43.682	479.5	542.2	1.2	1.2	34051	-39.47	302	67	2.34	27.6
215400	-92.455	43.658	477.7	539.3	1.2	0.0	34100	-39.38	302	64	2.37	28.2
215500	-92.255	43.638	474.9	538.3	0.6	1.0	34088	-39.45	302	63	2.22	24.4
215600	-92.060	43.633	471.0	500.2	1.7	-30.8	34027	-41.19	308	74	2.60	34 8
215700	-91.992	43.738	467.5	396.2	2.1	-30.0	34027	-38.50	305	63	-0.17	0.1
215800	-92.118	43.777	467.1	392.3	1.9	-0.3	34124	-38.28	304	88	2.29	26.1
215900	-92.268	43.785	470.8	400.1	1.8	0.7	34112	-38.92	305	85	2.27	25 7
220000	-92.425	43.792	476.4	405.3	1.1	1.0	34100	-39.18	304	86	2.29	26.2
220100	-92.582	43.793	480.4	407.2	1.3	0.7	34112	-39.18	302	85	2.29	26.2
220200	-92.737	43.798	482.1	411.1	1.8	0.5	34112	-39.20	304	86	2.26	25.4
220300	-92.883	43.750	483.6	455.3	1.0	-1.0	34051	-39.20	300	84	2.20	24.1
220400	-93.005	43.662	484.4	458.2	1.4	-20.5	34100	-38.52	298	81	2.23	24.7
220500	-93.030	43.535	483.6	543.2	1.7	-29.7	34051	-38.54	298	69	2.39	28.7
220600	-92.850	43.467	480.9	542.2	1.2	1.7	34136	-38.52	298	63	2.46	30.8
220700	-92.648	43.443	481.8	545.2	1.3	-0.1	34075	-38.58	300	64	2.49	31.5
220800	-92.445	43.423	475.8	540.3	1.3	0.6	34088	-38.60	300	67	2.48	31.1
220900	-92.238	43.400	476.8	537.3	1.2	-16.5	34051	-38.74	300	62	2.49	31.5
221000	-92.087	43.458	467.5	436.3	2.0	-31.2	34100	-38.36	309	80	4.34	103.2*
221100	-92.138	43.547	457.8	375.2	1.8	-5.7	34003	-38.38	303	84	2.40	29.2
221200	-92.265	43.600	459.6	375.2	1.9	-0.7	34112	-38.34	306	86	2.30	26.5
221300	-92.390	43.650	476.0	373.3	1.9	0.4	34088	-38.44	304	105	2.32	27.1
221400	-92.513	43.702	471.9	373.3	1.4	0.9	34088	-38.36	303	95	2.32	27.1
221500	-92.640	43.755	463.2	375.2	1.6	0.4	34039	-38.34	303	88	2.30	26.5
221600	-92.763	43.807	460.5	375.2	1.2	0.2	34051	-39.16	303	87	2.30	26.4
221700	-92.888	43.660	461.7	378.2	0.6	0.2	34112	-38.90	301	84	2.29	26.2
221800	-93.028	43.862	471.9	426.3	1.7	-29.1	33359	-36.98	292	90	2.44	30.2
221900	-93.078	43.742	466.0	502.2	2.6	-15.0	33347	-36.28	291	80	2.34	27.6
222000	-92.998	43.612	477.6	550.3	-1.5	-30.3	32509	-36.14	299	71	2.59	34.3
222100	-92.827	43.515	484.8	554.2	1.0	5.6	32108	-33.53	290	70	4.50	111.4*
222200	-92.665	43.422	478.2	552.2	1.0	1.4	32133	-34.43	295	74	2.65	36.0
222300	-92.502	43.325	478.7	551.3	0.7	-1.1	32133	-34.35	298	71	2.67	36.8
222400	-92.320	43.243	485.4	550.3	2.4	-26.6	32679	-34.85	304	67	2.79	40.3
222500	-92.143	43.280	477.7	480.2	2.1	-26.6	33650	-36.10	307	70	3.12	51.5
222600	-92.050	43.392	473.6	460.2	3.3	1.4	34780	-38.78	310	73	3.09	50.4
222700	-91.958	43.502	464.0	442.1	3.6	-8.1	36213	-41.63	313	80	2.88	43.2
222800	-91.898	43.607	451.7	408.2	2.2	-6.9	37220	-42.59	309	83	2.53	32.6

•CI

*ROLL

Table 4. Aircraft Navigation, Meteorological, and Water Vapor Data--July 12, 1971, 2145-2311 UT (continued)

TIME	POSITION		SPEED		PITCH	ROLL	ALT.	TEMP.	WIND		RADIATION	
	LONG	LAT	AIR	GRND					DIR	AMP	VOLT	WATER
GMT	DEG	DEG	KNOTS	KNOTS	DEG	DEG	FEET	DEG C	DEG	KNOTS		VAPOR
222900	-91.890	43.718	472.5	409.2	1.8	-5.8	37038	-45.74	308	84	2.28	25.9
223000	-91.908	43.833	468.5	410.1	3.1	1.8	37633	-45.64	306	83	2.20	24.1
223100	-91.922	43.947	464.0	413.3	2.4	-0.3	38240	-48.97	303	76	2.17	23.3
223200	-91.958	44.057	469.1	400.1	2.7	-11.5	38435	-47.71	302	79	2.08	21.1
223300	-92.078	44.115	473.4	400.1	2.8	-25.7	38593	-47.87	296	84	2.01	19.6
223400	-92.208	44.057	461.7	430.2	3.5	3.1	39321	-49.05	292	71	1.74	14.1
223500	-92.325	43.975	456.9	424.3	3.1	0.6	39916	-49.05	288	65	1.64	12.3
223600	-92.450	43.897	461.3	423.3	2.1	4.1	39928	-52.00	290	61	1.61	11.9
223700	-92.592	43.835	468.0	430.2	1.7	-1.5	39953	-51.74	289	59	1.56	10.9
223800	-92.730	43.773	474.0	435.3	2.2	-7.6	39989	-53.71	268	47	1.59	11.4
223900	-92.875	43.707	471.4	445.3	1.5	-2.4	39904	-51.62	282	39	1.52	10.2
224000	-93.013	43.635	477.9	451.2	2.1	2.3	39965	-51.20	287	49	1.45	9.2
224100	-93.150	43.558	480.4	454.3	1.6	0.5	39892	-51.12	291	51	1.50	10.0
224200	-93.200	43.442	470.9	500.2	2.1	-29.0	39892	-51.66	289	41	1.58	11.2
224300	-93.107	43.322	471.1	503.2	1.3	0.1	39953	-51.66	291	38	1.39	8.3
224400	-93.007	43.200	469.1	504.1	1.0	0.5	39940	-51.18	300	37	1.41	8.5
224500	-92.908	43.080	461.5	505.1	2.5	1.1	39892	-51.18	304	46	1.37	7.9
224600	-92.808	42.962	458.6	504.1	1.6	-0.3	39940	-50.58	304	46	5.06	142.0•
224700	-92.707	42.842	461.0	508.3	1.6	-1.5	39953	-51.68	305	49	1.30	7.0
224800	-92.633	42.713	461.9	500.2	2.7	-27.1	39965	-51.98	309	43	1.37	8.0
224900	-92.492	42.633	458.3	496.3	1.9	-6.9	39880	-52.83	316	48	1.92	17.6
225000	-92.317	42.650	450.0	468.3	4.6	-11.2	40147	-52.73	312	50	1.60	11.7
225100	-92.182	42.727	429.7	434.3	3.7	0.4	40888	-52.64	303	48	1.96	18.6
225200	-92.065	42.812	437.5	448.2	2.1	0.6	40669	-52.54	300	50	1.81	15.5
225300	-91.952	42.907	449.3	447.3	3.0	-8.6	40633	-52.56	303	49	1.83	15.9
225400	-91.883	43.017	447.2	439.2	3.5	2.2	40900	-52.77	300	49	1.67	12.8
225500	-91.817	43.130	463.1	447.3	2.5	0.4	40960	-52.81	309	53	1.64	12.4
225600	-91.750	43.242	457.8	455.3	1.7	0.4	40936	-52.81	295	49	1.73	13.9
225700	-91.673	43.363	460.1	464.3	2.8	-0.1	40936	-54.33	287	47	1.80	15.2
225800	-91.602	43.478	468.2	470.2	1.8	0.1	40900	-54.49	287	45	1.71	13.5
225900	-91.528	43.597	466.8	473.1	1.7	1.2	40936	-54.45	288	50	1.72	13.7
230000	-91.470	43.722	466.3	447.3	2.4	-21.1	40875	-54.07	284	57	1.42	8.7
230100	-91.550	43.815	465.3	405.3	2.8	-17.3	40912	-54.05	286	63	1.27	6.6
230200	-91.697	43.853	464.3	406.2	2.5	-0.8	40888	-54.71	285	60	1.13	4.9
230300	-91.848	43.892	470.1	408.2	2.3	0.8	40948	-54.03	283	64	1.16	5.3
230400	-91.997	43.928	468.7	413.3	1.8	1.0	40888	-54.07	279	58	1.12	4.7
230500	-92.143	257.350	466.6	415.3	2.0	1.5	40960	-54.05	273	56	1.09	4.5
230600	-92.298	44.005	462.7	415.3	2.5	2.2	40924	-54.07	278	49	1.11	4.7
230700	-92.448	44.042	450.2	420.2	2.3	1.7	40815	-53.93	273	32	1.03	3.8
230800	-92.600	44.075	468.8	422.4	2.1	2.4	40973	-54.01	282	50	1.07	4.3
230900	-92.760	44.082	468.9	425.3	2.4	-4.4	40875	-54.09	285	60	1.07	4.2
231000	-92.907	44.035	466.9	420.2	1.7	-0.3	40948	-54.11	287	65	1.02	3.7
231100	-93.050	43.985	467.1	423.3	1.5	1.3	40875	-53.79	295	67	1.04	3.9

•CI

We can now speculate on the vertical mass transport of water vapor over larger areas into the upper troposphere and stratosphere. Plains thunderstorms east of Colorado reach much higher altitudes than do storms nearer the Rockies, the former pushing well into the lower stratosphere. In addition, the tropopause is lower in the eastern portion of the Plains during the thunderstorm season than it is in the western portion, resulting in a much higher stratospheric penetration to the east. Recently Lee and McPherson (1971) reported on an observational survey of the tops of Oklahoma thunderstorms, stating that 469 thunderstorms exceeded 12.2 km during April, May, and June of 1967 through 1969; of that number, 33

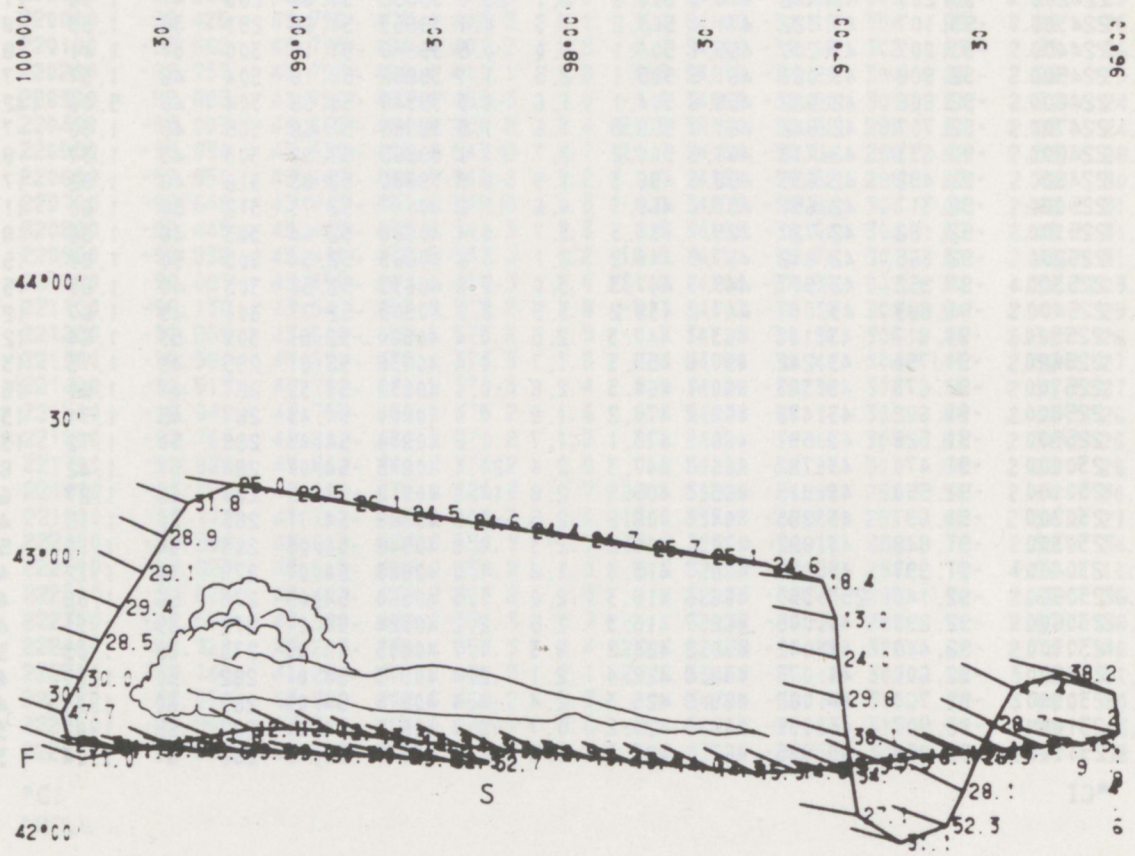

Figure 12. Flight track around O'Neill, Nebr., thunderstorm, 2223-2331 UT, July 14, 1971. Short segment lines indicate wind direction (point into wind) and speed (1 cm = 100 kt), and the numerals indicate water vapor (in g cm^{-2} × 10^4). Latitude and longitude measurements in 10-minute intervals are to the left and top, respectively.

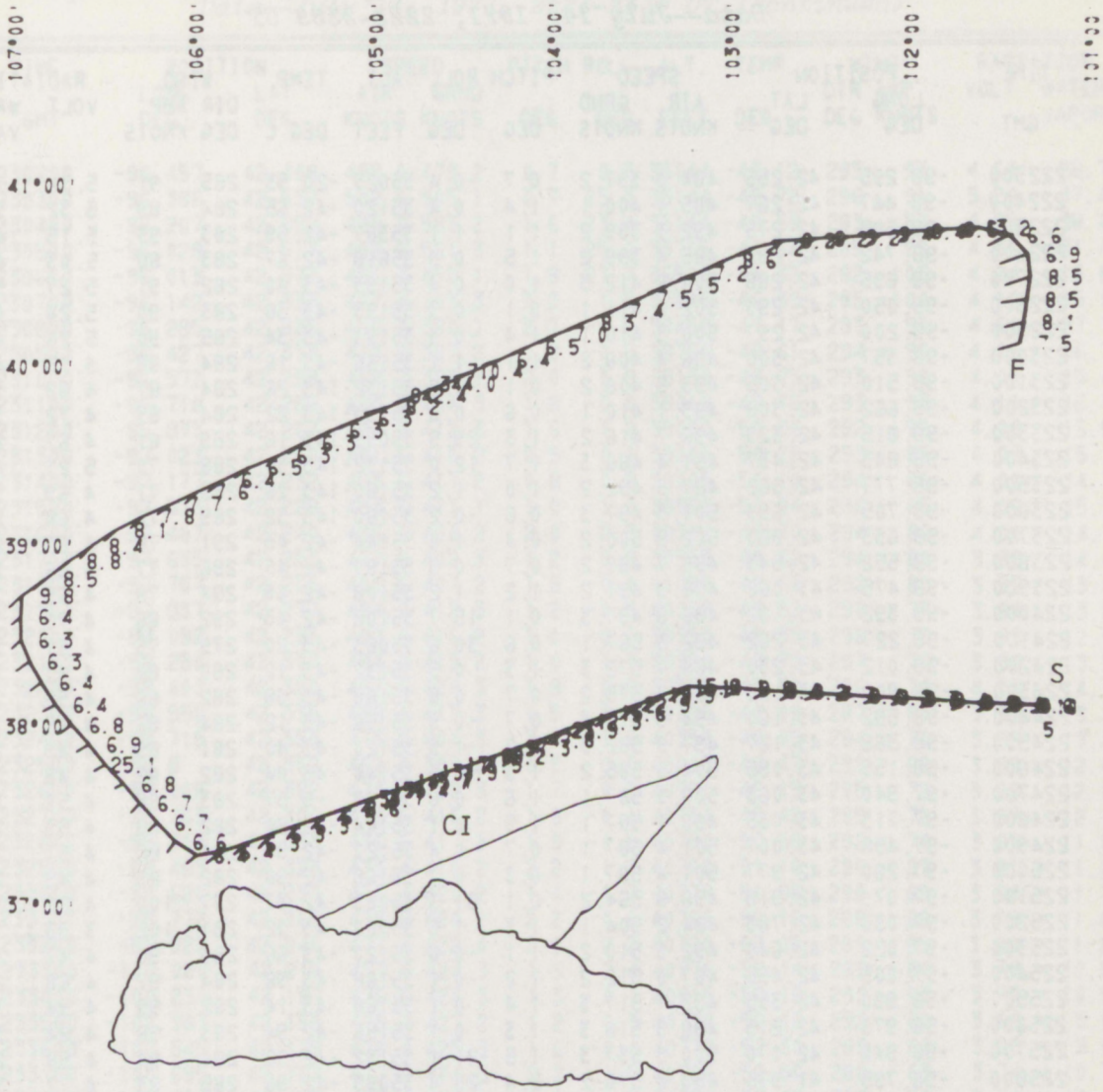

Figure 13. Flight for southwestern Colorado-New Mexico storm system, 2259-0025 UT, July 13-14, 1971. Short segment lines indicate wind direction (point into wind) and speed (1 cm = 100 kt), and the numerals indicate water vapor (in g cm^{-2} × 10^4). Latitude and longitude measurements in 10-minute intervals are to the left and top, respectively.

percent exceeded 15.2 km. They found the average base of the stratosphere during the period of observation to be 12.2 km. On the other hand, only 25 percent of all Colorado thunderstorms penetrate into the stratosphere during the May through September thunderstorm season.

Table 5. Aircraft Navigation, Meteorological, and Water Vapor Data--July 14, 1971, 2223-2339 UT

TIME	POSITION		SPEED		PITCH	ROLL	ALT.	TEMP.	WIND		RADIATION	
	LONG	LAT	AIR	GRND					DIR	AMP	VOLT	WATER
GMT	DEG	DEG	KNOTS	KNOTS	DEG	DEG	FEET	DEG C	DEG	KNOTS		VAPOR
222300	-98.295	42.255	484.0	397.2	0.7	-0.4	35023	-20.53	285	91	5.34	52.7*
222400	-98.447	42.267	485.1	400.1	1.4	0.4	35120	-42.65	284	89	5.32	52.3*
222500	-98.595	42.275	492.3	399.2	1.1	1.1	35387	-42.59	283	93	5.15	45.3*
222600	-98.742	42.283	485.4	399.2	1.5	0.9	35618	-42.67	283	88	5.03	40.9*
222700	-98.895	42.288	504.6	412.3	1.0	0.4	35193	-43.40	282	91	5.27	50.3*
222800	-99.050	42.293	502.6	411.1	-0.1	-0.3	35193	-43.38	283	90	5.24	49.0*
222900	-99.200	42.297	500.3	410.1	1.4	-0.3	35193	-43.34	285	90	5.26	49.9*
223000	-99.357	42.300	496.4	408.2	1.1	1.1	35156	-43.16	284	98	5.15	45.6*
223100	-99.510	42.305	493.9	408.2	0.1	-0.2	35132	-143.26	284	87	4.82	33.9
223200	-99.662	42.308	493.1	410.1	0.6	0.6	35193	-143.22	284	83	4.72	31.1
223300	-99.815	42.323	496.7	416.2	1.3	29.5	35095	-143.16	289	81	4.67	29.3
223400	-99.843	42.437	491.4	486.3	1.7	12.0	35132	-143.30	288	70	5.21	47.7
223500	-99.777	42.562	487.5	492.2	1.0	1.2	35180	-143.26	285	71	4.69	30.0
223600	-99.705	42.693	501.3	497.3	0.6	-0.2	35180	-143.32	289	70	4.64	28.5
223700	-99.633	42.820	502.9	500.2	0.4	1.6	35144	-42.43	291	76	4.67	29.4
223800	-99.552	42.943	499.7	489.2	0.7	-0.3	35180	-42.45	296	77	4.66	29.1
223900	-99.475	43.068	498.9	491.2	1.2	1.2	35108	-42.49	294	78	4.65	28.9
224000	-99.392	43.192	496.8	497.3	0.1	15.7	35108	-42.43	292	86	4.75	31.8
224100	-99.227	43.262	492.3	567.1	0.6	30.6	35083	-43.20	279	75	4.51	25.0
224200	-99.012	43.230	484.7	572.3	1.3	0.5	35132	-43.12	280	84	4.41	22.5
224300	-98.800	43.195	486.2	575.2	0.7	0.8	35168	-43.08	282	86	4.55	26.1
224400	-98.592	43.160	494.3	579.3	0.7	-0.9	35156	-43.12	284	86	4.49	24.5
224500	-98.368	43.127	497.9	582.3	0.2	-1.5	35120	-43.40	281	85	4.49	24.6
224600	-98.155	43.095	504.5	585.2	1.3	0.6	35144	-43.04	282	82	4.48	24.4
224700	-97.940	43.063	500.3	587.1	1.6	0.8	35193	-5.57	283	88	4.50	24.7
224800	-97.713	43.035	499.1	587.1	1.5	0.1	35144	-42.94	282	89	4.53	25.7
224900	-97.498	43.007	501.4	587.1	0.7	0.4	35120	-42.90	281	86	4.51	25.1
225000	-97.280	42.977	501.4	587.1	0.3	0.7	35168	-42.98	282	89	4.49	24.6
225100	-97.07_	42.918	496.8	564.2	0.1	31.3	35083	-42.37	277	100	4.22	18.4
225200	-97.030	42.783	484.2	504.1	1.3	1.5	35180	-43.32	281	102	3.93	13.0
225300	-97.022	42.640	492.3	510.2	1.1	-0.6	35120	-43.66	283	98	4.47	24.0
225400	-97.005	42.495	487.0	512.2	1.2	-0.1	35168	-43.38	284	97	4.68	29.8
225500	-96.990	42.355	492.7	517.3	1.4	0.1	35168	-43.14	285	99	4.94	38.1
225600	-96.973	42.215	498.5	518.3	1.3	0.7	35156	-42.94	283	98	4.84	34.7
225700	-96.948	42.070	500.5	537.3	1.5	-21.1	35132	-42.96	281	94	4.58	27.1
225800	-96.795	41.975	493.8	576.2	2.4	-29.4	35095	-42.96	285	83	4.72	31.1
225900	-96.625	42.035	479.9	486.3	1.6	-27.9	35193	-43.04	290	93	5.33	52.3
230000	-96.568	42.160	497.0	472.2	0.9	-0.6	35132	-42.82	296	93	4.62	28.1
230100	-96.515	42.287	495.2	474.4	1.0	1.0	35193	-42.94	294	94	4.58	26.9

*CI

Table 5. Aircraft Navigation, Meteorological, and Water Vapor Data--July 14, 1971, 2223-2339 UT (continued)

TIME	POSITION		SPEED		PITCH	ROLL	ALT.	TEMP.	WIND		RADIATION	
	LONG	LAT	AIR	GRND					DIR	AMP	VOLT	WATER
GMT	DEG	DEG	KNOTS	KNOTS	DEG	DEG	FEET	DEG C	DEG	KNOTS		VAPOR
230200	-96.457	42.408	498.0	479.2	0.7	0.3	35144	-43.12	295	93	4.64	28.7
230300	-96.388	42.537	502.5	505.1	0.7	25.3	35144	-42.72	296	91	5.20	47.4*
230400	-96.207	42.592	498.0	583.2	1.6	23.4	35144	-42.59	283	87	4.95	38.2*
230500	-96.028	42.517	492.9	561.3	1.1	25.0	35715	-44.64	285	99	4.36	21.4*
230600	-96.013	42.377	496.7	452.1	1.8	27.7	36528	-44.32	282	103	4.24	18.6*
230700	-96.142	42.333	477.4	383.3	3.2	1.5	37645	-46.39	285	100	4.10	15.9
230800	-96.285	42.325	466.0	380.1	2.7	-0.5	38459	-47.17	293	93	4.61	27.7•
230900	-96.427	42.313	470.8	387.2	1.2	-0.5	38750	-48 61	294	96	4.14	16.7
231000	-96.572	42.298	469.7	390.1	2.0	0.9	39139	-48.75	293	90	4.07	15.4
231100	-96.718	42.285	483.0	404.3	1.8	-0.0	39018	-49.76	293	93	4.11	16.1
231200	-96.873	42.267	494.2	412.3	1.6	1.2	39030	-50.28	292	92	4.08	15.5
231300	-97.023	42.250	491.6	416.2	0.9	0.1	39005	-50.28	293	85	4.07	15.3
231400	-97.177	42.232	493.6	417.2	0.8	-0.2	39005	-50.10	294	86	4.01	14.3
231500	-97.333	42.228	493.6	411.1	1.0	1.0	38969	-50.04	296	85	4.06	15.3
231600	-97.487	42.240	486.7	408.2	2.0	2.3	39382	-49.70	294	86	4.01	14.3
231700	-97.635	42.253	477.6	402.3	1.2	0.8	39953	-49.62	294	80	3.99	14.0
231800	-97.787	42.265	481.6	407.2	1.8	-0.1	40025	-49.66	292	80	3.95	13.4
231900	-97.937	42.277	484.7	412.3	1.2	-0.5	40038	-49.52	290	77	3.94	13.2
232000	-98.092	42.293	492.8	416.2	1.0	-0.1	39953	-49.35	296	79	3.93	12.9
232100	-98.250	42.307	494.0	419.2	1.0	1.1	39989	-48.75	297	76	3.96	13.5
232200	-98.403	42.320	497.6	424.3	1.9	0.7	39965	-47.51	296	74	4.01	14.3
232300	-98.558	42.335	499.1	413.3	1.5	3.0	40098	-47.09	287	83	3.95	13.3
232400	-98.715	42.353	475.8	404.3	2.4	1.6	40353	-48.45	294	75	3.95	13.3
232500	-98.8	42.368	462.5	398.2	1.9	0.6	40803	-48.47	299	68	3.89	12.4
232600	-99.008	42.382	470.6	402.3	1.7	0.2	40790	-49.15	295	72	3.86	12.0
232700	-99.163	42.380	473.6	416.2	1.8	-0.1	40754	-49.42	295	72	3.87	12.1
232800	-99.313	42.353	476.6	417.2	1.9	-0.1	40790	-50.56	292	74	3.85	11.8
232900	-99.463	42.323	473.4	418.2	2.2	1.2	40766	-51.16	294	67	3.81	11.2
233000	-99.620	42.297	476.4	420.2	1.4	-1.7	40778	-51.98	290	69	3.84	11.7
233100	-99.772	42.268	478.9	420.2	2.2	-0.6	40766	-52.16	288	68	3.79	11.0
233200	-99.922	42.240	477.4	422.4	2.0	2.2	40790	-52.06	289	65	3.80	11.2
233300	-100.080	42.215	477.5	424.3	1.5	2.4	40778	-52.14	289	64	3.78	10.8
233400	-100.230	42.187	476.5	426.3	1.3	0.1	40815	-52.16	293	63	3.75	10.5
233500	-100.387	42.155	475.7	427.2	1.2	0.3	40778	-52.16	292	60	3.69	9.8
233600	-100.545	42.128	478.4	425.3	1.6	-0.4	40778	-52.30	289	64	3.69	9.8
233700	-100.695	42.102	477.9	424.3	2.2	1.5	40766	-52.56	288	63	3.74	10.3
233800	-100.850	42.075	472.4	421.1	1.0	-0.8	40778	-53.05	288	58	3.71	10.1
233900	-101.005	42.048	475.5	420.2	1.8	-4.5	40766	-52 95	285	64	3.71	10.0

•CI
*ROLL

The Oklahoma thunderstorm statistics are at least typical for continental climates for all of the United States to the east. If each of these approximately eight cells per day areally averaged 10 km^2 and exhibited a stratospheric injection per cell of 20×10^{-4} g cm^{-2}, twice

Table 6. Aircraft Navigation, Meteorological, and Water Vapor Data--July 13-14, 1971, 2259-0025 UT.

TIME	POSITION		SPEED		PITCH	ROLL	ALT.	TEMP.	WIND		RADIATION	
	LONG	LAT	AIR	GRND					DIR	AMP	VOLT	WATER
GMT	DEG	DEG	KNOTS	KNOTS	DEG	DEG	FEET	DEG C	DEG	KNOTS		VAPOR
225900	-101.252	38.148	485.2	459.2	3.5	-0.5	39285	-50.12	253	29	3.75	10.5
230000	-101.407	38.152	453.5	429.2	3.4	0.8	40875	-50.54	247	27	3.57	8.6
230100	-101.562	38.160	460.4	438.2	2.6	1.6	40790	-52.22	244	27	3.61	9.0
230200	-101.715	38.165	463.8	444.3	1.5	0.6	40827	-53.03	239	25	3.60	8.9
230300	-101.872	38.173	470.4	448.2	2.0	0.5	40827	-53.01	246	26	3.65	9.4
230400	-102.030	38.182	467.5	442.1	2.6	0.7	41240	-53.05	248	27	3.54	8.3
230500	-102.182	38.187	462.4	439.2	2.1	0.1	41543	-53.15	247	26	3.53	8.2
230600	-102.337	38.195	466.8	441.2	2.4	0.9	41568	-53.41	252	26	3.55	8.4
230700	-102.495	38.198	464.3	438.2	2.5	0.1	41798	-55.67	255	30	3.47	7.7
230800	-102.647	38.208	454.2	430.2	3.3	2.2	42163	-56.14	243	28	3.53	8.2
230900	-102.797	38.218	450.0	428.2	2.6	-0.5	42296	-56.10	241	27	3.55	8.4
231000	-102.947	38.228	450.7	426.3	2.2	0.6	42357	-56.12	244	30	3.69	9.8
231100	-103.097	38.237	455.4	428.2	3.3	2.1	42260	-56.14	244	32	3.80	11.1
231200	-103.243	38.238	453.8	419.2	2.8	-13.9	42308	-56.16	235	37	4.10	15.9
231300	-103.382	38.193	455.5	416.2	2.9	0.2	42333	-56.20	234	40	4.30	19.9
231400	-103.515	38.143	455.5	417.2	2.5	-1.2	42296	-56.36	232	39	4.42	22.9
231500	-103.650	38.095	454.3	419.2	2.4	-1.2	42260	-57.08	237	37	4.08	15.6
231600	-103.783	38.048	455.6	419.2	2.4	-1.1	42296	-56.88	231	39	3.88	12.3
231700	-103.918	37.998	456.3	419.2	2.5	2.1	42284	-57.24	235	39	4.47	23.9
231800	-104.050	37.948	453.7	421.1	2.6	3.0	42248	-57.36	225	36	5.21	47.8
231900	-104.185	37.900	455.2	423.3	2.4	2.1	42260	-57.16	221	39	6.24	97.3•
232000	-104.320	37.852	447.2	421.1	2.6	3.0	42308	-55.89	215	33	6.10	89.2•
232100	-104.457	37.805	446.7	422.4	2.5	-2.2	42284	-55.83	197	39	7.34	171.5•
232200	-104.597	37.763	454.3	420.2	2.6	-0.8	42357	-55.89	220	37	6.80	131.8•
232300	-104.730	37.715	450.2	421.1	2.4	2.4	42296	-55.77	227	31	7.00	145.7•
232400	-104.863	37.665	456.8	428.2	2.1	0.5	42320	-55.69	214	36	7.13	155.4•
232500	-105.003	37.617	456.7	433.3	2.4	1.5	42320	-57.28	222	26	4.81	33.7•
232600	-105.138	37.568	458.4	434.3	3.0	1.3	42369	-57.20	220	28	3.57	8.6
232700	-105.277	37.517	461.1	436.3	2.0	-1.3	42320	-57.20	225	29	3.20	6.5
232800	-105.420	37.468	465.4	440.2	2.6	-0.5	42272	-57.18	218	30	3.10	6.3
232900	-105.558	37.418	467.1	438.2	2.5	0.4	42308	-57.18	224	33	3.04	6.3
233000	-105.698	37.368	464.6	437.2	2.1	1.0	42357	-57.26	230	29	3.09	6.3
233100	-105.840	37.318	468.6	439.2	1.4	0.8	42320	-57.28	235	31	3.13	6.4
233200	-105.987	37.295	462.8	449.2	2.1	21.1	42320	-57.30	233	18	3.17	6.4
233300	-106.103	37.370	461.3	464.3	2.2	2.6	42296	-57.22	219	20	3.25	6.6
233400	-106.200	37.478	461.6	465.3	1.6	-2.1	42333	-57.26	227	19	3.26	6.7
233500	-106.293	37.583	464.3	469.2	2.2	0.6	42260	-56.90	225	21	3.28	6.7

•CI

Table 6. Aircraft Navigation, Meteorological, and Water Vapor Data--July 13-14, 1971, 2259-0025 UT (continued)

TIME	POSITION		SPEED		PITCH	ROLL	ALT.	TEMP.	WIND		RADIATION	
	LONG	LAT	AIR	GRND					DIR	AMP	VOLT	WATER
GMT	DEG	DEG	KNOTS	KNOTS	DEG	DEG	FEET	DEG C	DEG	KNOTS		VAPOR
233600	-106.387	37.690	471.2	471.2	1.9	0.2	42272	-56.86	236	14	3.29	6 8
233700	-106.483	37.797	467.8	470.2	2.2	1.3	42320	-56.90	238	21	4 51	25.1
233800	-106.573	37.907	466.5	469.2	1.6	-0.2	42308	-56.88	234	22	3 32	6.9
233900	-106.665	38.013	466.7	469.2	1.6	0.1	42393	-56.86	230	23	3.31	6.8
234000	-106.755	38.125	471.2	472.2	1.4	4.9	42248	-56.88	239	22	3.17	6.4
234100	-106.828	38.245	465.1	472.2	1.7	-0.6	42333	-56.92	233	22	3.18	6.4
234200	-106.897	38.362	467.5	473.1	1.4	1.9	42296	-56.82	232	25	3.09	6.3
234300	-106.968	38.482	470.6	472.2	2.2	4.9	42296	-56.86	246	25	3.10	6.3
234400	-107.007	38.612	467.8	483.1	2.5	17.4	42284	-56.82	226	19	3.16	6.4
234500	-106.937	38.728	461.3	491.2	2.9	5.9	42296	-56.80	223	27	3.69	9 8
234600	-106.807	38.820	465.2	493.2	2.2	1.1	42296	-56.84	227	25	3.56	8 5
234700	-106.680	38.918	471.6	494.1	2.6	1.3	42308	-56.92	228	19	3.59	8.8
234800	-106.552	39.005	455.4	484.1	3.0	-2.6	42721	-60.71	220	27	3.55	8.4
234900	-106.420	39.093	461.7	485.3	3.1	4.8	42588	-57.94	224	24	3.51	8.1
235000	-106.272	39.165	457.7	483.1	3.0	0.2	42673	-57.42	226	26	3.48	7.8
235100	-106.125	39.232	455.0	481.2	2.4	2.1	42867	-57.50	231	25	3.46	7.7
235200	-105.973	39.300	456.1	485.3	1.6	-0.3	42745	-58.44	226	27	3.45	7.6
235300	-105.827	39.368	450.9	483.1	2.6	0.7	42830	-58.96	233	31	2.96	6.4
235400	-105.678	39.437	456.7	485.3	1.8	-2.0	42818	-58.92	235	29	2.92	6.5
235500	-105.523	39.503	454.0	479.2	2.5	2.3	43049	-58.88	227	26	3.07	6.3
235600	-105.380	39.573	449.8	482.2	2.3	1.8	43098	-59.12	235	31	3.06	6.3
235700	-105.228	39.640	450.4	484.1	2.3	1.5	43025	-59.89	242	31	3.06	6.3
235800	-105.070	39.707	455.9	492.2	2.0	2.1	42928	-60.35	245	37	3.05	6.3
235900	-104.918	39.773	451.2	491.2	2.1	-0.9	43000	-60.55	253	39	2.62	8.2
000000	-104.763	39.838	455.3	492.2	1.8	-1.9	42976	-59.93	25	37	-7.10	942.4•
000100	-104.603	39.902	456.7	495.4	3.4	-0.1	42964	-59.73	247	37	-3.04	344.0•
000200	-104.448	39.970	465.7	496.3	1.6	2.1	42915	-59.77	254	31	-5.75	710.4•
000300	-104.295	40.037	466.0	493.2	1.7	2.7	43000	-59.77	253	26	2.96	6.4
000400	-104.135	40.103	465.0	495.4	2.6	1.0	42940	-59.53	246	28	3.19	6.5
000500	-103.982	40.173	464.8	494.1	1.6	0.6	42940	-59.20	244	29	3.34	7.0
000600	-103.828	40.240	464.9	494.1	2.2	2.0	42952	-59.20	245	27	3.53	8.3
000700	-103.665	40.307	467.4	496.3	1.3	0.0	42915	-59.18	247	29	3.42	7.4
000800	-103.512	40.377	466.6	496.3	2.3	-1.4	42976	-59.37	248	27	3.43	7.5
000900	-103.357	40.443	463.1	496.3	2.6	0.5	42952	-59.14	249	33	3.43	7.5
001000	-103.198	40.512	467.5	497.3	2.1	0.7	42915	-59.18	252	28	3.37	7.2
001100	-103.040	40.582	466.3	496.3	2.4	-1.4	42964	-59.16	244	28	3 57	8.6
001200	-102.885	40.652	471.2	497.3	2.7	5.5	42891	-59.24	240	25	3.39	7.2
001300	-102.715	40.690	464.7	494.1	2.3	-1.2	42952	-59.18	236	32	3.64	9.2
001400	-102.533	40.705	468.1	495.4	1.9	1.0	42952	-59.18	239	29	3.63	9.2
001500	-102.353	40.718	467.3	496.3	2.4	1.2	42915	-59.16	243	30	3.63	9.2
001600	-102.175	40.732	465.6	494.1	2.1	-2.2	42988	-59.18	231	31	3.66	9.4
001700	-101.992	40.750	470.3	498.3	1.2	-0.4	42915	-59.18	235	29	3.65	9.4
001800	-101.815	40.765	468.6	497.3	2.5	0.8	42940	-59.12	246	29	3.57	8.6
001900	-101.635	40.773	466.0	495.4	1.1	10.0	43000	-59.16	238	33	3.94	13.2
002000	-101.463	40.735	465.9	485.3	1.4	14.9	42940	-59.10	243	38	2.92	6.6
002100	-101.362	40.630	466.6	464.3	2.4	16.8	42891	-59.18	249	47	2.82	6.9
002200	-101.350	40.507	464.9	447.3	2.0	0.7	42940	-59.18	251	43	3.56	8.5
002300	-101.370	40.382	460.8	449.2	3.3	1.0	42940	-59.14	263	42	3.56	8.5
002400	-101.388	40.260	449.7	438.2	3.5	1.6	43401	-59.73	254	31	3.51	8.1
002500	-101.408	40.138	451.1	436.3	3.1	1.6	43438	-60.73	254	37	3.44	7.5

•CI

Table 7. Summary of Data on Vertical Transport of Water Vapor by Thunderstorms

Date/Time* 1971	Cloud top	Tropopause	Flight altitude	Mean upstream water vapor	Mean downstream water vapor	Difference increase	Percentage increase
(UT)	(ft)	(ft)	(ft)	(g $cm^{-2} \times 10^{-4}$)	(g $cm^{-2} \times 10^{-4}$)	(g $cm^{-2} \times 10^{-4}$)	(%)
7/15 0047-0107	48,000	47,000	43,500	4.6	13.6	+ 9.0	195
7/15 0000-0116	48,000	47,000	40,700	20.1	27.4	+ 7.3	36
7/12 2150-2228	49,000	40,000	33,500	27.9	43.6	+15.7	56
7/12 2234-2259	49,000	40,000	40,000	11.5	14.6	+ 3.1	27
7/14 2233-2302	50,000	41,000	35,600	31.8	35.2	+ 3.4	11
7/14 2309-2339	46,000	41,000	40,700	10.2	14.6	+ 4.4	43
7/13-14 2311-2344	44,000	43,000	42,300	6.5	21.2	+14.7	226

* 7/15, 0000-0130 location: between latitudes 40°00' to 41°20' and longitudes 103°00' to 104°20'.
7/12, 2147-2310 location: between latitudes 42°40' to 44°10' and longitudes 91°30' to 93°20'.
7/12, 2147-2310 location: between latitudes 42°40' to 44°10' and longitudes 91°30' to 93°20'.
7/14, 2223-2331 location: between latitudes 42°00' to 43°30' and longitudes 96°00' to 100°00'.
7/13, 2259-0025 location: between latitudes 37°20' to 40°40' and longitudes 101°30' to 107°00'.

that of the drier Colorado thunderstorms, the cells can vertically transport 1.6×10^9 g of water vapor per day into the Oklahoma stratosphere. Since the annual variability in the number of thunderstorms ranges from one-half of the average to one and one-half times the average, we should strongly consider this variability when speculating on the effects of manmade additions of water vapor into the stratosphere.

The final life history of this injected water vapor remains a topic for further study because it may be swept out during the storm's dissipating stage. Thus, the residence time for the water vapor mass injection is not completely analyzed, but it appears that its residence time may not exceed 90 minutes. Higher altitude flights with a higher (radiance) resolution radiometer are required for a solution.

2. UPPER TROPOSPHERE OZONE AND CARBON DIOXIDE MEASUREMENTS IN THE VICINITY OF THUNDERSTORMS

2.1 Introduction

Ozone and carbon dioxide measurements were made aboard the NASA Ames Research Center Convair 990 (CV-990) aircraft from July 12 to 15, 1971, in conjunction with the NOAA Atmospheric Physics and Chemistry Laboratory's study of water vapor injection into the stratosphere by thunderstorms. Observations were made above 30,000-feet altitude in a triangular traverse of the country, with vertices of the triangle roughly bounded by San Francisco, Calif., Minneapolis-St. Paul, Minn., and Santa Fe, N. Mex.

There were three objectives for obtaining these measurements. First, to use the excellent tracer qualities of both ozone and carbon dioxide to study air circulation and mixing processes in the troposphere and low stratosphere. Measurements of these trace gases, together with aerosol data obtained simultaneously aboard the aircraft by W. E. Marlatt, were expected to yield information on upward mixing of near ground-level air in the vicinity of updrafts around thunderstorms and on downward mixing of stratospheric air across the tropopause. Because ozone concentrations generally increase markedly just above the tropopause, ozone measurements taken aboard aircraft can also serve to indicate whether the aircraft flight is within the troposphere or stratosphere at any time. Second, to correlate ozone, aerosol, and water vapor data obtained simultaneously to discern whether ozone is destroyed to any significant extent by aerosols or by water vapor in the upper troposphere through chemical or catalytic action. Water vapor measurements were made onboard the aircraft by P. M. Kuhn, using a radiometric technique. Third, to test a new atmospheric-constituents sampling system designed to function in aircraft to flight altitudes of 45,000 feet. The sampling system permitted air to flow continuously without contamination from the outside into the cabin of the aircraft where measurements on the air could be performed conveniently.

2.2 The Sampling System

A block diagram of the new atmospheric-constituents sampling system employed aboard the aircraft is shown in figure 14. Air from outside the boundary layer of the NASA CV-990 aircraft enters the cabin by means of an air-sampling probe mounted in a 65° aircraft port, located in the fuselage forward of the aircraft wings. Because ram pressure (even at speeds near 500 kt) is insufficient to force air from outside into the inside of the aircraft (e.g., against a pressure differential of about 600 mb at 44,000-ft altitude), we employed a vacuum-pressure diaphragm pump to force airflow into the desired direction. Air flows from the probe to the pump and then to the sampling manifold through a 7/16-inch I.D. hose lined with Teflon[4]. Excess air, not used for analyses, empties into the aircraft cabin through a flexible extension tube connected to the end of the sampling manifold.

The vacuum-pressure pump used was a Thomas Industries, Inc., series 726-CA-39 unit, operated by a $\frac{1}{4}$-hp split-phase motor drawing 6 amperes current at 110-V AC. Flow rate through the pump under normal conditions of temperature and pressure (20°C and 760-mm Hg) is about 100 l/min. As the air becomes rarified and as the back pressure on the pump increases during aircraft ascent in the atmosphere, the flow rate decreases progressively to a low value of about 5 l/min near the 44,000-foot flight altitude. All internal metal components of the pump that contact sampled air are coated with Teflon to insure that no ozone destruction occurs within the pump. The Buna-N rubber nylon-reinforced diaphragm of the pump is also covered with a thin sheet of adhesive-backed Teflon.

The sampling manifold shown in figure 14 is fabricated from a solid block of Teflon measuring 2 inches by 6 inches by 1 inch. It contains a $\frac{1}{2}$-inch-diameter chamber that runs throughout its length and is connected to three sampling ports from which air is drawn for analysis. An airflow gage is connected to a fourth sampling port. The gage provides a means of

---

[4]Teflon is a highly nonreactive polytetrafluoroethylene resin that does not destroy ozone after a minimal amount of conditioning with ozone.

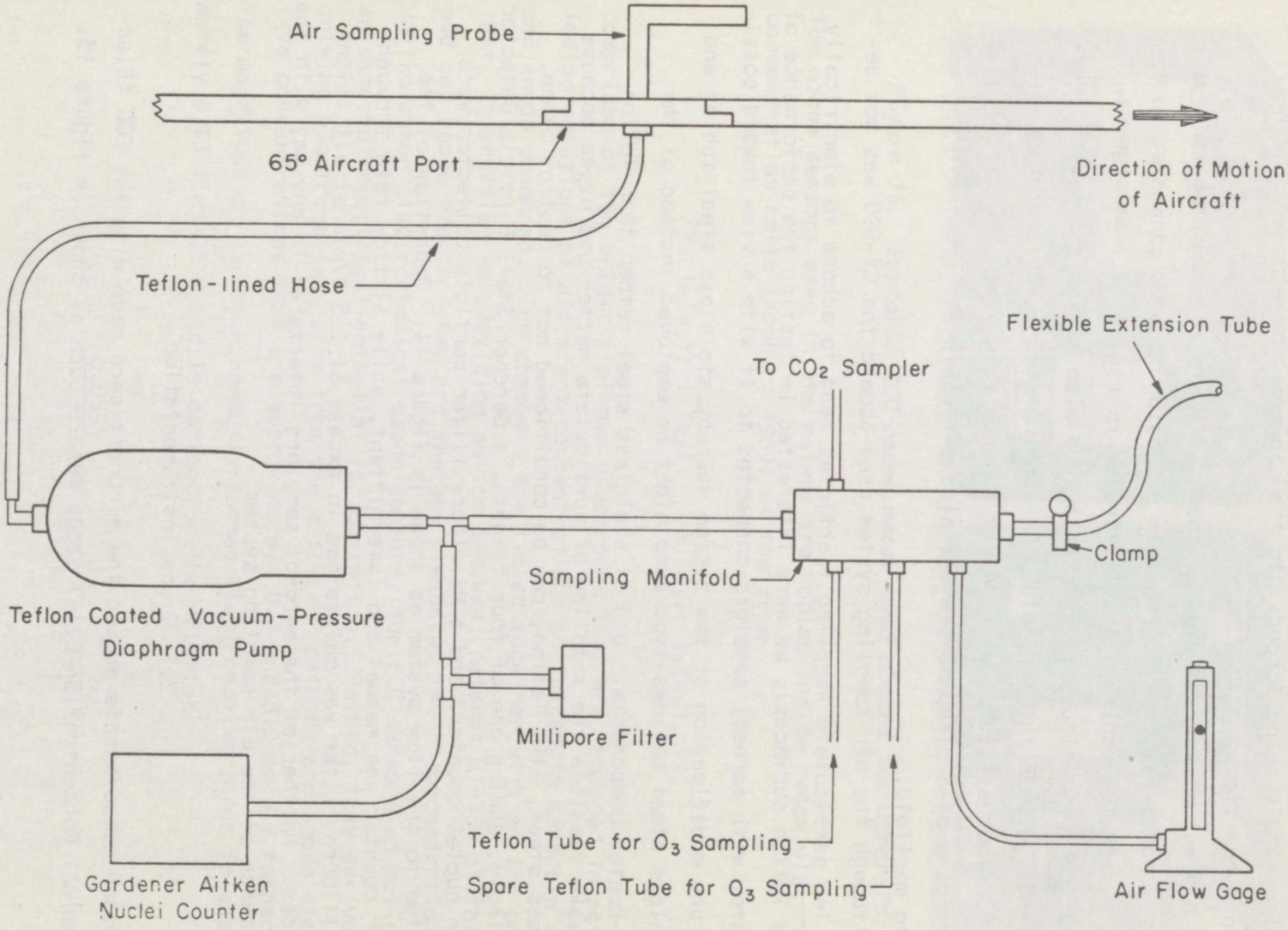

Figure 14. Block diagram of the atmospheric-constituents sampling system used aboard the NASA Convair 990.

verifying that the pump functions correctly and that a sufficient amount of outside air is being forced into the cabin of the aircraft under all operating conditions.

To prevent backward mixing of cabin air into the sampling manifold, a 3-foot long, 3/8-inch I.D. flexible extension tube is connected to the exhaust end of the manifold as illustrated in figure 14. At high airflow rates during low-altitude flight, this tube also serves to prevent pressure buildup within the manifold. As pumping efficiency decreases near the 40,000-foot altitude, we found it necessary to close the extension tube by means of a clamp to prevent aircraft cabin air from entering the sampling manifold.

Although the air sampling system used aboard the CV-990 was not designed for particulate sampling (particles tend to adhere to electrically charged Teflon surfaces), we were interested in testing the performance of the system with aerosol samplers connected to it with a view toward possible future modification of the system whereby stainless steel tubing and a stainless steel bellows-type pump might be employed instead of the Teflon-coated components. Use of stainless steel rather than Teflon might make feasible the sampling of particulate matter and ozone because stainless steel, like Teflon, can be conditioned not to destroy ozone. Accordingly, during one of four flights, a Gardner Small Particle Detector (Aitken nuclei counter) and a Millipore filter particle collector were connected to the flow system as shown in figure 14. Operation of the Gardner counter was manual and intermittent, while airflow rate through the Millipore filter was maintained in excess of 0.5 l/min at all flight altitudes. Neither of the aerosol samplers interfered in any way with the performance of the air sampling system.

2.3 Ozone Instrumentation

Ozone measurements aboard the aircraft were made with two ECC (Electrochemical Concentration Cell) ozone meters such as shown in figure 15.

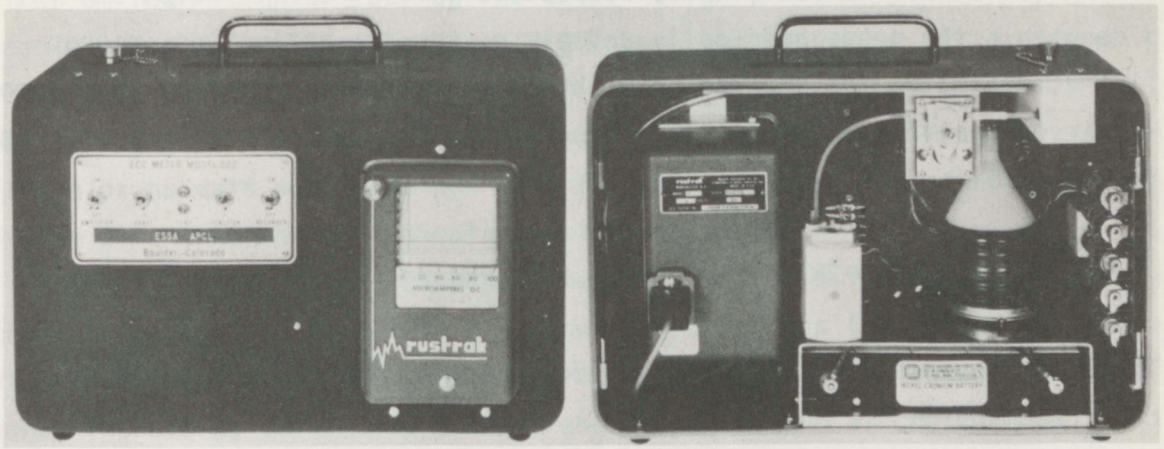

Figure 15. Portable ECC ozone meter used aboard the aircraft.

The ozone sensors used in the meters are iodine/iodide redox electrode concentration cells (Komhyr, 1969) of the type

$$Pt,\ I_2(a_1);\ I^-(a_2) \qquad I^-(a_3);\ I_2(a_4),\ Pt, \tag{2.1}$$

comprised of two bright platinum electrodes that are immersed in potassium iodide solutions of different concentrations contained in separate cathode and anode chambers. The chambers are linked together with an ion bridge that, in addition to providing an ion pathway, retards mixing of the cathode and anode electrolytes and thereby preserves their concentrations. Unlike other electrochemical ozone sensors, the ECC sensors do not require an external electrical potential for operation. Rather, they derive their driving electromotive force from the different cathode and anode electrolyte concentrations that are approximately 0.1 and 8.0 molal, respectively. The magnitude of the spontaneously formed electromotive force is approximately 0.13 V at 25°C and is defined by the relation

$$E = -\frac{0.0591}{2} \log \frac{(a_1)_{I_3^-}\,(a_3)^2_{I^-}}{(a_4)_{I_2}\,(a_2)^3_{I^-}}, \tag{2.2}$$

where a_1, a_2 are the activities, respectively, of the tri-iodide and iodide within the anode half-cell, and a_3, a_4 are the activities, respectively, of the iodide and iodine within the cathode half-cell. When ozone in air enters the sensor, I_2 is formed in the cathode half-cell according to the relation

$$2KI + O_3 + H_2O \rightarrow 2KOH + I_2 + O_2 \ . \qquad (2.3)$$

The cell converts the iodine to iodide in accordance with the overall cell reaction

$$3I^-(a_2) + I_2(a_4) \rightarrow I_3^-(a_1) + 2I^-(a_3), \qquad (2.4)$$

and the ozone concentration in the sampled air may be derived from

$$PPHMV(O_3) = 0.431 \frac{iT_r t}{P} \ , \qquad (2.5)$$

where $PPHMV(O_3)$ is the ozone concentration in parts per hundred million by volume, P is the ambient air pressure in mb, i is the sensor current due to ozone in microamperes, T_r is the temperature in ^oK of the environment in which the ozone meter is located, and t is the time in seconds taken by the ozone meter pump to force 100 ml of air through the sensor.

One of the two ozone meters used aboard the aircraft sampled ventilating air emanating from one of a number of air vents located within the cabin of the aircraft. By comparing the vent-air ozone readings with ozone measurements made in air that entered the aircraft directly through the flow system described above, we intended to obtain information on possible destruction of ozone within the aircraft's air conditioning system. The use of dual ozone-measuring instrumentation was a favorable circumstance resulting in acquisition of reliable ozone data for all flights that would not otherwise have been possible because inadvertent contamination of a portion of the airflow system occurred. The initial hookup of the flow system was slightly different from that shown in figure 14 in that the airflow meter was installed in front of the sampling manifold during the

first of four flights. During the second flight, we discovered that the needle valve of the flow gage was highly contaminated with oil, leading to contamination of the sampling manifold as well as to contamination of one of the two ozone sampling tubes shown in figure 14. Fortunately, reliable ozone data were obtained with the second ozone meter during most of the time that the contaminated system was in use.

The ECC ozone-meter response time is such that a 90-percent step change in ozone is indicated in 1 minute. Variations in the horizontal distribution of ozone that had a characteristic length of about 75 miles were, therefore, well measured from aboard the CV-990 aircraft whose cruising speed was about 450 knots. Changes in ozone concentrations were recorded by the meters over distances as short as 10 miles, although for such short paths the ozone profile fine-structure was not well resolved.

2.4 Carbon Dioxide Instrumentation

Carbon dioxide air samples were collected during three of four flights in 500-ml Pyrex glass flasks that had previously been evacuated to about 5-μm Hg pressure. The method of collecting an air sample for subsequent CO_2 analysis is as follows: The output tube of a pressure-vacuum Neptune Dyna-Pump, permanently coupled to the airflow sampling manifold, is connected to a stopcock at one end of the glass flask. This stepcock is then opened to allow air from the sampling manifold to fill the flask. A second stopcock, at the opposite end of the flask, is then opened, and air from the sampling manifold passes through the flask at a rate of about 3 l/min for about 1 minute. The air sample is finally confined in the flask by closing the stopcocks at the output and input ends of the flask, respectively.

The flask air samples were analyzed for carbon dioxide at Boulder, Colo., by means of a Mine Safety Appliance LIRA 200 nondispersive infrared gas analyzer. This instrument consists of a source of infrared radiation, an absorption (or sample) cell, a comparison (or reference) cell, and an infrared radiation detector. In measuring CO_2, the instrument

compares the attenuation of infrared radiation at 4.3 μm by CO_2 in the air sample with the attenuation of radiation by two CO_2 reference gases of known concentrations. The reference-gas concentrations are chosen to span the air sample CO_2 concentration which is then determined using a linear interpolation technique. The CO_2 reference gases are comprised of CO_2 in N_2 and were calibrated by C. D. Keeling at the Scripps Institute of Oceanography, La Jolla, Calif., to a precision of about $\pm$0.3 ppm by volume.

2.5 Interpretation of the Data

Ozone and carbon dioxide data obtained during flights 1 to 4 (July 12 to 15, 1971) are shown in figures 16, 18, 19, and 22. (No carbon dioxide data were collected during flight 1, July 12.) The ozone plots represent data averaged over 1-minute time intervals. Included in the plots, as a possible aid in interpretation of the results, are the aerosol data of Marlatt. Figures 17, 20, and 21 give ozone concentrations measured in the vicinity of three thunderstorms that were singled out for special study, namely, the La Crosse, Wis., O'Neill, Nebr., and Grover, Colo., storms.

In an initial analysis of the results, we included the water vapor data of Kuhn in the correlations. Because these data were not derived from in situ measurements in the vicinity of the aircraft but rather represented integrated values above flight altitude, no useful comparisons could be made between variations in water vapor amounts and variations in the concentrations of ozone, carbon dioxide, or aerosols. Water vapor data were, therefore, not included in the final plots.

2.5.1 Flight No. 1

The flight of July 12 originated in San Francisco, proceeded in a northeastward direction into northern South Dakota, and then southeastward to a storm area located in the vicinity of Rochester, Minn., and La Crosse (about 200 miles west of Lake Michigan). After making several circuits around an area of cumulus activity (the La Crosse storm), the aircraft headed for Denver, Colo.

National Weather Service radar observations at 1200Z on July 12 showed no echoes in the western United States, but revealed a storm area that stretched from the northeastern corner of Kansas, northeastward into Iowa, then northward into eastern Minnesota to the Canadian border. This storm area was associated with a cold front that moved slowly eastward.

The data for a portion of the flight, commencing about 100 miles west of Salt Lake City, Utah, are plotted in figure 16. The most striking aspect of the plots is the generally excellent correspondence between the broad highs and the lows in the ozone and aerosol values. Until about 2136Z, the aircraft flew outside the storm area at a flight altitude of 32,800 feet. Ozone amounts observed were typically tropospheric, ranging from 1.8 to 3.1 pphmv. The air was also relatively clean, with aerosol counts varying between 1,000 and 180 nuclei/cm^3. Upon entering the storm area and increasing the flight altitude by 1,000 feet, significant structure was observed in the ozone and aerosol horizontal profiles. The ozone and aerosol concentrations also increased to peak values of 4.0 pphmv and 3,000 nuclei/cm^3, respectively. At about 2225Z, while still in the vicinity of the La Crosse storm, the aircraft began a climb to 39,700 feet and later to 40,800 feet. Ozone and aerosol amounts then increased markedly to peak values of 7.2 pphmv and nearly 7,000 nuclei/cm^3, respectively. At 2320Z, the aircraft turned from the storm area and headed toward Denver. Ozone values quickly fell to 2.5 pphmv, even though the aircraft flight altitude was maintained at 40,800 feet. A more gradual decrease in aerosol counts was observed during this time.

It is of interest to examine the ozone and aerosol profiles in more detail. Figure 17 depicts ozone values measured along the La Crosse storm flight trajectory. Careful examination of the plot reveals that significantly lower than average ozone values generally occurred downwind from the storm. This is more readily seen from the plot in figure 16 where the downwind trajectory-flight times are indicated by three of four "half moons." (The first of the four half moons marks a time that the aircraft flew upwind, but along the edge of the cloud.) With regard to small-scale fluctuations in the aerosol profiles, no particularly striking correlations with changes in ozone are evident. At about 2150Z, for example,

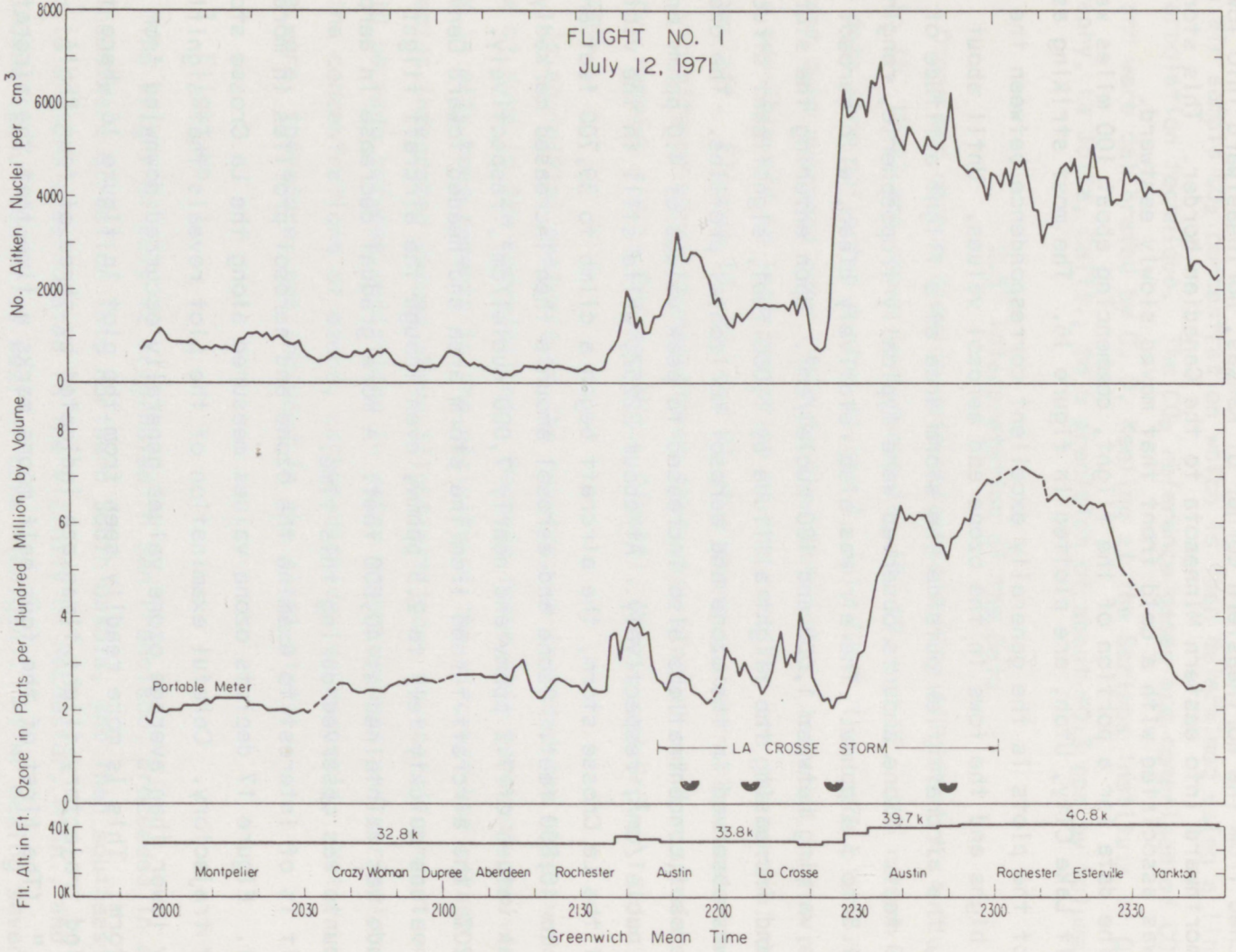

Figure 16. Plots of ozone and Aitken nuclei data measured during the flight of July 12, 1971.

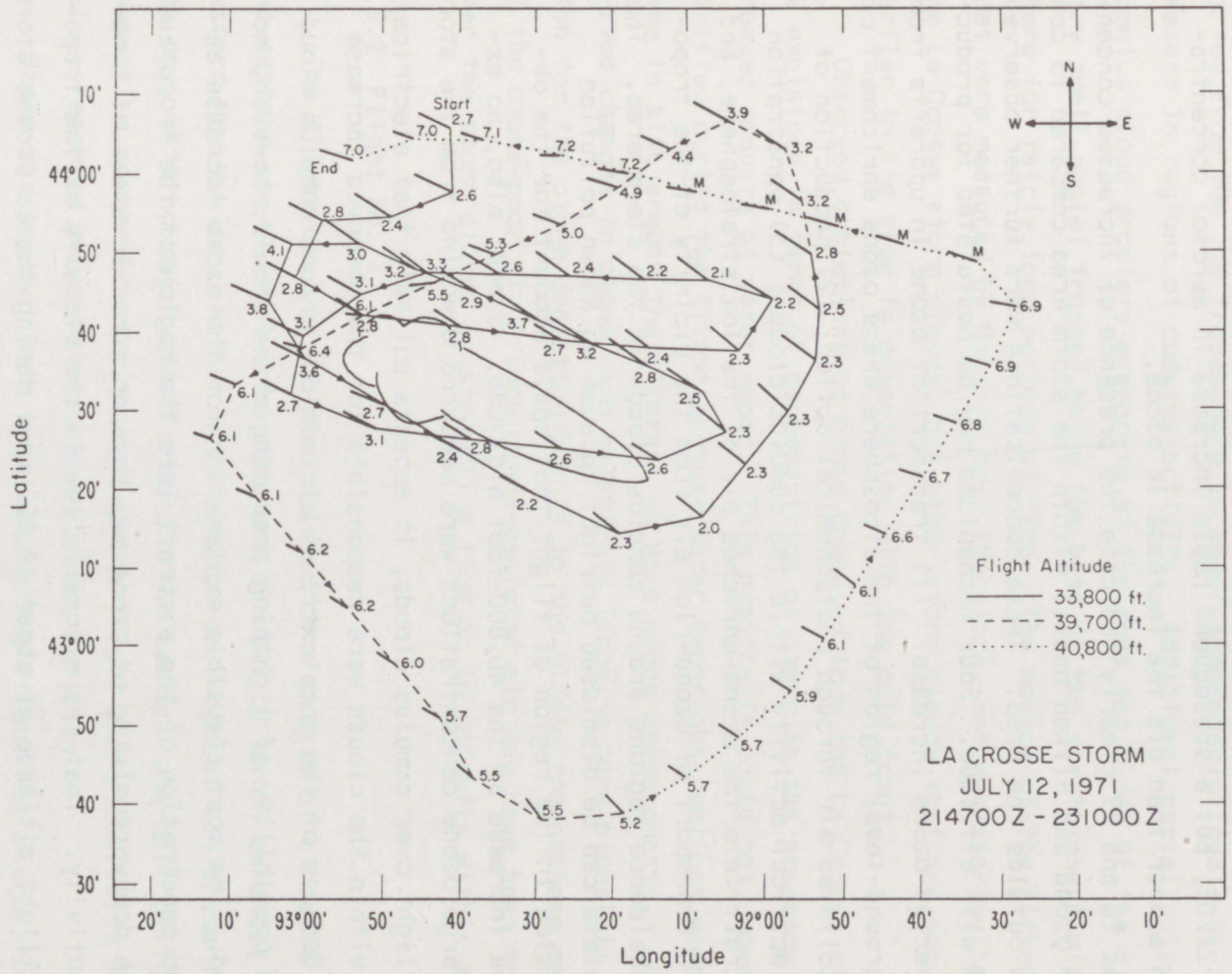

Figure 17. Ozone concentrations in pphmv along the flight trajectory around the La Crosse, Wis., storm. Values are given at intervals of one minute. Bars point into the direction of the wind, and the length of each bar denotes wind velocity (1 cm = 100 kt).

during flight along the upwind edge of the cloud, aerosol concentrations increased while ozone values decreased. Near 2210Z, when another dip in ozone values appeared, no significant change in aerosol concentrations was measured. Lows appeared in both the ozone and the aerosol profiles just after 2220Z, but a subsequent rapid increase in aerosol concentrations began sooner than did the increase in ozone.

Figures 16 and 17 clearly indicate the presence of increased concentrations of ozone and Aitken nuclei within the storm area compared to concentrations outside the area. These concentrations were further observed to increase with altitude. Four mechanisms may be postulated for producing the observed ozone increase: (1) transport of ozone in updrafts from some near ground-level region of the atmosphere where ozone enrichment occurred in polluted air through photochemical action; (2) production of ozone by electrical activity within the cumulus clouds; (3) penetration of the aircraft into the ozone-enriched air of the low stratosphere; and (4) downward transport of ozone-rich air from the vicinity of the tropopause in subsidence regions around cumulus clouds in the storm area. The first postulate can be dismissed outright because no known pollution sources existed in the region of flight that could account for the observed ozone increase at the 40,800-foot altitude. Since, also, no excessively large ozone concentrations were measured downwind from the storm or during flight over cumulus clouds, it appears unlikely that electrical discharges within the clouds were responsible for the observed increase in ozone. Because of the complexity of air motions around cumulus cloud storms, the possibility of lightning producing ozone should, however, not be dismissed. The most plausible explanation for the ozone increase appeared to be penetration of the aircraft into the region of the tropopause, across which downward mixing of ozone may have occurred in areas of cumulus cloud activity. That the aircraft flew in the vicinity of the tropopause at a flight altitude of about 40,000 feet during the La Crosse storm is verified by radiosonde observation (RAOB) data from St. Cloud, Minn., which located the tropopause at about 200 mb. The RAOB data from Denver indicated the tropopause at about 150 mb. This difference in tropopause

elevations probably accounted for the observed decrease in ozone measured at a constant flight altitude of 40,800 feet as the aircraft returned to Denver.

According to Marlatt, it is possible that Aitkin nuclei are transported from the low troposphere to upper atmospheric levels by updrafts present in regions of cumulus activity. Additional nuclei arise when cumulus cloud droplets evaporate at the tops and sides of the clouds. Very small nuclei trapped below the base of the stratosphere might remain there for fairly long periods of time. The source of the Aitken nuclei that were measured by Marlatt may, therefore, not necessarily have been the La Crosse storm clouds, but other storm clouds that had occurred earlier in the area in association with the cold front.

Observed depletions of ozone downwind from the La Crosse storm might be explained in terms of decomposition of ozone in the presence of increased amounts of water vapor. This hypothesis could not, however, be verified during the flight because water vapor observations were not made in situ around the aircraft as were ozone measurements. Because observed changes in ozone were relatively large, a more plausible explanation for the ozone depletion points to the middle troposphere as the source of the ozone-poor air. Such ozone-depleted air may have been transported over the storm clouds in streamline flow or in updrafts within the clouds.

2.5.2 Flight No. 2

The flight of July 13-14 consisted of a couple of circuits made over the eastern one-half of Colorado, one circuit of which extended into northwestern New Mexico. Rather weak cumulus development was present during the day, with no major storm areas in the western one-half of the country. However, a number of stations along the flight path, including Alamosa, Colo., reported thunderstorms and cumulus activity.

Ozone and aerosol data obtained during flight No. 2 are plotted in figure 18. Carbon dioxide measurements were made for the first time on this flight. These carbon dioxide concentrations are indicated in figure 18 by crosses.

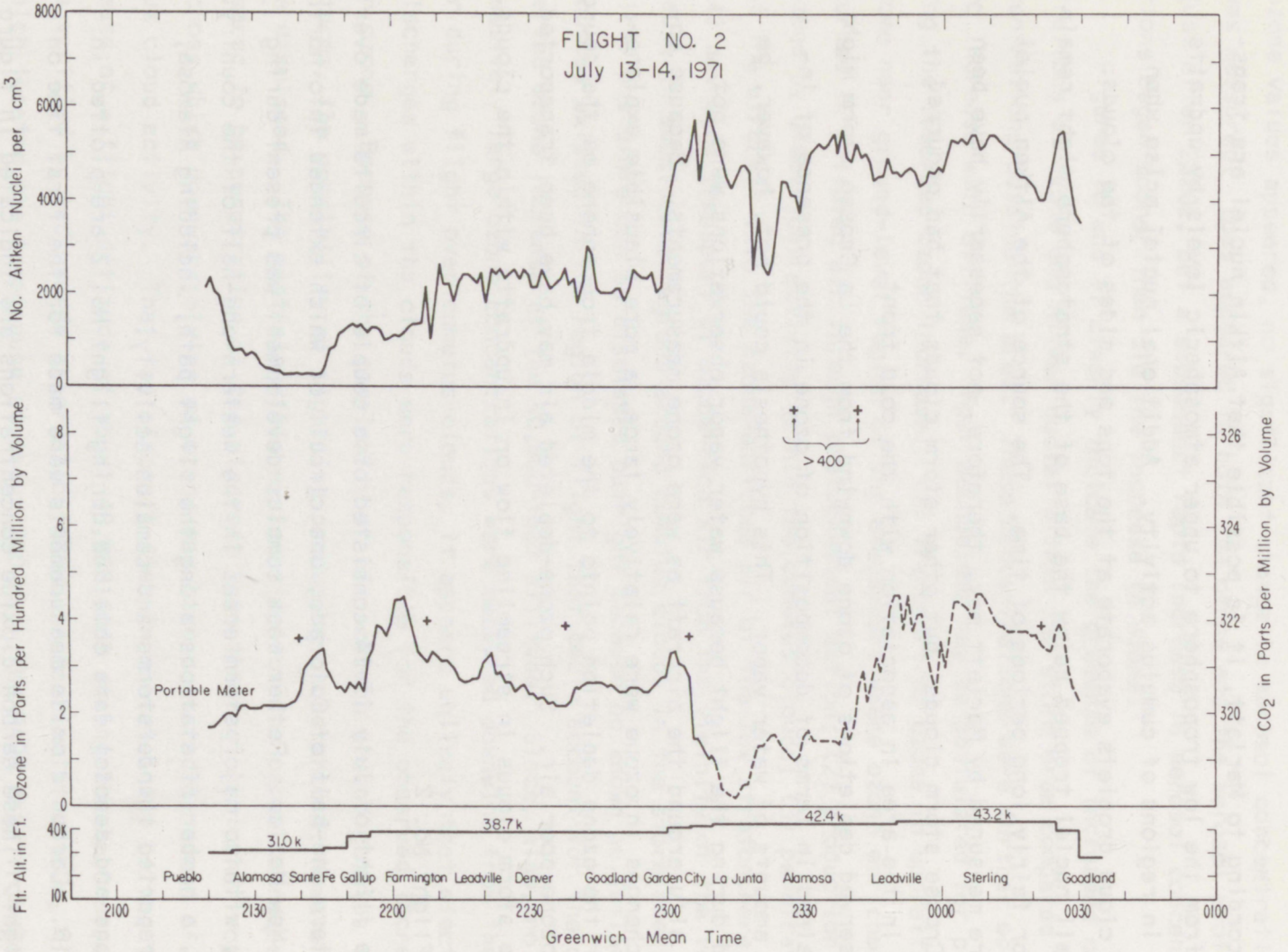

Figure 18. Plots of ozone, carbon dioxide, and Aitken nuclei data measured during the flight of July 13-14, 1971.

Examination of the ozone profile of figure 18 reveals no significant downward mixing of ozone from the ozone-rich low stratosphere. Whereas ozone concentrations at the 40,800-foot flight altitude exceeded 7.0 pphmv during the previous day, maximum ozone concentration measured only 4.5 pphmv during the July 13-14 flight even though the aircraft flew at a higher altitude (43,200 ft) during a portion of its trajectory. Flight altitude was at all times well below the tropopause which at Denver was located at about 120 mb. Interpretation of the aerosol data is more difficult. In general, aerosol concentrations measured during flight No. 2 were somewhat lower, but not greatly so, than they were at corresponding flight altitudes during flight No. 1 of the preceding day. Note that during both flights No. 1 and 2, air at about the 32,000-foot altitude was very clean (Aitken nuclei concentrations were approximately 250 nuclei/cm^3), but the concentration of aerosols increased with height to about the 40,000-foot altitude. It is difficult to postulate a source for the Aitken nuclei in the 32,000- to 40,000-foot atmospheric layer. One possible source may be that very small nuclei, having a long residence time, were injected into the upper troposphere by highly convective cumulus clouds at some earlier time. Another source for the nuclei may have been a forest fire that raged over several thousand acres in the Red Feather Lakes region of northern Colorado. Neither speculation, however, appears entirely satisfactory.

Of considerable interest are the carbon dioxide concentrations measured during flight No. 2; these concentrations were lower by about 2.5 ppmv than the values measured during flights on the following 2 days. Using the average CO_2 data of Bolin and Keeling (1963) and assuming a mean global rate of increase in CO_2 of 0.8 ppmv per year since 1960 (based on the Mauna Loa Observatory, Hawaii, record), we estimate that the average upper troposphere CO_2 concentration over Colorado in July 1971 was approximately 324.5 ppmv. Actual measured values during flight No. 2 were 321.8 ± 0.1 ppmv where the indicated error is the mean deviation of the measurements. (Two samples that yielded extremely high values were not considered in deriving this result.) Bolin and Keeling have also shown that a very strong latitudinal gradient in CO_2 exists during the month of July, that is, CO_2 concentrations decrease by about 6 ppmv in the

latitudinal direction of 20° to 70°N. A possible explanation, therefore, for the low CO_2 values measured during flight No. 2 is that the air mass in which the aircraft flew during July 13 originated in northern latitudes. This hypothesis, however, is not substantiated by applicable meteorological charts which indicate that a generally southerly airflow prevailed at 200 mb over Colorado. Because near ground-level air in the latitude of Colorado during the time of rapid plant growth is depleted of CO_2 relative to its concentration in upper troposphere air, the possibility should not be overlooked that the air in the upper troposphere over Colorado on July 13 originated at low levels in the middle latitudes. Kelly (1969) measured a 2-ppmv difference in CO_2 concentrations in air between the west coast and Denver at a 500-mb flight level.

One puzzling feature of the ozone plot in figure 18 is the ozone low that occurred after 2305Z. Two CO_2 samples taken during the period of the low yielded CO_2 concentrations in excess of 400 ppmv. At about the time that the ozone decrease started, the turbo-assist unit of the aircraft was activated to augment the flow of ventilating air through the aircraft cabin. Because the turbo-assist unit may introduce some contamination into the air conditioning system of the aircraft, we adopted the procedure throughout all flights to discontinue sampling ozone in the aircraft ventilating air once the turbo-assist unit was activated. Ozone data plotted in figure 18, following 2310Z (dashed curve), were, therefore, obtained from measurements in air coming directly from outside the aircraft through the air sampling system. The plotted values have been corrected for the flow system contamination described earlier. Now, activation of the turbo-assist unit occurred during other flights, yet, at those times, no deep ozone lows were observed. Note that almost complete depletion of ozone occurred at 2315Z. Surprisingly, also, the two CO_2 samples obtained at the time of the ozone low yielded much higher CO_2 concentrations than was the case with the four samples taken before that time and with the one sample taken later, all of which exhibited a scatter of only $\pm$ 0.2 ppmv in CO_2 concentration. Because some cirrus clouds were present in the vicinity of the ozone low, it was speculated that

this region of the atmosphere may have been contaminated by military or commercial aircraft passing through at some earlier time.

2.5.3 Flight No. 3

The flight of July 14-15 proceeded from Denver to northeastern Nebraska where a circuit was made around the O'Neill storm. The aircraft then returned to northeastern Colorado where it flew several times around an area of rather intensive cumulus activity (the Grover storm) near Sterling.

The plots in figure 19 show two ozone profiles--one obtained with a portable ozone meter and the second obtained with a panel ozone meter. The higher meter readings are the correct ones; the panel meter values have been plotted simply to illustrate the effect of contamination upon the air sampling system discussed earlier. Note that in spite of the contamination, the variations in the ozone profiles given by the two meters are very similar.

Fifteen samples of carbon dioxide were obtained on this day. The mean CO_2 concentration was found to be 324.7 $\pm$ 0.2 ppmv where the indicated error is the mean deviation of the measurements. As pointed out in the preceding subsection, 2.5.2, this concentration is about what might be expected in the upper troposphere over Colorado during the month of July, based on the data of Bolin and Keeling. It was also 2.9 ppmv greater than that measured during the previous day's flight. The difference in concentrations was undoubtedly related to a difference in air masses in which the aircraft flew on both days. During flight No. 3, the aircraft's flight path was in a region of high pressure located northeast of a cold front that stretched from northwest to southeast over Colorado. During the previous day, the aircraft flight trajectory was more or less south of the cold front.

Although large variations occur in the ozone profiles plotted in figure 19, there exists no clear-cut evidence that significant downward mixing of ozone, from the region of the tropopause, occurred in the areas of the O'Neill and Grover storms. Some slight mixing from above may be

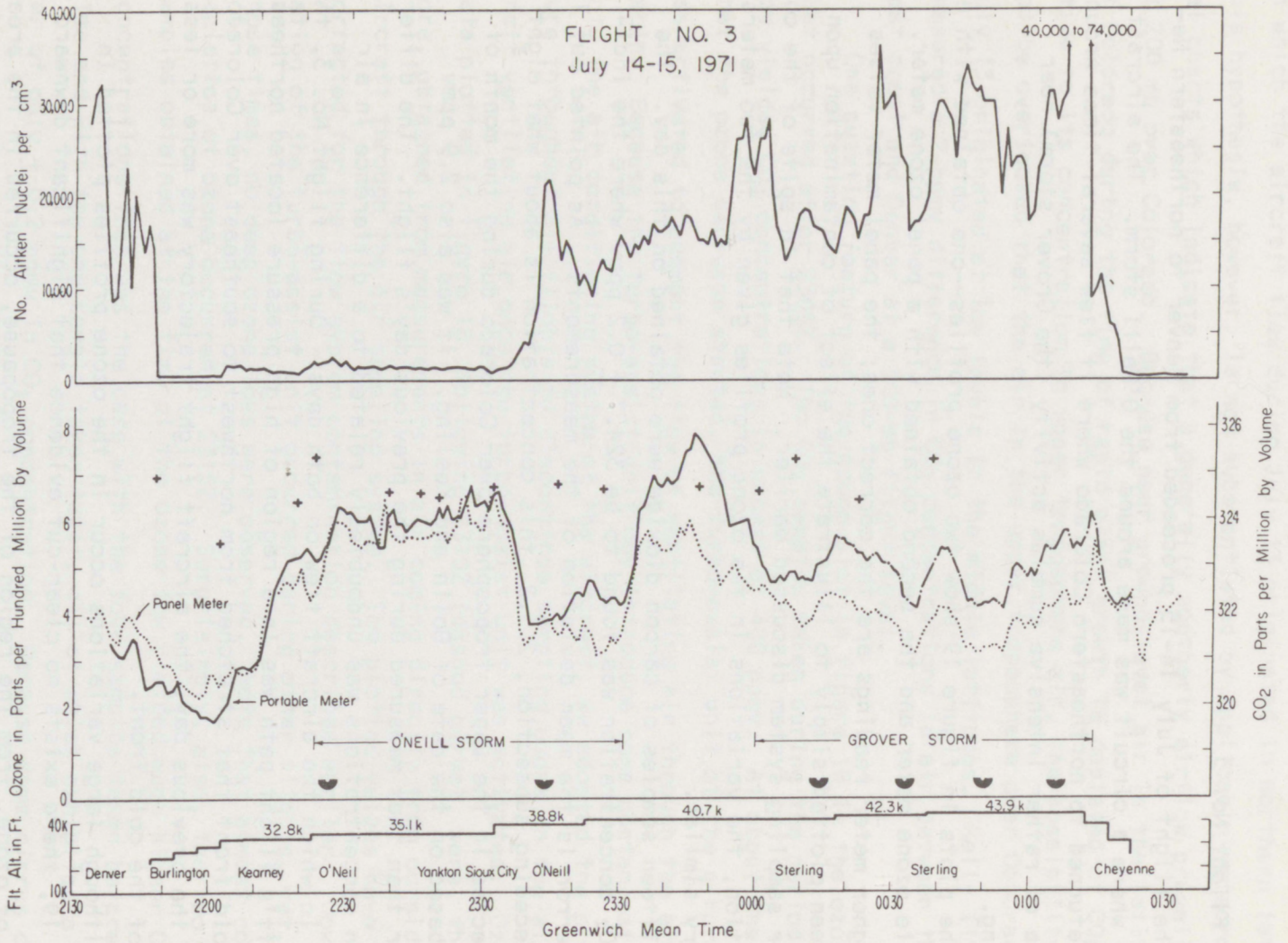

Figure 19. Plots of ozone, carbon dioxide, and Aitken nuclei data measured during the flight of July 14-15, 1971.

inferred from the scatter in the individual CO_2 measurements if the value of 325.3 ppmv is interpreted as representative of the upper troposphere while the value of about 324.6 ppmv is interpreted as representative of upper troposphere air mixed with stratospheric air. (During July in mid-latitudes, stratospheric CO_2 concentrations are several ppmv lower than average upper troposphere values.) Examination of the ozone values around the flight trajectories of the O'Neill and Grover storms (figs. 20 and 21) and also of the ozone profiles in figure 19 where the flight paths downwind from the storm are marked by half moons indicates further, as in flight No. 1, that ozone lows generally occurred over the storm clouds or downwind from them. As stated in the discussion of the flight No. 1 data, the significance of the lows has not been resolved. Interpretation of the phenomenon will have to await future measurements with more diverse instrumentation than was used during the July 1971 series of flights.

The aerosol data of flight No. 3 present a particular dilemma in that very high concentrations were measured (up to 74,000 nuclei/cm^3) as compared to concentrations observed during the other three flights (7,000 nuclei/cm^3 maximum). Marlatt has suggested that the source of the nuclei may have been the Red Feather Lakes forest fire, located about 150 miles west of the Grover storm.

During flight No. 3, P. A. Allee made spot measurements of Aitken nuclei simultaneously with Marlatt's aerosol observations, using a Gardner Small Particle Detector connected to the airflow system described earlier in subsection 2.2. Allee's values were completely different from those of Marlatt. For example, at 40,700-foot altitude, Marlatt measured 25,000 nuclei/cm^3 while Allee measured 770 nuclei/cm^3; at 43,400-foot altitude, Marlatt measured nearly 30,000 nuclei/cm^3 while Allee measured 410 nuclei/cm^3. The possibility was raised that a leak was present in Marlatt's instrumentation which operates at outside air pressure rather than at aircraft cabin air pressure. Nuclei from within the cabin of the aircraft leaking into the instrument would then contaminate samples of outside air in which aerosol measurements were made, giving rise to the high readings observed by Marlatt. This argument is difficult to substantiate because aerosol counts measured with the same equipment did not

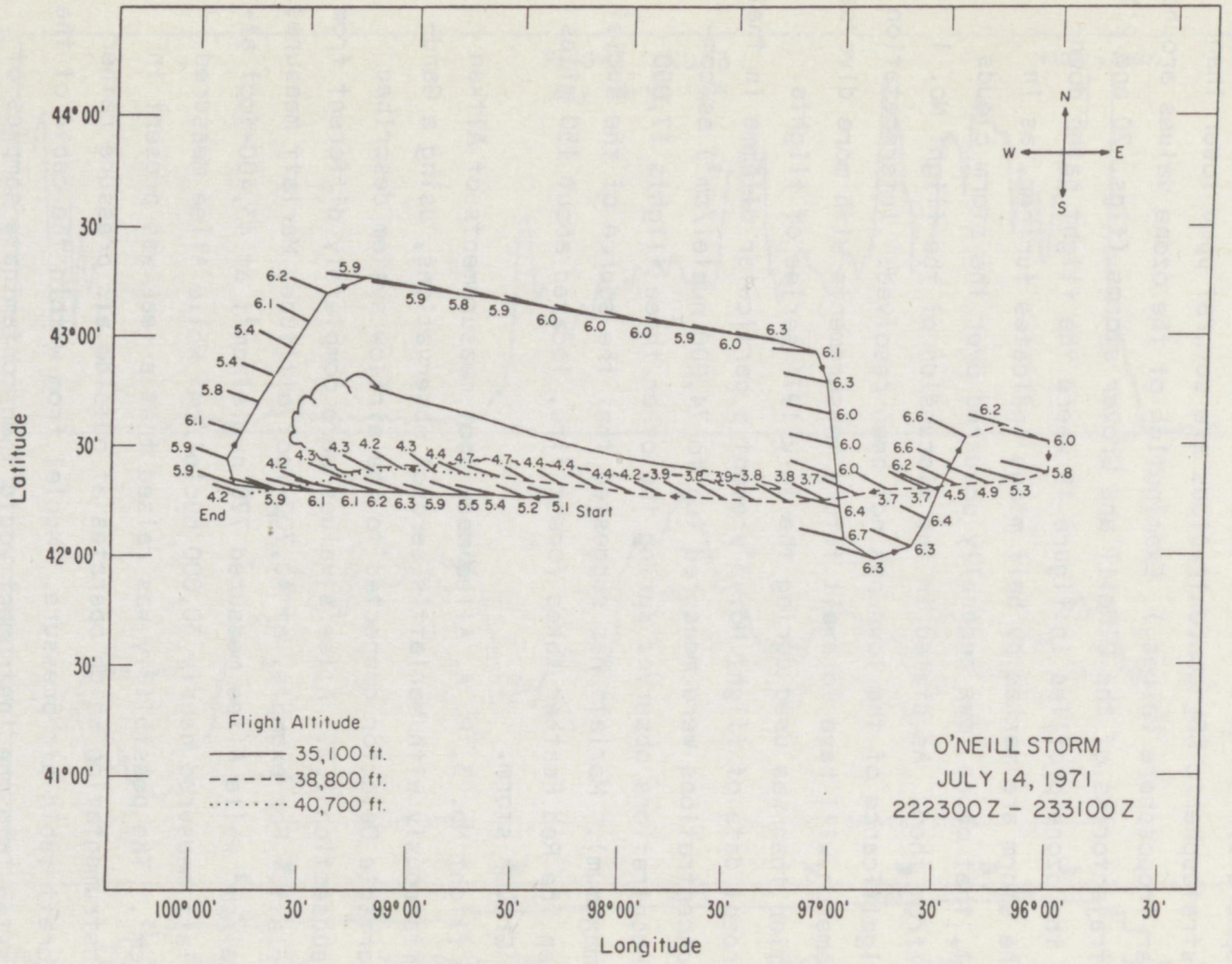

Figure 20. Ozone concentrations in pphmv along the flight trajectory of the O'Neill, Nebr., storm. Values are given at intervals of one minute. Bars point into the direction of the wind, and the length of each bar denotes wind velocity (1 cm = 100 kt).

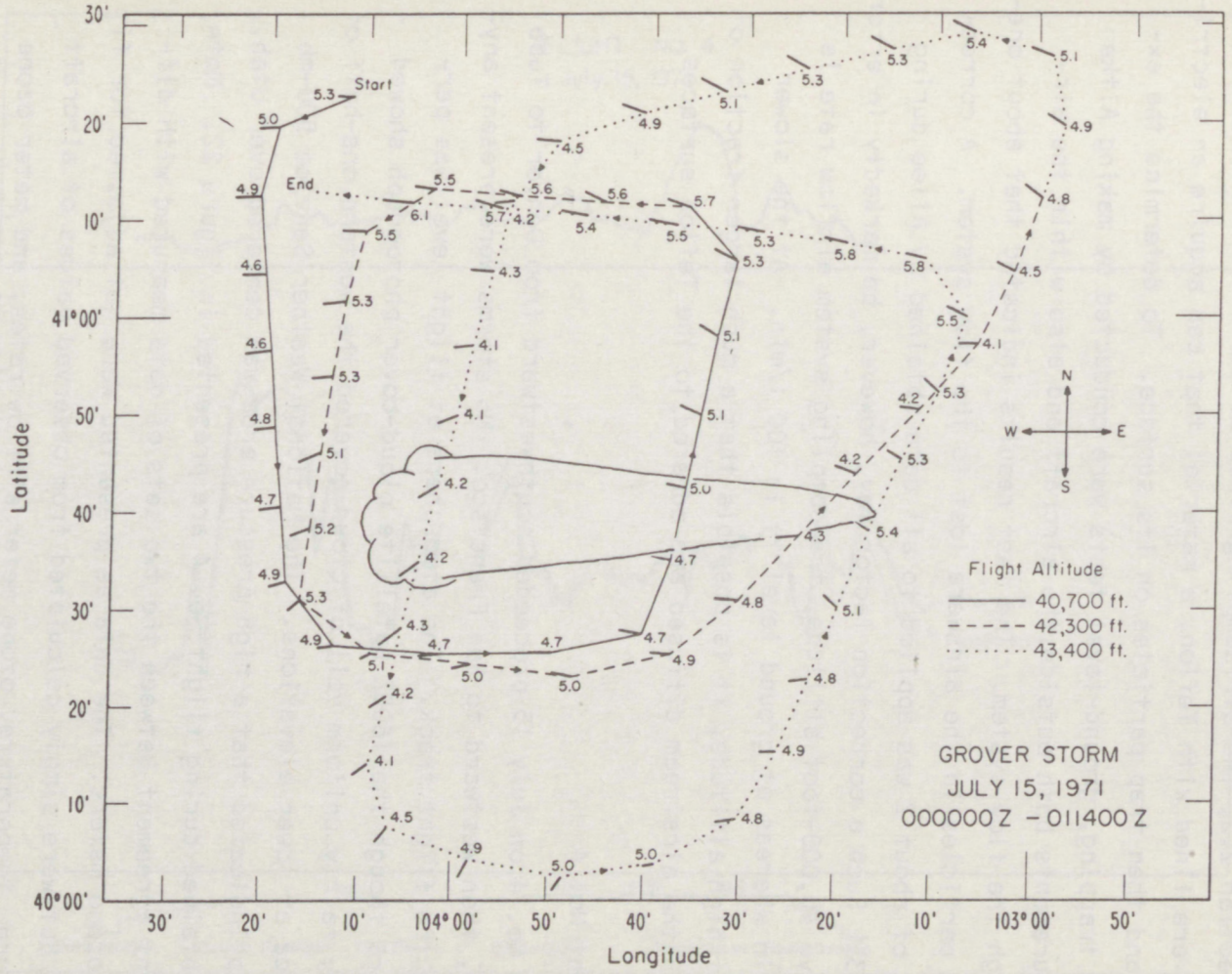

Figure 21. Ozone concentrations in pphmv along the flight trajectory around the Grover, Colo., storm. Values are given at intervals of one minute. Bars point into the direction of the wind, and the length of each bar denotes wind velocity (1 cm = 100 kt).

exceed 1,500 nuclei/cm^3 during the next day's flight, as will be shown later. The possibility exists that somehow the leak failed to occur the next day. The data of Allee are also subject to question. As was pointed out in subsection 2.2, the air sampling lines as well as the pump of the flow system are lined with Teflon, a material that can acquire an electrical charge and then trap particles on its surface. To determine the extent of the trapping, ground-level tests were conducted by making Aitken nuclei measurements both outside the aircraft and also within the aircraft through the flow system. The test results indicated that about one-half of the particles in the air were lost to the flow system. A correction factor of about 2 was applied to all data obtained by Allee during flight No. 3. Such a correction factor may, however, be markedly in error because above 40,000-foot altitude, the sampling system airflow rate is about 5 l/min whereas at ground level it is 100 l/min. At the slower flow rate at high altitude, it is possible that a much larger fraction of particles in the airstream diffused and adhered to the Teflon surfaces.

2.5.4 Flight No. 4

Flight No. 4 on July 15 proceeded southwestward from Denver to Tuba City, Ariz., then westward to San Francisco. No storms were present anywhere along the flight track. The atmosphere at flight level was perfectly clear, though the 1600Z satellite cloud-cover photograph showed that a thin, fairly uniform veil of cloud covered the western one-half of North America at lower elevations. The National Weather Service 500-mb analysis map indicated that a high pressure area was centered over Utah.

Data obtained during flight No. 4 are presented in figure 22. Note the excellent agreement between the two sets of data measured with different ECC ozone meters. The data as presented were not adjusted for fit in any way, but were simply calculated from observed values of aircraft cabin pressure, temperature, ozone meter airflow rates, and meter ozone currents in accordance with equation (2.5) given previously in subsection 2.3. Both meters sampled air from the specially designed air sampling system (which by this time had been decontaminated) during most of the

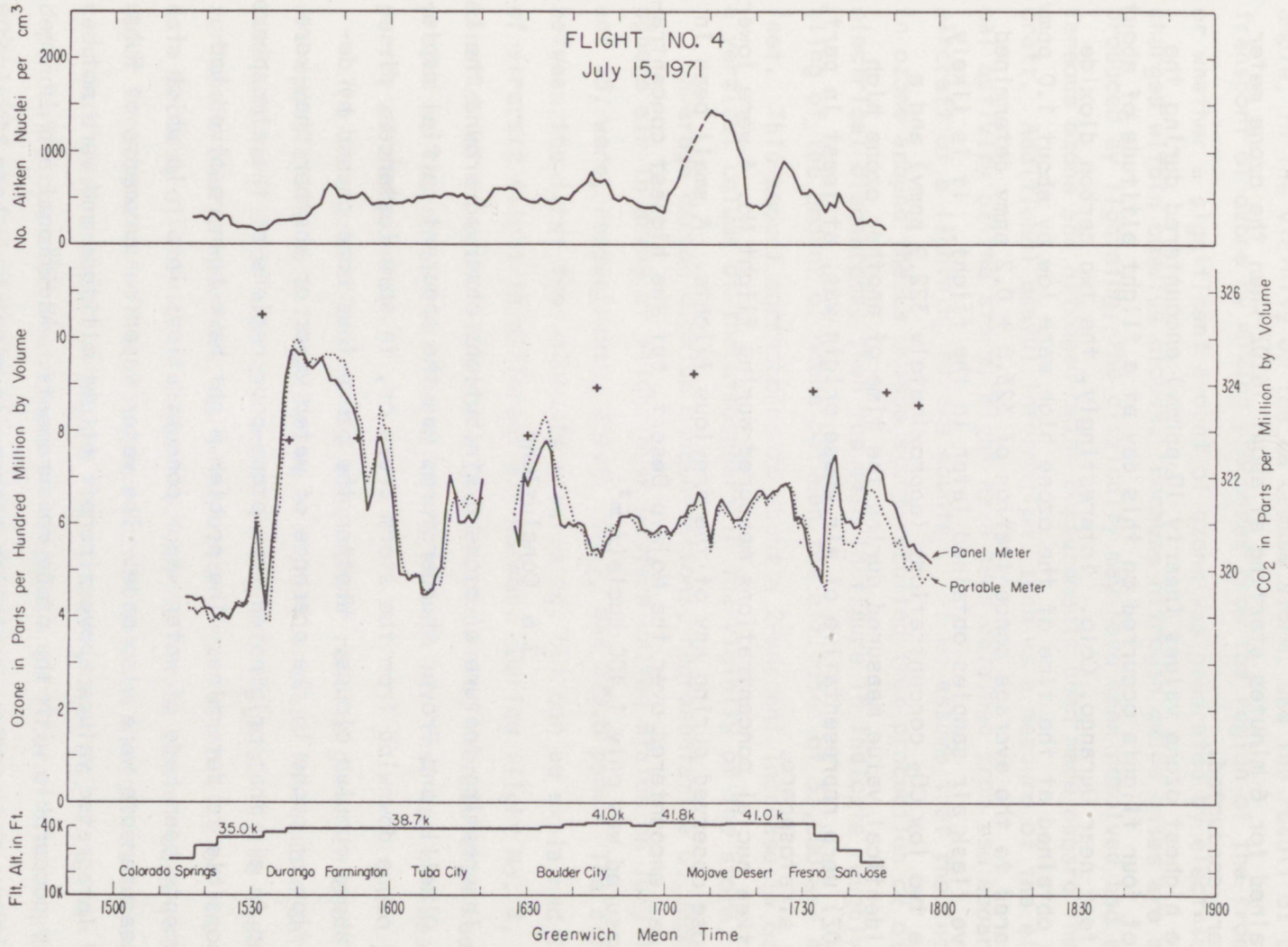

Figure 22. Plots of ozone, carbon dioxide, and Aitken nuclei data measured during the flight of July 15, 1971.

flight, except from about 1607Z to 1639Z when the portable meter sampled air from one of the vents in the cabin of the aircraft. Ozone data were not obtained for 6 minutes starting at about 1620Z when the ozone meter tests were conducted.

The highest ozone values (nearly 10 pphmv) encountered during the series of four flights occurred on this day at a flight altitude of about 38,000 feet near Durango, Colo. Interestingly, the two carbon dioxide samples obtained at the time of the ozone high were low by about 1.0 ppmv as compared to the average concentration of 323.8 $\pm$ 0.2 ppmv determined from five flask air samples obtained later in the flight. It is likely that the two low CO_2 concentrations (approximately 322.9 ppmv) and a nearly identical value measured during the time of another ozone high (at 1630Z) were representative of air whose origin was, at least in part, the low stratosphere.

Aitken nuclei concentrations measured during flight No. 4 were lower than those observed during any of the previous flights. A small peak in nuclei was encountered over the Mojave Desert, but the highest concentration measured was only 1,400 nuclei/cm^3.

2.6 Conclusions

An interesting feature of ozone distributions observed around the La Crosse, O'Neill, and Grover thunderstorms was the apparent partial depletion of ozone downwind from the storm areas or, in some instances, directly above cumulus clouds. Whether the ozone lows were caused by decomposition of ozone in the presence of water vapor or whether they were measured in air that originated from ozone-poor regions of the atmosphere was impossible to determine. The problem might have been resolved had measurements been made of water vapor concentrations in air in which ozone measurements were also made. The water vapor measurements of Kuhn yielded integrated values above aircraft flight altitude and were not directly comparable with the ozone measurements. Additional aid in interpretation of the ozone depletion phenomenon might have been obtained from vertical-distribution ozone data had such data been available. Unfortunately, no ozonesondes were flown in the storm areas.

It is difficult to know whether the observed ozone increase, for example, in the vicinity of the La Crosse storm, was the result of downward transport of ozone by mixing processes from the region of the tropopause or whether a significant amount of ozone was generated by electrical discharges within cumulus clouds. Because nitrogen oxide gases are also produced by lightning, the difficulty may have been resolved had simultaneous ozone and nitrogen oxide measurements been made aboard the aircraft. Additional useful information, such as a measure of the electrical activity of the storm, might have been obtained from use aboard the aircraft of a lightning stroke counter. If we assume that the increase in ozone around the La Crosse storm resulted from production of ozone by electrical discharges, then the data in figure 16 indicate roughly a doubling of the amount of ozone between the altitudes of 33,000 and 41,000 feet. This amount corresponds to about a 2-percent increase in ozone in a vertical column of the atmosphere in the vicinity of the storm.

Average carbon dioxide concentrations, representative of upper troposphere air in areas of flight over western United States on July 13, 14, and 15, were, respectively, 321.8, 324.7, and 323.8 ppmv. The difference between the first two values is surprising, but can be explained in terms of aircraft flight in different air masses. During flight No. 4, a combination of an ozone high and a CO_2 low occurring over Durango was interpreted as the passage of the aircraft through air that was at least partly stratospheric.

The interpretations of the measurement results given in section 2 are speculative to a large degree primarily because inadequate data of complementary kinds were collected during the flights. It is also unfortunate that a question has arisen about the reliability of the aerosol data because of the large concentrations of Aitken nuclei observed in the upper troposphere. This situation points out the usefulness of employing redundant instrumentation aboard the aircraft, that is, more than one independently operated instrument to measure a particular atmospheric property. Had we not used two ECC meters to measure ozone, for example, the contamination problem that occurred may not have been recognized, and the ozone data obtained would have been considerably less reliable.

The flights of July 12 to 15, 1971, on board the NASA Ames Research Center CV-990 aircraft afforded an opportunity to test a newly developed air sampling system suitable for use to flight altitudes of 45,000 feet. The system conducts uncontaminated air from the outside into the cabin of the aircraft where various kinds of analysis can be performed on the air at convenient operating conditions. Airflow rate through the system is about 100 l/min near ground level, decreasing to about 5 l/min at a flight altitude of 44,000 feet. It is likely that the airflow rate at high altitudes can be doubled with minor modification of the pump. Further, it may be possible to build a similar air sampling system using a stainless steel bellows pump and stainless steel tubing rather than Teflon-coated components. The modified system might then be suitable for measurements of gaseous atmospheric constituents and aerosols.

An attempt was made during the flights to determine the extent to which atmospheric ozone is destroyed within the air conditioning system of the CV-990. Two ECC meters were used to get the required information: one sampled ozone in air brought directly into the aircraft through a specially designed air sampling system; the other sampled ventilating air emanating from one of several air vents present in the aircraft cabin. Unfortunately, a precise result for the amount of ozone destruction was not obtained because of an inadvertent contamination problem. Comparison data obtained during flight No. 4, however, as well as similar data obtained during earlier flights at low altitudes when airflow rates through the air sampling system were large enough to minimize the contamination problem indicate that less than 10-percent ozone destruction occurred within the ventilation system of the CV-990 aircraft.

3. AITKEN AND ICE NUCLEI CONCENTRATION OBSERVATIONS AROUND THUNDERSTORMS

Air from the air intake manifold, described by Komhyr and Harris in section 2, was sampled with a Gardner Small Particle Detector to determine the Aitken nuclei concentration during the NASA CV-990 flight No. 3 of July 14-15, 1971. The data have been corrected for air intake attenuation, detector altitude correction, and ambient atmospheric pressure and temperature at flight altitude. Figure 23 shows the corrected Aitken nuclei concentration, pressure altitude, and time for each observation during the flight. Figure 24 is the altitude profile of the Aitken nuclei concentration of flight No. 3 and the temperature profile measured by a Rosemont temperature probe.

Junge (1961a, 1961b) made seven balloon-borne Aitken-nuclei-concentration profiles in the same general area of the Great Plains during anticyclonic conditions. Data obtained on NASA CV-990 flight No. 3, flown in the same type of anticyclonic condition, are in good agreement with the measurements of Junge. Figure 23 shows variation of Aitken nuclei concentration with time along portions of the flight path that were at constant pressure altitude because of the penetration of air parcels with differing histories and trajectories. The Aitken nuclei concentration and temperature profiles in figure 24 are smoother than one of Junge's individual flight profiles as the result of averaging the Aitken nuclei concentrations and temperatures obtained within each 0.5-km altitude interval. Individual profiles of the seven Junge flights can be selected to show Aitken nuclei concentrations that are either greater or less than the Aitken nuclei concentration obtained on NASA CV-990 flight No. 3 at a comparable altitude.

Membrane-filter air samples to determine the ice nuclei concentration were taken by Gerhard Langer, National Center for Atmospheric Research, Boulder, from the intake manifold used by Komhyr and Harris. A special filter holder, only partially exposing the filter to the sample air, was used; an annular area served as a blank reference. Results are tabulated in table 8. The first filter was used to check the flow system and was

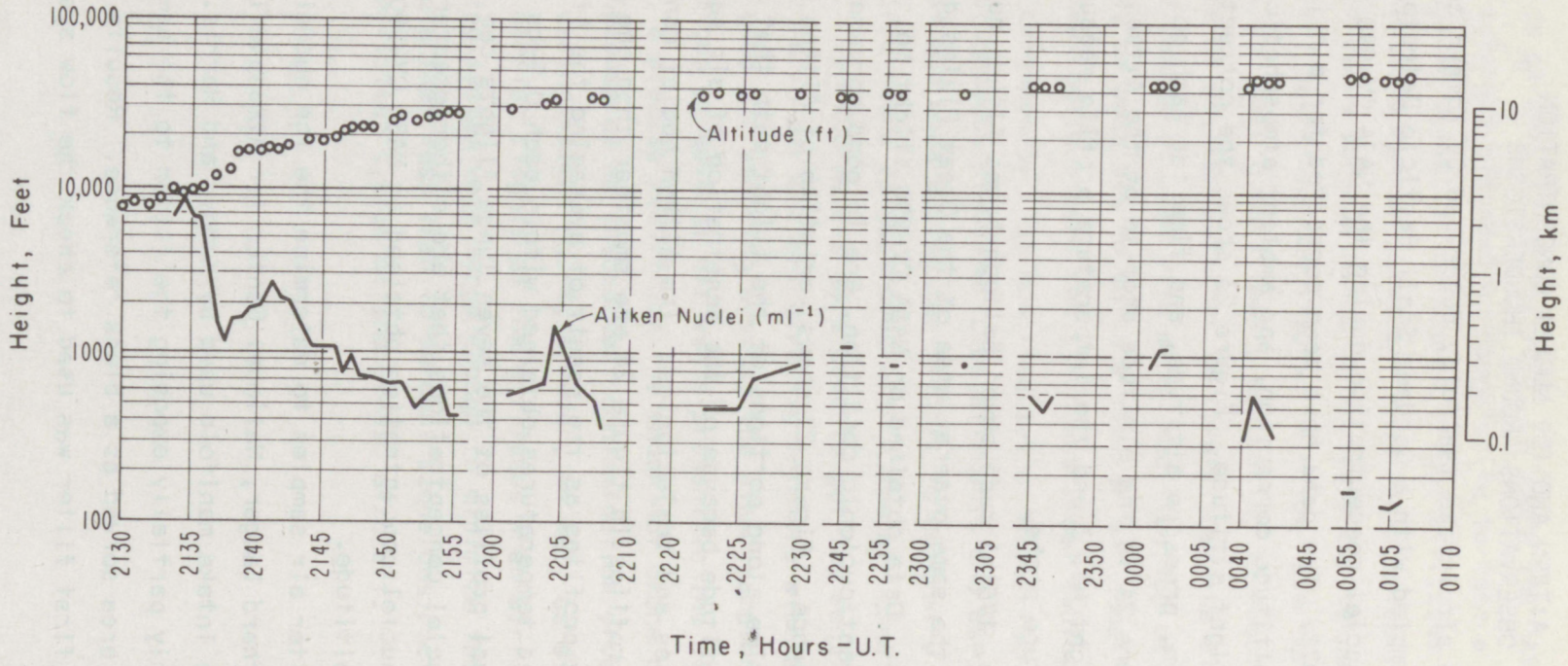

Figure 23. Profile of the Aitken nuclei concentration with altitude, 2130-0105 UT, July 14-15, 1971.

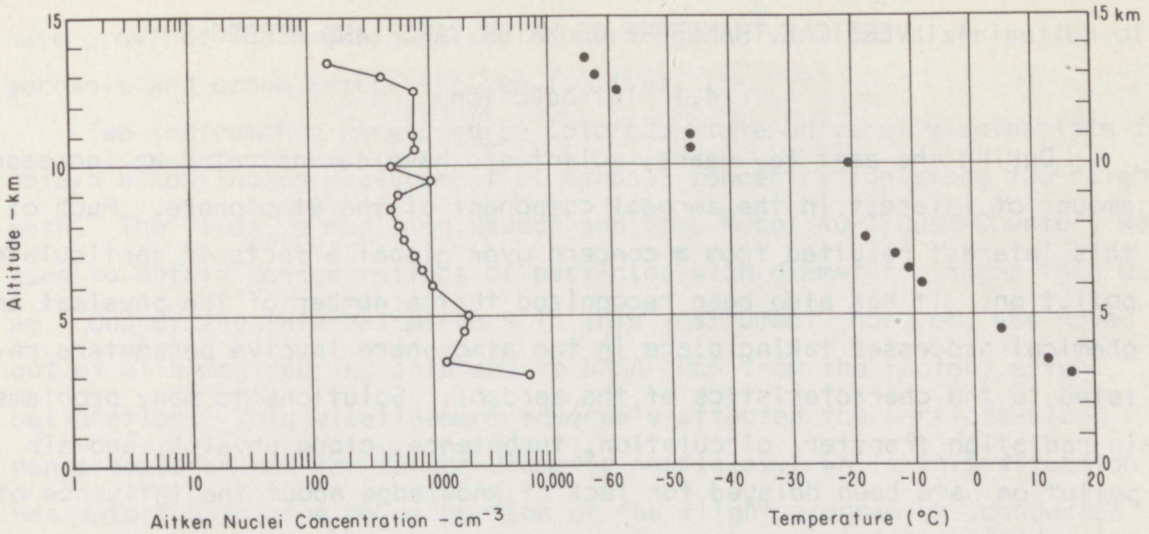

Figure 24. Vertical profiles of Aitken nuclei concentration and temperature, 2130-0105 UT, July 14-15, 1971.

not exposed to more than a few liters of air. Counts of ice nuclei on the active area of all filters are low and are not substantially different from the background count of the filter determined from the unexposed reference area of the filter. The actual ice nuclei concentration of the air sample, using the membrane filter method, was below the threshold of accurate measurement. The maximum possible ice nuclei concentration, as shown by filter 4, was not more than about 0.1 ice nuclei per liter; when considering the ice nuclei concentration determined from filters 2 and 3, it was probably much less.

Table 8. Ice Nuclei Concentration Counts, Flight of July 14-15, 1971.

Filter*	Altitude	Time	Flow	Corrected total volume	Count at -21°C		Net count	Concentration counts
					Active area	Reference area		
	ft	UT	l/min.	l				l
1	Ground	1515	0	---	28	22	6	---
2	32,000-39,000	1611-1714	1.3	103	24	20	4	0.04
3	40,000-42,000	1721-1822	.8	61	20	26	-6	0
4	42,000-45,000	1824-1917	.7	46	20	14	6	0.13

*0.8-μm membrane filter (Millipore Corp.).

4. VERTICAL TRANSPORT OF WATER VAPOR AND AEROSOLS

4.1 Introduction

During the past few years, scientists have demonstrated an increased amount of interest in the aerosol component of the atmosphere. Much of this interest resulted from a concern over global effects of particulate pollution. It has also been recognized that a number of the physical and chemical processes taking place in the atmosphere involve parameters related to the characteristics of the aerosol. Solutions to many problems in radiation transfer, circulation, turbulence, cloud physics, and air pollution have been delayed for lack of knowledge about the influence of atmospheric aerosols.

During midsummer 1970, a Department of Transportation-sponsored field program, involving NOAA, NASA Ames Research Center, and Colorado State University, was conducted to measure the distribution and concentration of water vapor, aerosols, ozone, and carbon dioxide in the environment of large thunderstorms over the Midwest and High Plains States of the United States. This report summarizes the aerosol measurements and discusses the comparison in distribution of aerosols and ozone around several thunderstorm tops.

4.2 The Measurement Program

To investigate simultaneously the radiative, chemical, and aerosol environments of thunderstorms which often tower to tropopause altitudes and even higher, it is necessary to carry a relatively large instrumentation payload to or above the maximum cloud altitude. The NASA Ames Research Center (NASA-AMES) made available its flying laboratory, a CV-990 aircraft. This aircraft is generally well suited for this type of research, having exceptional speed and range capability as well as a large capacity, in-cabin environment for in-flight calibration and servicing of instrumentation. For most studies of this type, the service ceiling of approximately 44,000 msl is adequate. For the storms investigated in this program, an additional 5,000- to 10,000-foot flight capability would

have provided the answers needed concerning the vertical distribution of aerosols and ozone around the cumulus tops.

Two instruments were used by Colorado State University scientists to obtain a continuous measurement of aerosol concentration along the flight path. The first, a modified Bausch and Lomb Model 40-1 Dust Counter, was used to obtain concentrations of particles with diameters larger than 0.3 μm. One of the internal mirrors in this instrument, however, was moved out of alinement during shipment to NASA-AMES from the factory after calibration. This misalinement adversely affected the particle-size range measurements for larger diameter particles. While this situation was unfortunate, the major portion of the flight program was conducted at altitudes above 30,000 feet msl where the concentration of large aerosol particles is normally very small.

The second aerosol-counting instrument used was the General Electric continuous Condensation Nuclei Counter. This instrument was adjusted to measure all particles with a radius between 0.005 and 9.2 μm (Aitken nuclei). Figure 25 shows the aerosol-measuring equipment aboard the CV-990. Figure 26 shows the isokinetic intake system mounted through the roof of the aircraft fuselage. This sampling system has been used by the author on nearly one hundred previous flights with the CV-990 aircraft, and its accuracy and reliability have been determined from fly-by comparisons with identical instrumentation on towers and other aircraft.

A block diagram of the NOAA atmospheric-constituents sampling system is shown in section 2 (fig. 14). Ozone measurements were made with two ECC ozone meters (fig. 15, section 2). Carbon dioxide air samples were collected by NOAA personnel during three flights using 500-ml Pyrex glass flasks which had previously been evacuated to about 5-mm flask pressure. These air samples were analyzed following each flight by means of a Mine Safety Appliance LIRA 200 nondispersive infrared gas analyzer.

During one of the flights, a Gardner Small Particle Counter (Aitken nuclei counter) and a Millipore filter particle collector (filter unit) were connected to the air intake system. The Millipore filter unit did not operate successfully, and no useful data on particulate material were obtained. A comparison of measurements made at high altitudes for the

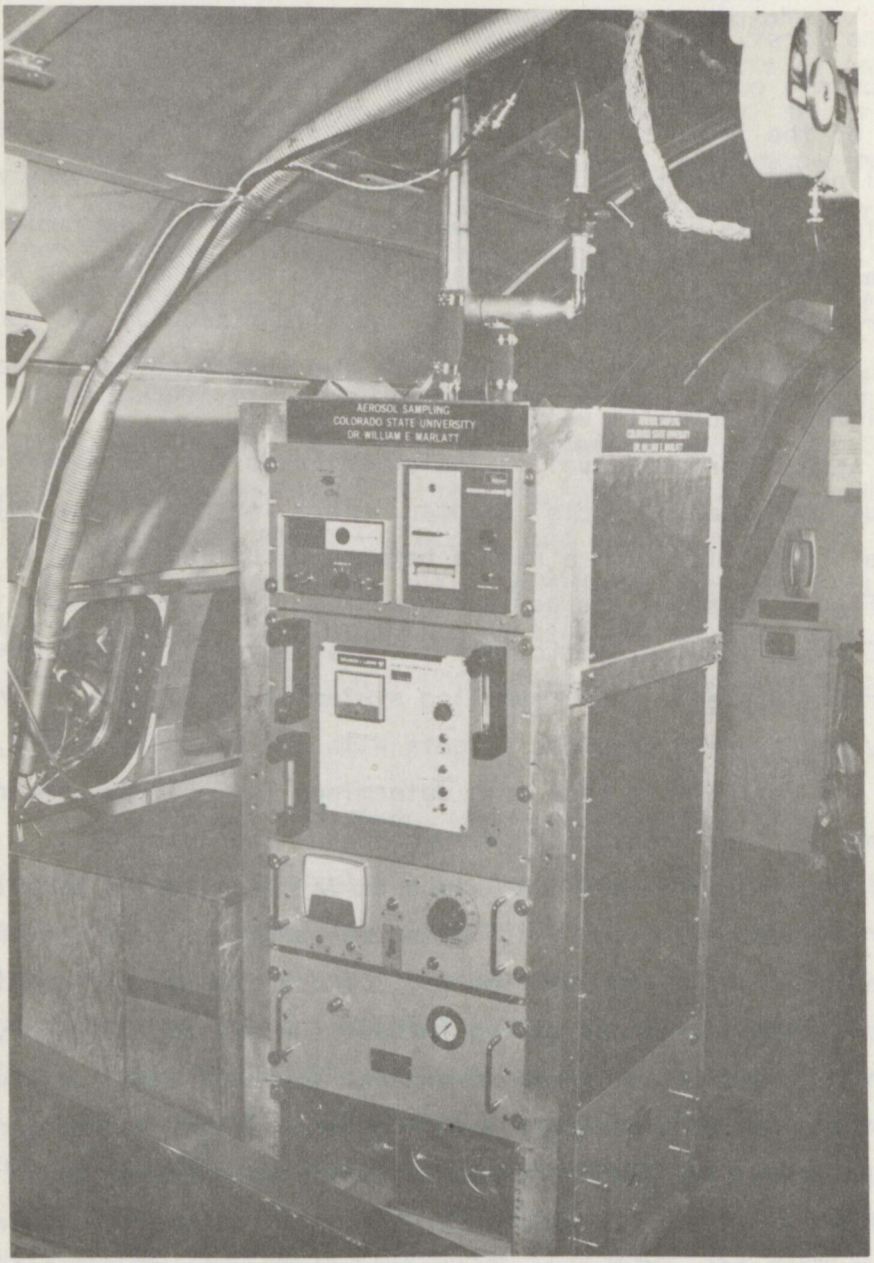

Figure 25. Instrumentation aboard Convair 990 used to measure aerosol concentrations.

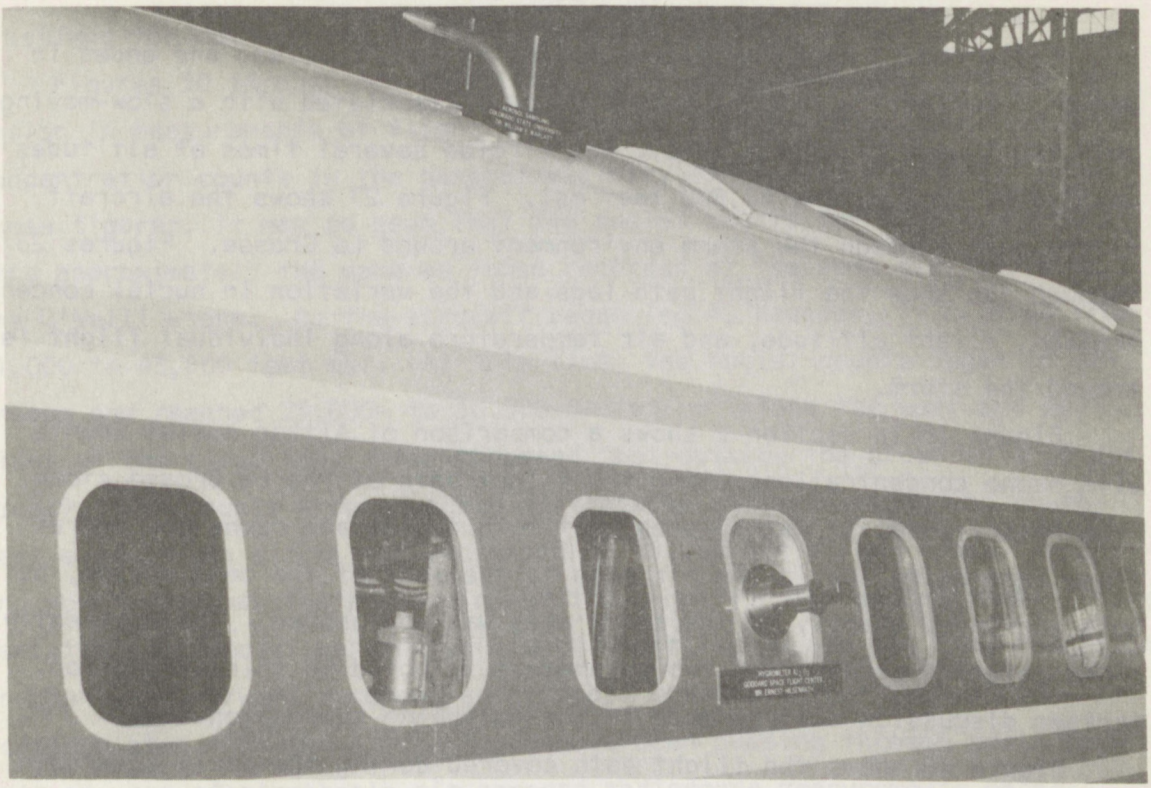

Figure 26. Aerosol intake system (mounted through roof) used aboard Convair 990.

same storm by the Gardner and the General Electric counters indicated that quite low counts were obtained using the Gardner unit, while exceptionally high counts were recorded using the General Electric counter. It was speculated later that the plastic (Teflon-coated) tubing used on the Gardner intake system may have collected a static surface charge, preventing the nuclei from reaching the counting chamber.

Figure 1 in section 1 shows a typical high-altitude flight path around a thunderstorm. Flights were conducted in this manner to obtain both upward and downward wind measurements of the various parameters around the top of the thunderstorm. The downstream crosswind leg was normally flown just below the anvil streamer of the cloud. The "boxed" thunderstorm enclosed an area ranging approximately from 150 to 200 nautical miles, north-south, to 300 to 375 nautical miles, east-west.

4.3 Results

Flight No. 1 (NASA-AMES) originated at San Francisco and ended in Denver. During the flight, a cumulus cell associated with a slow-moving cold front near La Crosse, Wis., was circled several times at altitudes of 33,800, 39,700, and 40,800 feet msl. Figure 27 shows the aircraft flight path through the storm environment around La Crosse. Figures 28 through 39A show the flight path legs and the variation in nuclei concentration, flight altitude, and air temperature along individual flight legs around the storm.

Figure 16 in section 2 shows a comparison of Aitken nuclei counts with ozone concentrations along the flight path of the La Crosse storm. From this figure, it may be seen that both nuclei and ozone concentrations were quite low in the air mass to the west of the cell system, but both increased sharply as the storm area was approached. The apparently close relation between the two parameters is noted in this subsection. Further discussion will be made in the following subsection 4.4.

Figure 40 shows the flight path covered during the early afternoon of July 14 around an isolated cumulus near O'Neill, Nebr. Figures 41 through 48 show the flight path legs and the variation in nuclei concentration, flight altitude, and air temperature along individual flight legs around this storm. Nuclei counts remained low (<3,000 nuclei/cm^3) until the aircraft passed over Sioux City, Iowa, on leg 5 downstream crosswind where it climbed from 35,000 to 38,000 feet msl. It may have been expected that the increase in nuclei counts at this time was associated with the cirrus anvil portion of the thunderstorm. The concentrations measured along legs 6 and 7, during which the aircraft passed over the top of the storm at 40,000 feet msl, indicated that the nuclei counts above about 38,000 feet were approximately 10 times those below that altitude.

Figure 49 shows the flight path of the aircraft around a towering, building cumulus associated with a violent rain and hailstorm in the late afternoon of July 14 (approximately 30 to 40 minutes' flying time after leaving the O'Neill storm). The storm, located southeast of Cheyenne,

Wyo., was centered near Grover, Colo., and passed over the Pawnee National Grassland for most of the flight period.

Figures 50 through 58A show individual flight path legs and the variation in measurements of flight altitude, air temperature, and nuclei concentration counts in the general vicinity of the Grover storm. From these figures, it may be seen that the nuclei counts for legs 1 and 2 were approximately the same as those recorded at the same altitude over the O'Neill storm. As the aircraft began leg 4, however, it climbed from 41,000 to 43,000 feet msl. At this time, the nuclei counts began to increase and reached 25,000- to 30,000-nuclei/cm^3 along the west and south sides of the cloud (and a few thousand feet outside the cloud wall in all cases). The counts dropped again at the same altitude along the southeast side of the storm, but increased to 30,000 nuclei/cm^3 along the east and north sides as the plane circled the cloud for the second time. Sharp variations of nuclei were noted along flight legs 9 and 10. The reduction in counts was always accompanied by small changes in air temperature; it is speculated that the aircraft may have been passing through small parcels of warm stratospheric air because radiosonde measurements of the temperature profile indicate that the aircraft was approaching the tropopause altitude.

The aircraft moved away from the cumulus cell during leg 12 and began its descent to land at Denver. From the original data, it appeared that the nuclei counts had already decreased slightly as the aircraft left the storm environment before starting its descent. Because the aircraft had not moved far from the storm vicinity at the ceiling altitude, it is not possible to state anything about the nuclei environment in undisturbed air at that altitude.

As the plane descended below 35,000 feet msl (fig. 58A), the nuclei concentration became extremely low with counts well below 500 nuclei/cm^3. Figure 19 in section 2 shows a plot of Aitken nuclei and ozone concentrations for the O'Neill and Grover storm flights. From this figure, it may be noted that as the aircraft climbed above the surface layer, the nuclei concentrations decreased to low values and remained low until the aircraft had turned to pass directly over the O'Neill storm. Ozone

concentrations, on the other hand, had started to increase when the plane was over Kearney, Nebr., more than one hundred miles from the storm system. At the point when nuclei concentrations were highest over the O'Neill storm, the ozone concentrations dropped sharply and did not increase until the aircraft was 50 miles west of the storm. Nuclei counts remained high and variable whenever the ozone again reached a maximum in the clear-sky area midway between the O'Neill and the Grover storms, then they decreased to approximately 4 to 5 pphm in the vicinity of the Grover storm.

4.4 Discussion

Reasons for the apparent positive correlation between the nuclei count and ozone concentration in the vicinity of the La Crosse storm and the lack of correlation or, on occasion, of negative correlation for the O'Neill and Grover storms are not immediately obvious. Komhyr has postulated that the most probable explanation for the high-ozone concentration in the vicinity of the La Crosse storm may be the downward transport of stratospheric air through the tropopause. This postulate is in line with measurements by Lovill (1969) who found stratospheric ozone at ground level following periods of strong chinook winds. Why high concentrations of ozone were not found in the vicinity of the O'Neill storm is not known.

On the other hand, it is surprising to find concentrations of 25,000- to 70,000-nuclei/cm^3 around the Grover storm, while the concentration was less than 25,000 nuclei/cm^3 in the vicinity of the O'Neill storm and less than 10,000 nuclei/cm^3 around the La Crosse storm. The Grover storm, however, was the only flight in which the aircraft climbed above 42,000 feet. Riehl (1962) has shown that the layer just below the tropopause is favored for accumulation of particulate matter, and this is an important feature of atmospheric heating and cooling.

The possibility of a partial leak in the General Electric counter which would permit cabin air to enter the air sampling system was considered. The counter is extremely sensitive; undoubtedly, if cabin air would have entered, the counts would have exceeded 1 million nuclei/cm^3.

The close relation between particle counts and small fluctuations in air temperature also would indicate that the instrument was working satisfactorily.

On the day of the Grover storm, a large (3,000-acre) forest fire was burning approximately 150 miles upwind from the storm. One logical hypothesis offered is that the large nuclei concentration reflected the material placed in the atmosphere by the fire. From previous measurements made during the Barbados Oceanographic and Meteorological Experiment (BOMEX), it is believed by the author that nuclei found at this altitude result from the evaporation of cloud drops at the top and sides of the cloud. These nuclei may have a fairly long residence time, depending upon the height of the tropopause and the wind velocities at cloud-top altitudes.

In conclusion, the field program provided measurements which indicate that the nuclei concentration at or near tropopause height near the tops of thunderstorms can be many times that of the free atmosphere at levels only a few thousand feet lower. Whether or not there is a correlation between variations in ozone and nuclei could not be determined. It is most apparent that the measurement program was sufficient only to point out several intriguing questions concerning the environment of atmospheric nuclei. It is strongly recommended that further studies be undertaken using an aircraft which would be capable of making profile flights between 40,000 and 55,000 feet msl, that is, through the layer just below the tropopause up to the lower layers of the stratosphere.

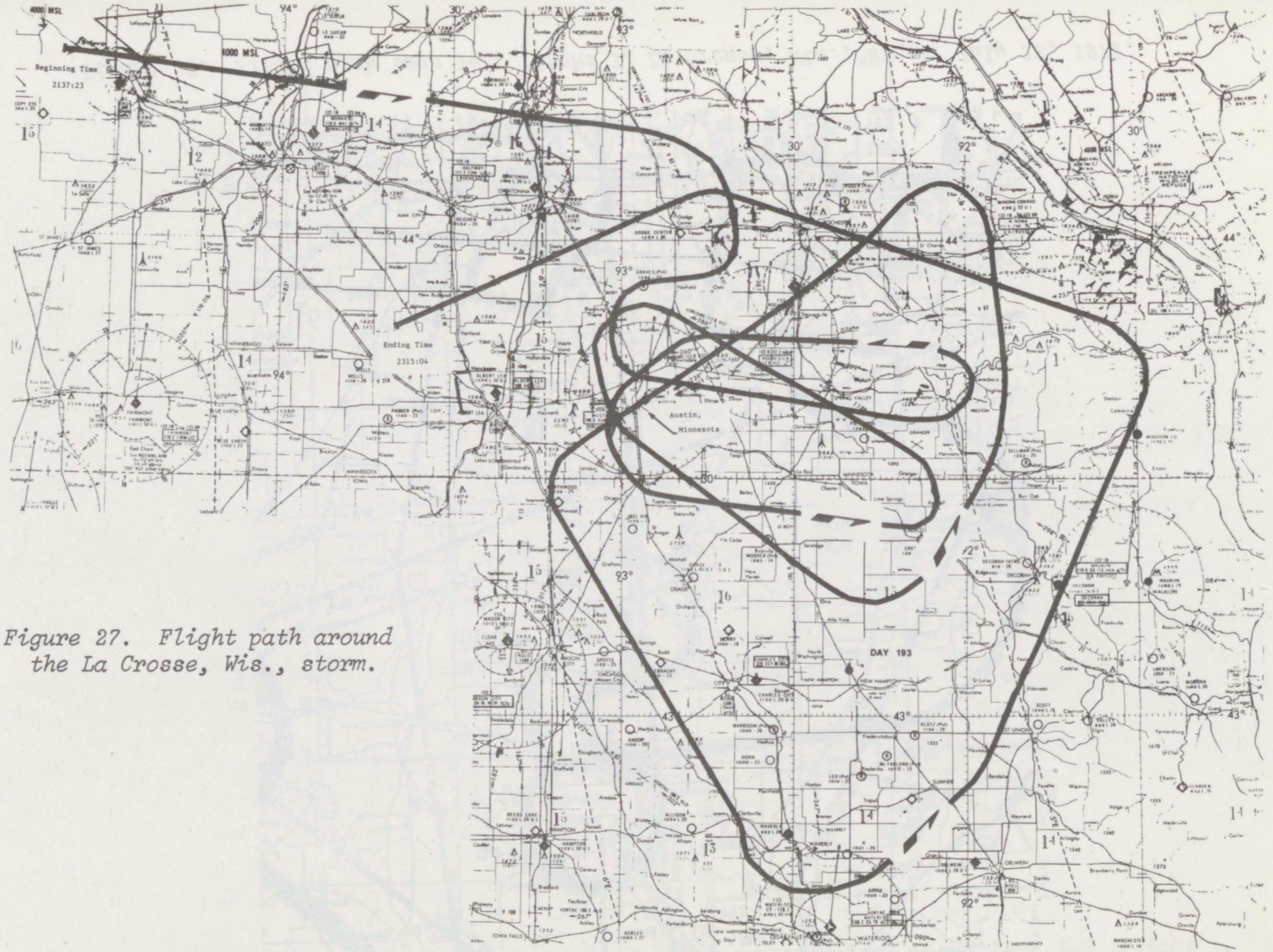

Figure 27. Flight path around the La Crosse, Wis., storm.

Figure 28. Flight path legs 1-2, flight 1, La Crosse, Wis., storm, July 12, 1971.

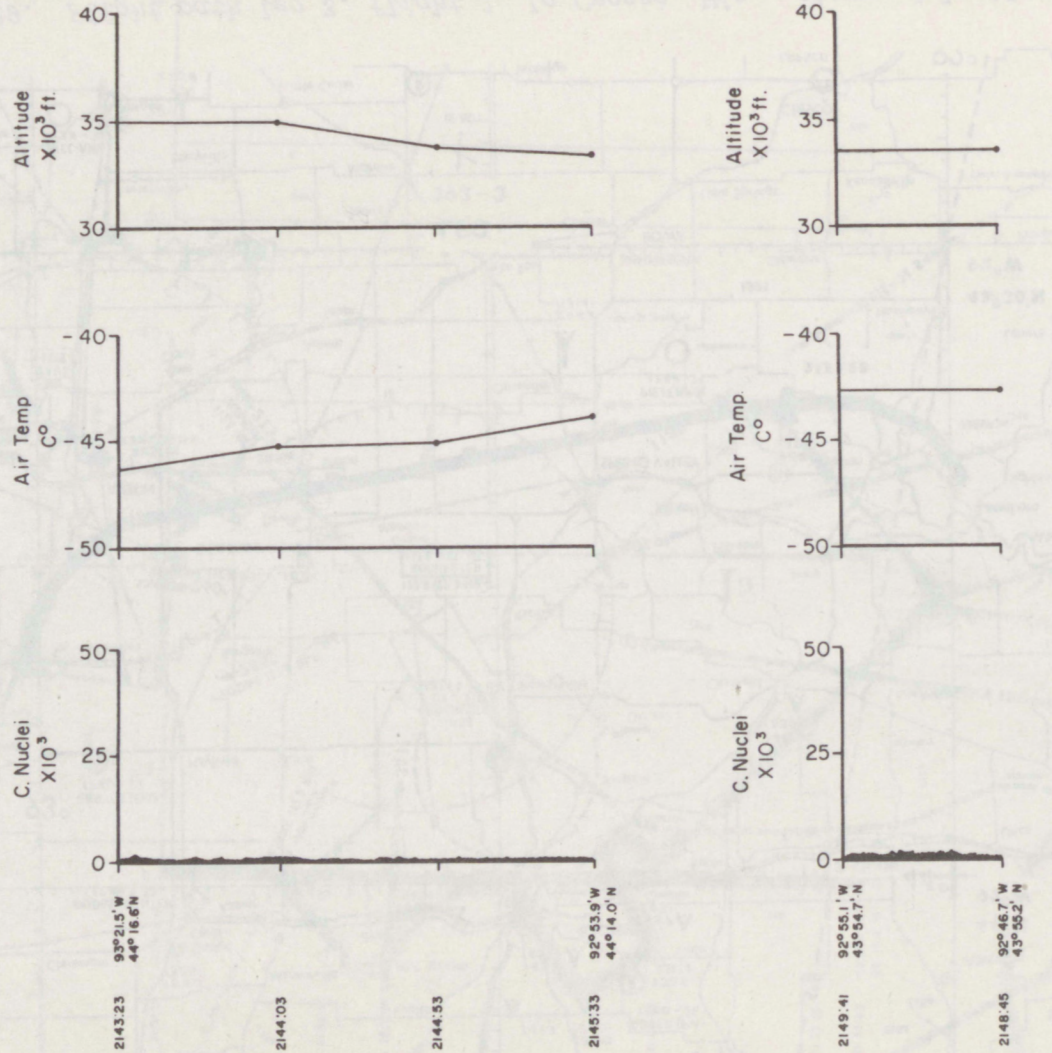

Figure 28A. Altitude, air temperature, and nuclei concentration along legs 1-2, flight 1, La Crosse, Wis., storm, July 12, 1971.

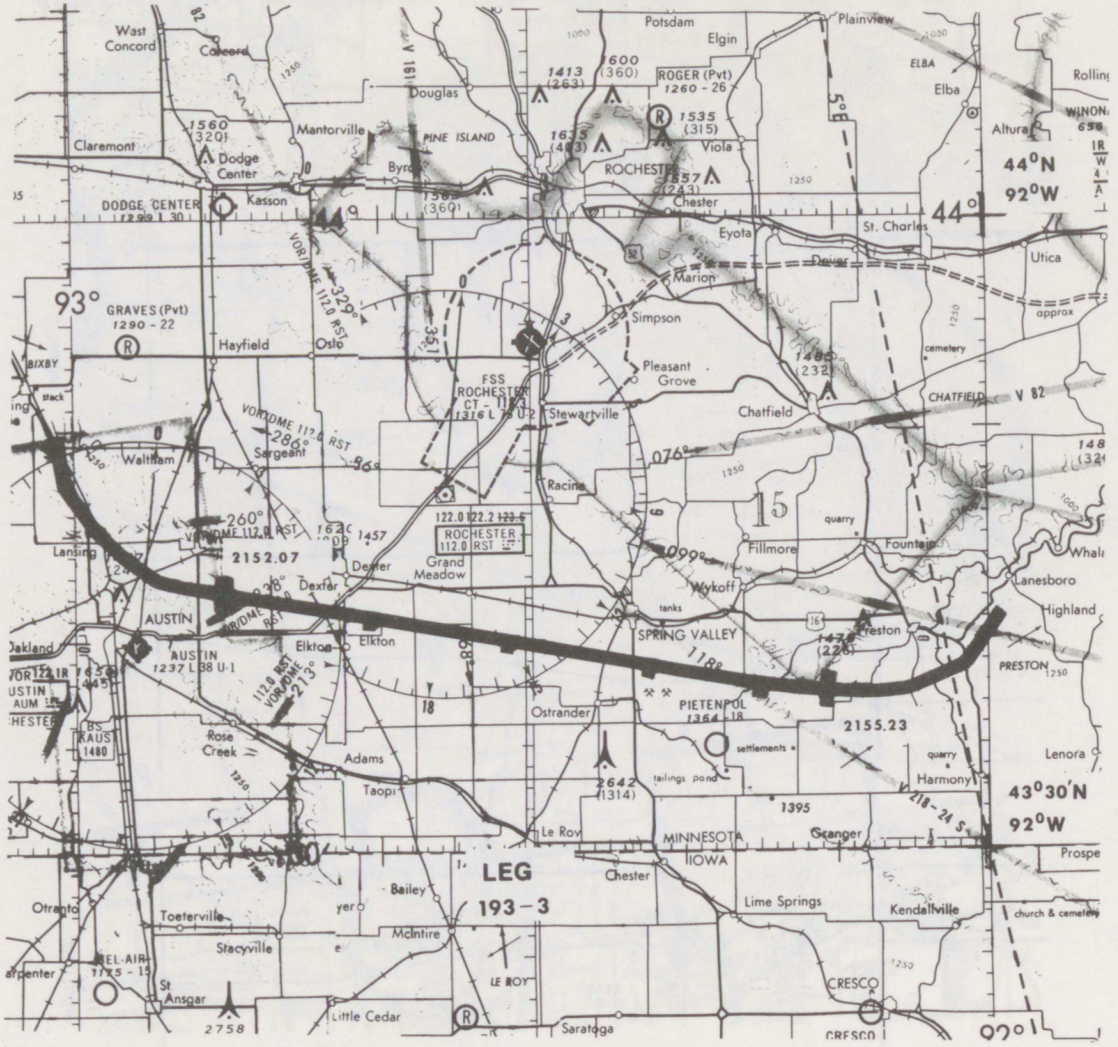

Figure 29. Flight path leg 3, flight 1, La Crosse, Wis., storm, July 12, 1971.

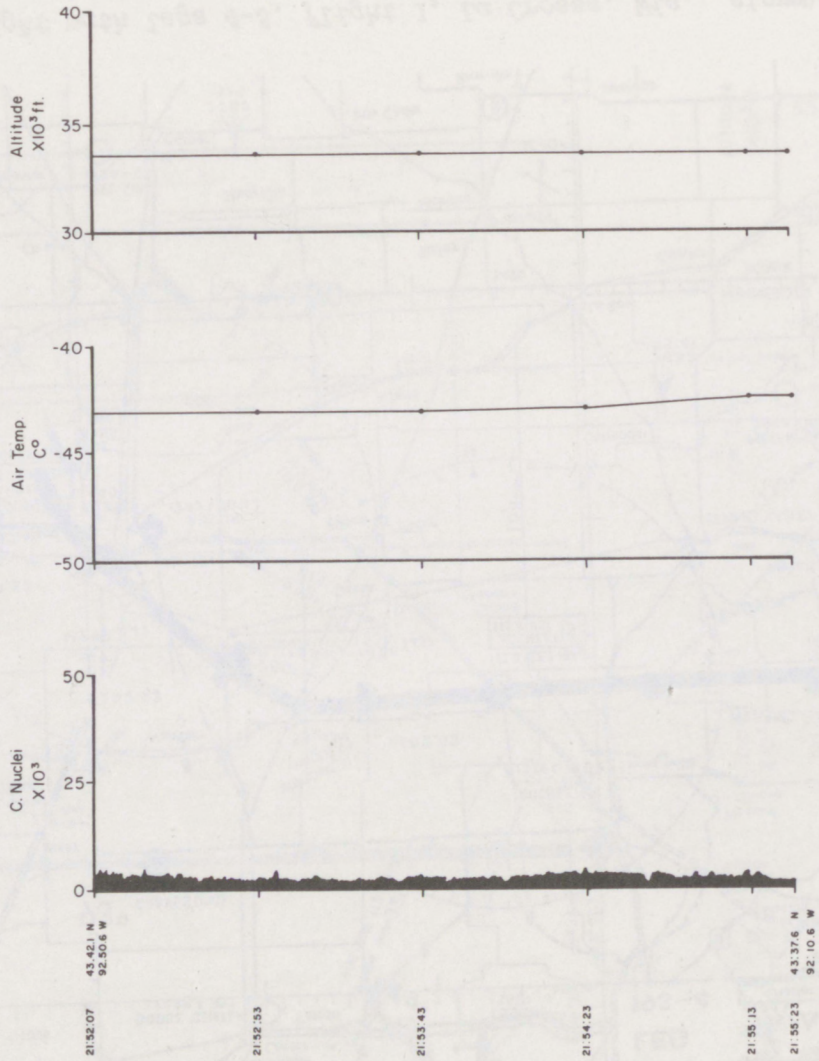

Figure 29A. Altitude, air temperature, and nuclei concentration along leg 3, flight 1, La Crosse, Wis., storm, July 12, 1971.

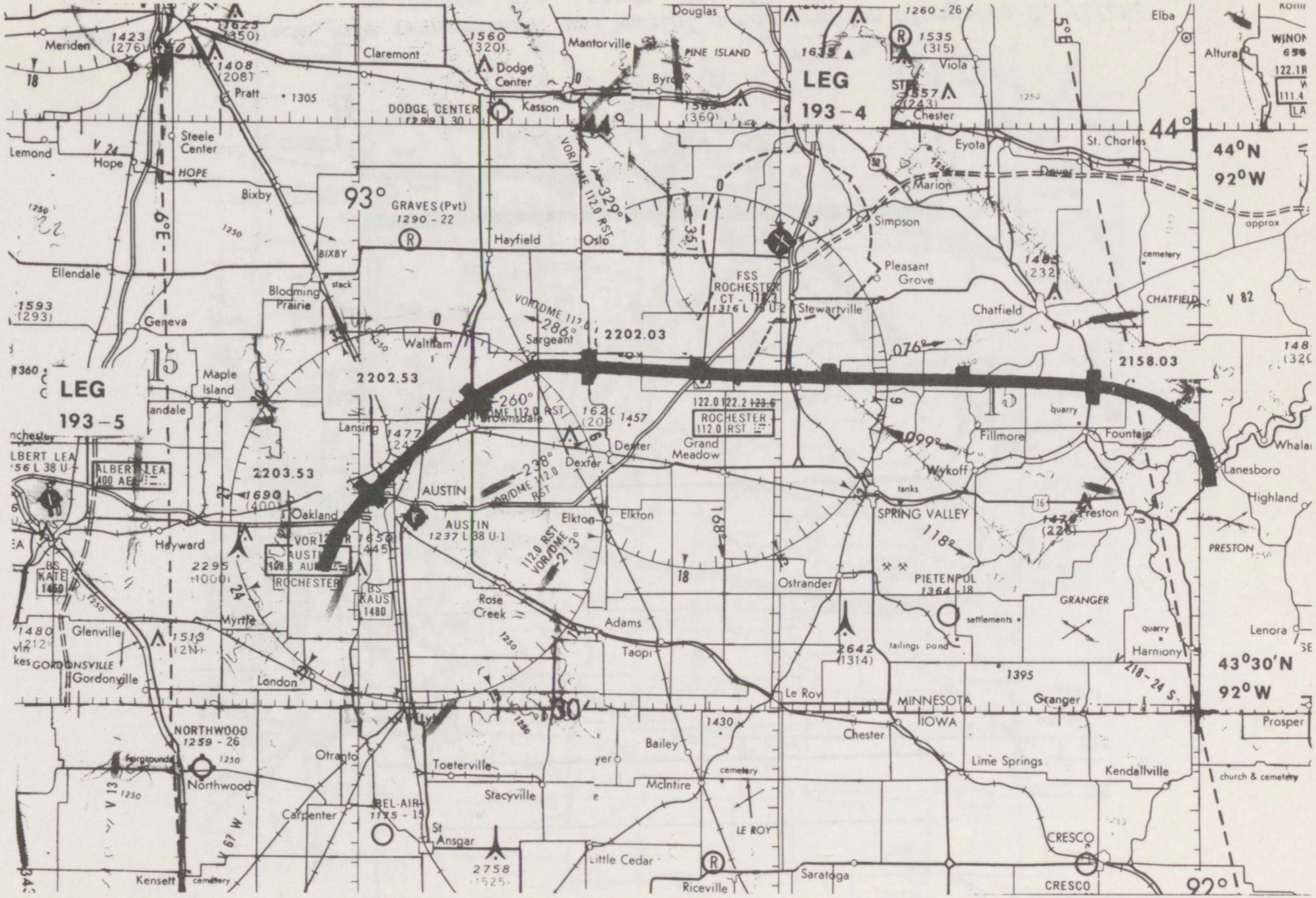

Figure 30. Flight path legs 4-5, flight 1, La Crosse, Wis., storm, July 12, 1971.

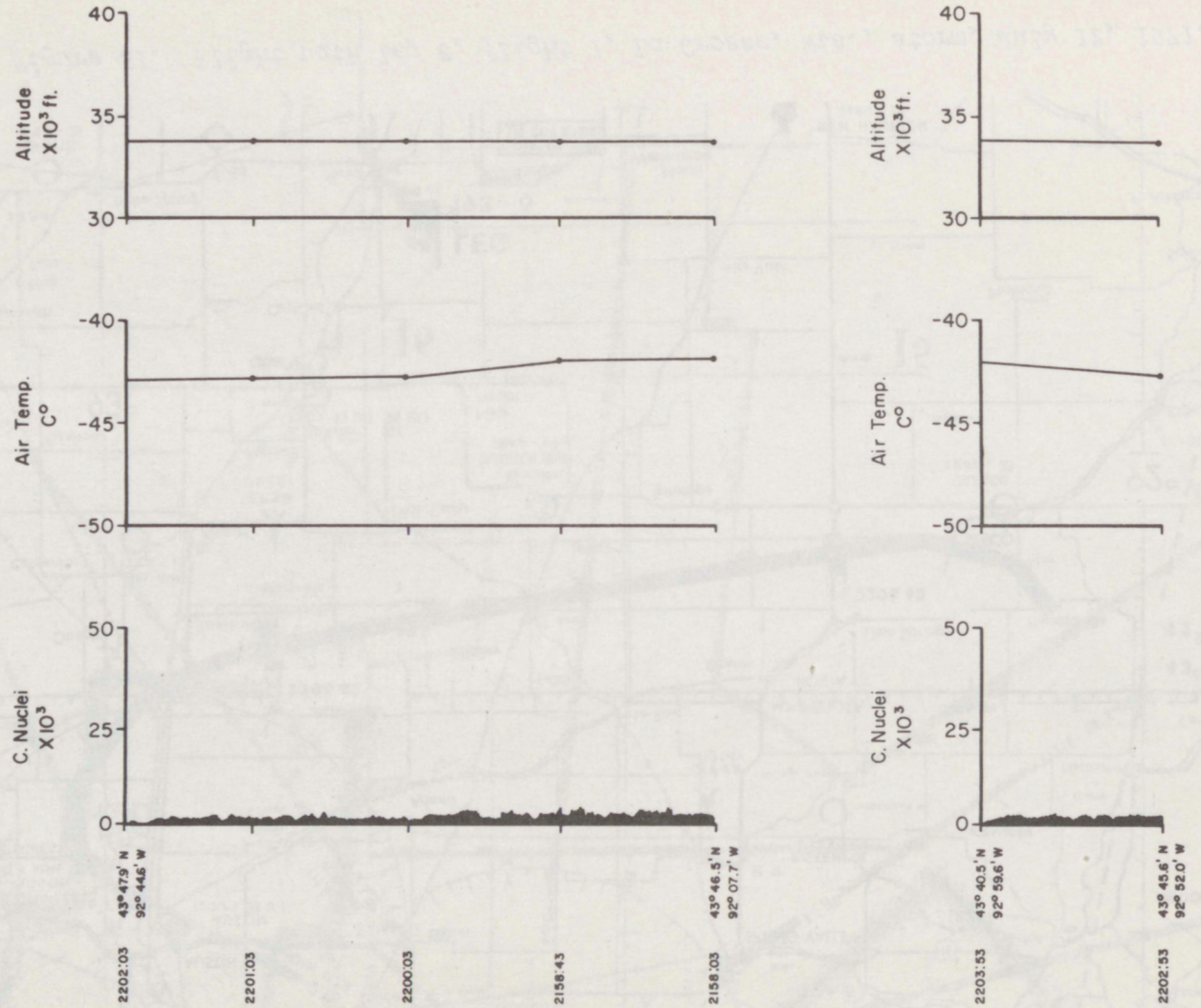

Figure 30A. Altitude, air temperature, and nuclei concentration along legs 4-5, flight 1, La Crosse, Wis., storm, July 12, 1971.

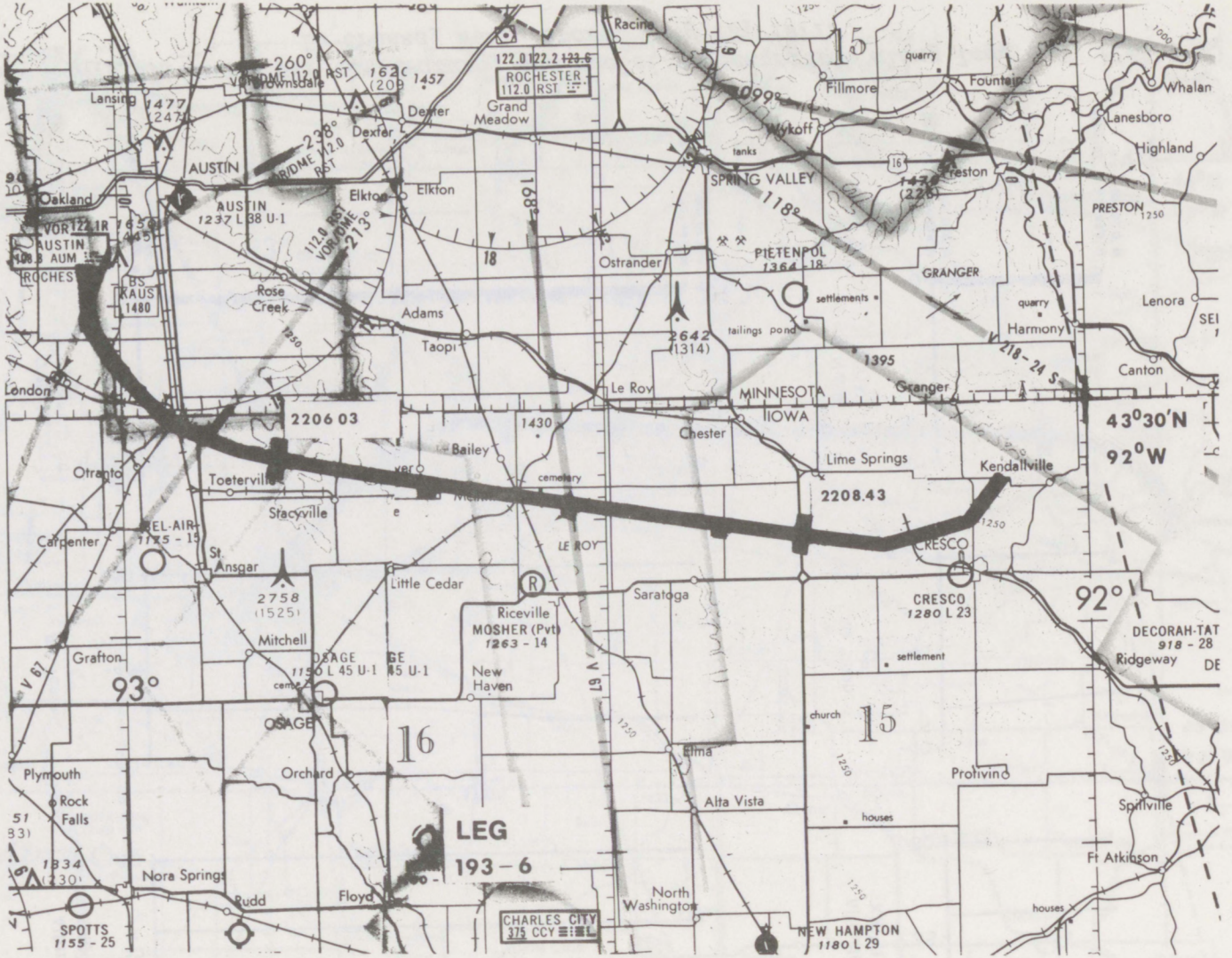

Figure 31. Flight path leg 6, flight 1, La Crosse, Wis., storm, July 12, 1971.

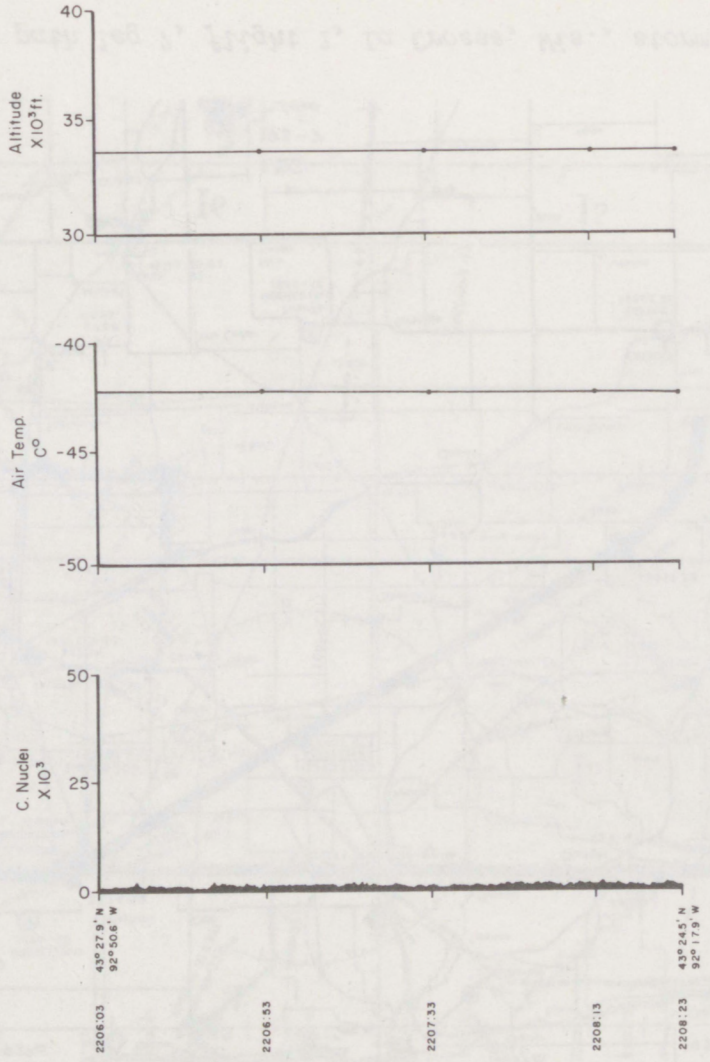

Figure 31A. Altitude, air temperature, and nuclei concentration along leg 6, flight 1, La Crosse, Wis., storm, July 12, 1971.

Figure 32. Flight path leg 7, flight 1, La Crosse, Wis., storm, July 12, 1971.

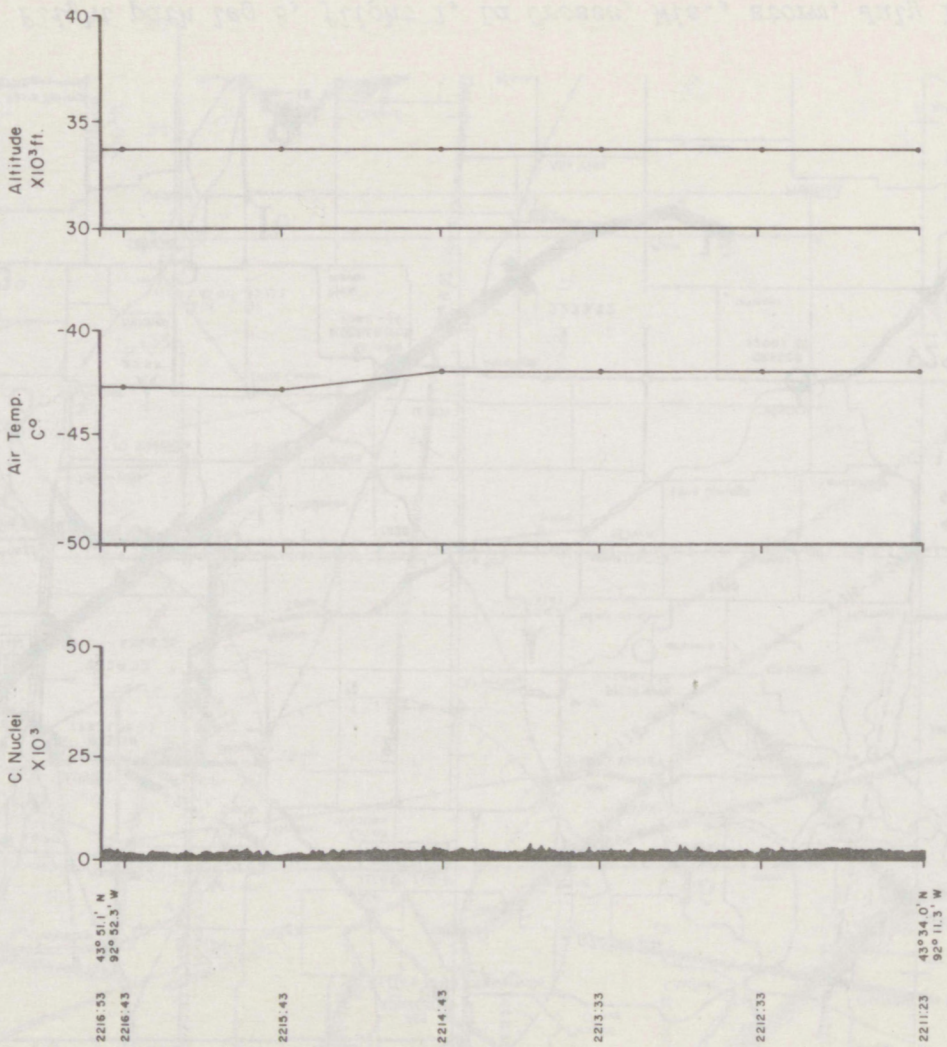

Flight 32A. Altitude, air temperature, and nuclei concentration along leg 7, flight 1, La Crosse, Wis., storm, July 12, 1971.

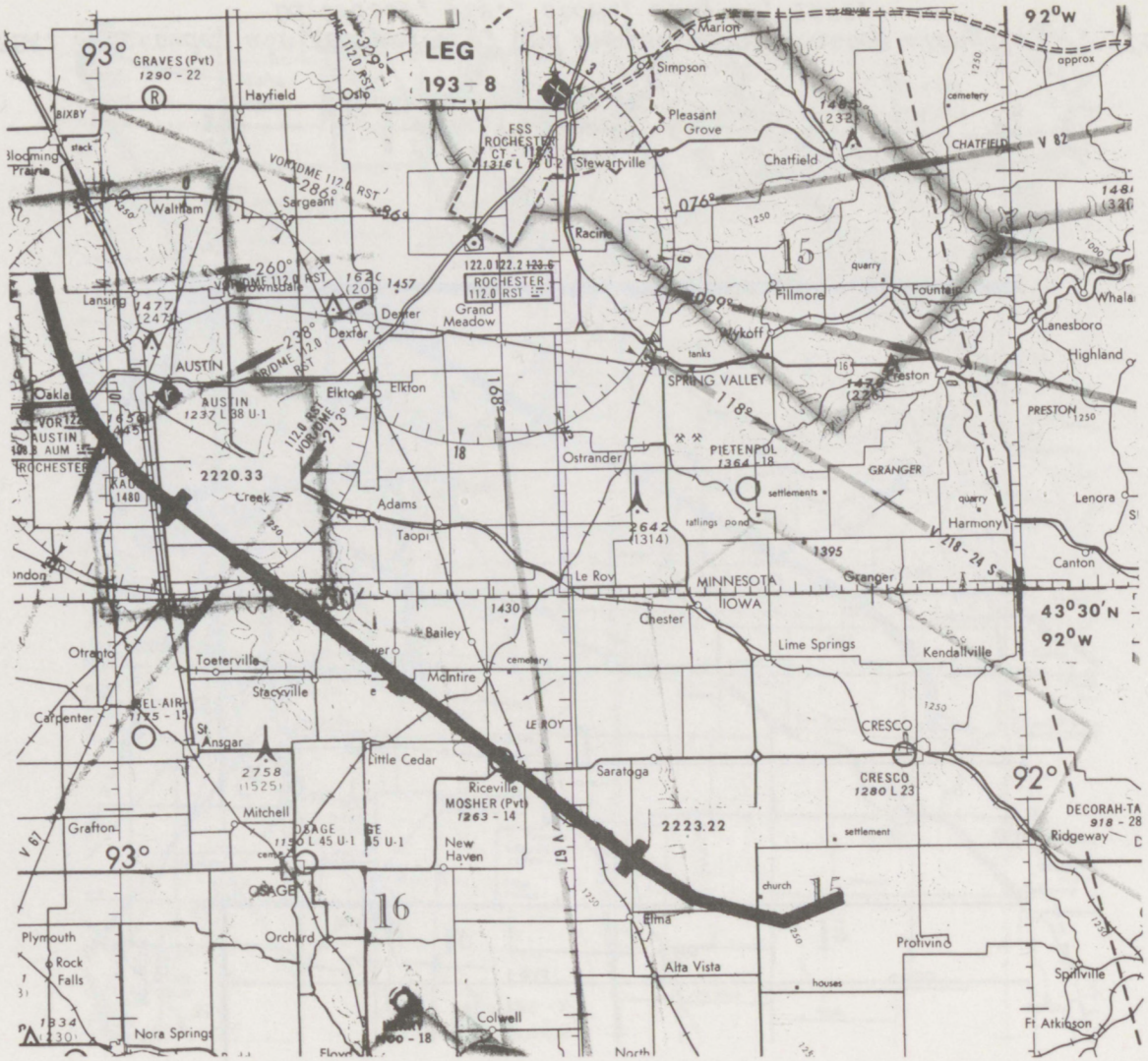

Figure 33. Flight path leg 8, flight 1, La Crosse, Wis., storm, July 12, 1971.

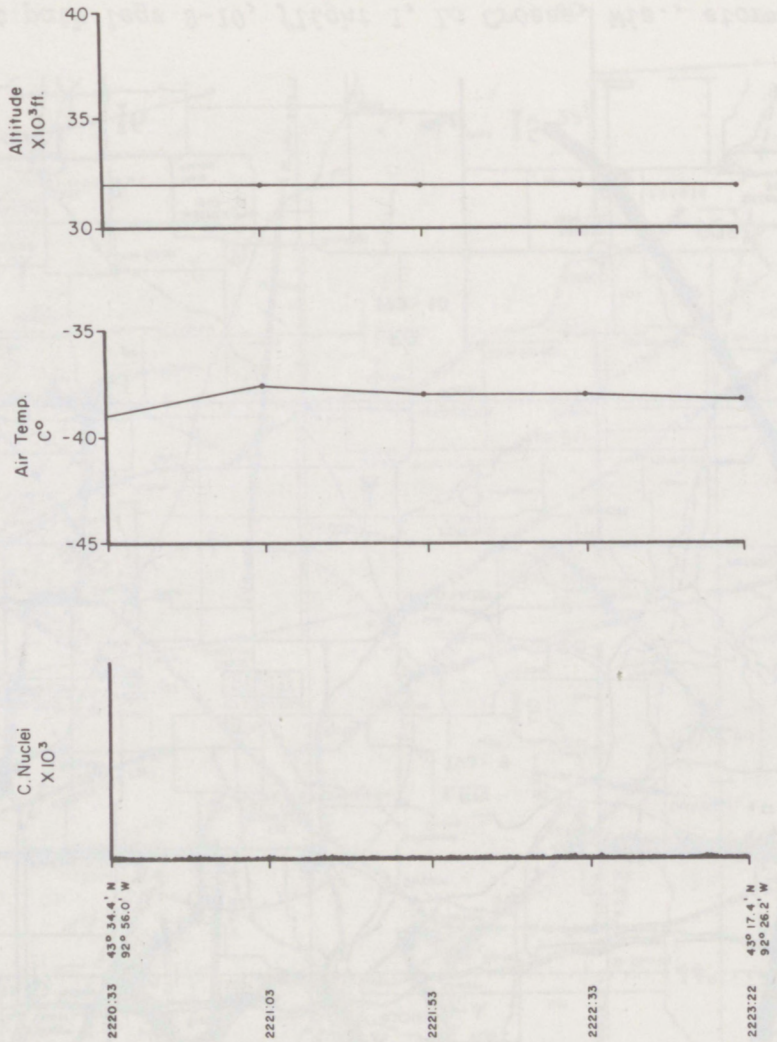

Figure 33A. Altitude, air temperature, and nuclei concentration along leg 8, flight 1, La Crosse, Wis., storm, July 12, 1971.

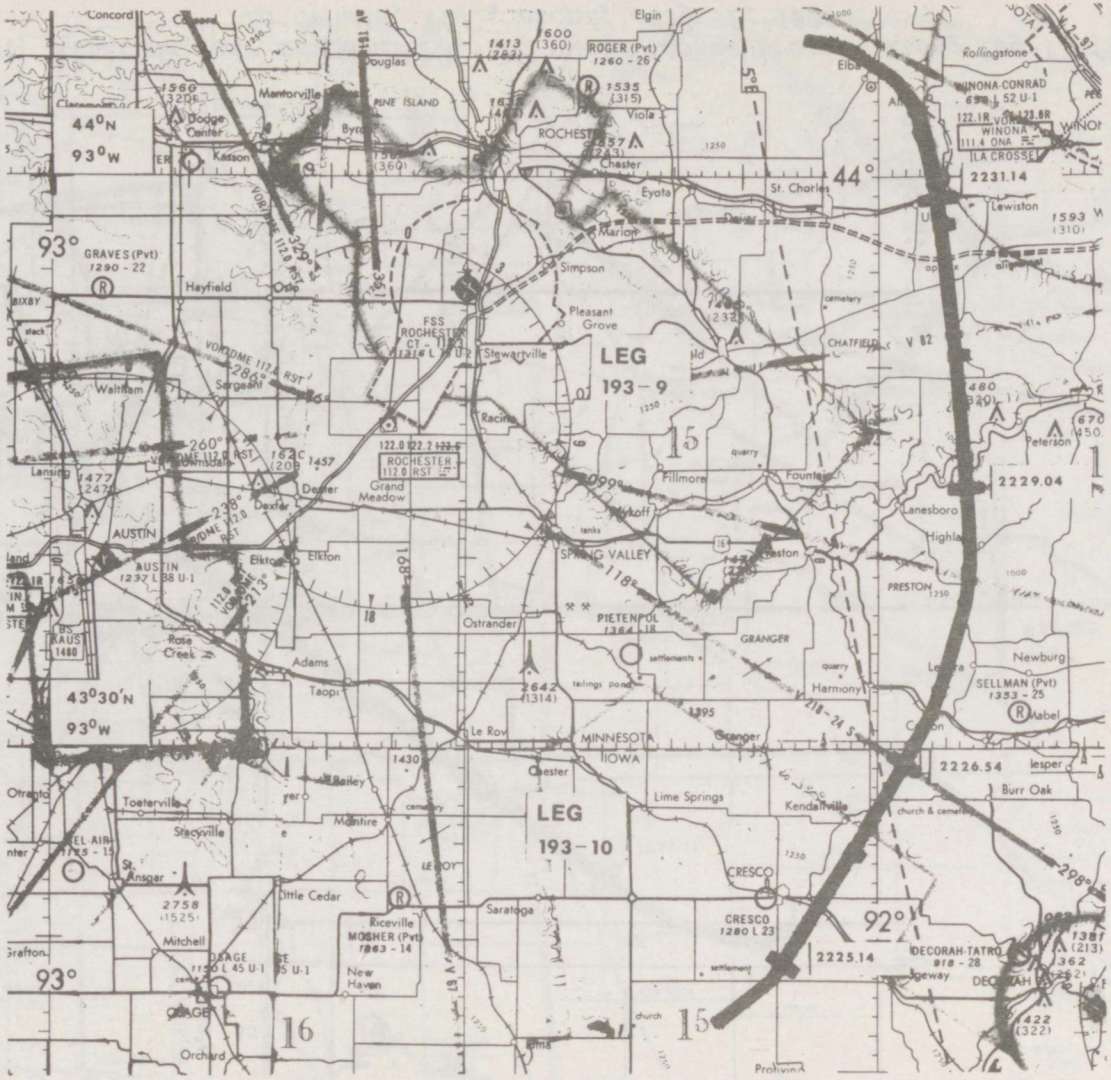

Figure 34. Flight path legs 9-10, flight 1, La Crosse, Wis., storm, July 12, 1971.

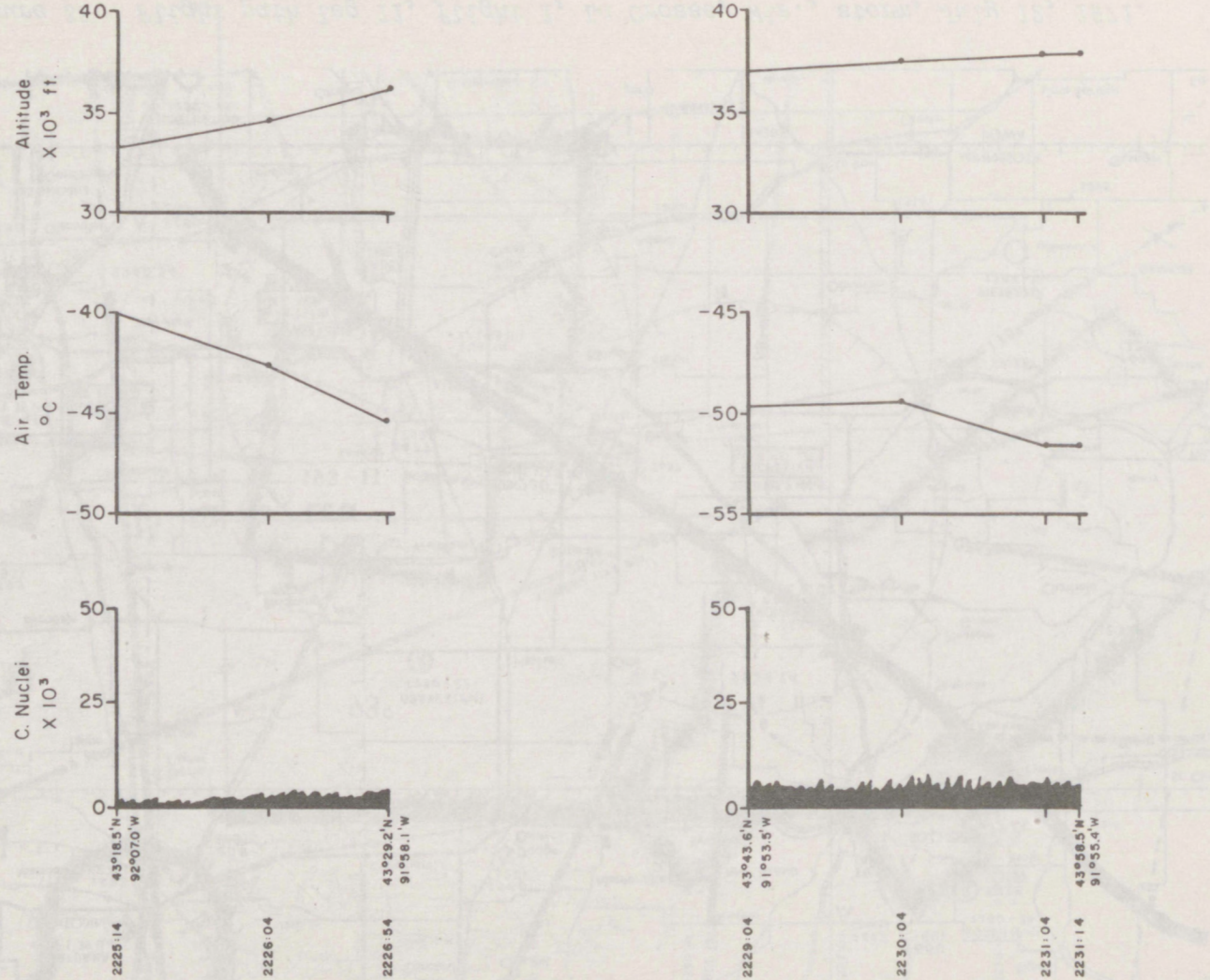

Figure 34A. Altitude, air temperature, and nuclei concentration along legs 9-10, flight 1, La Crosse, Wis., storm, July 12, 1971.

Figure 35. Flight path leg 11, flight 1, La Crosse, Wis., storm, July 12, 1971.

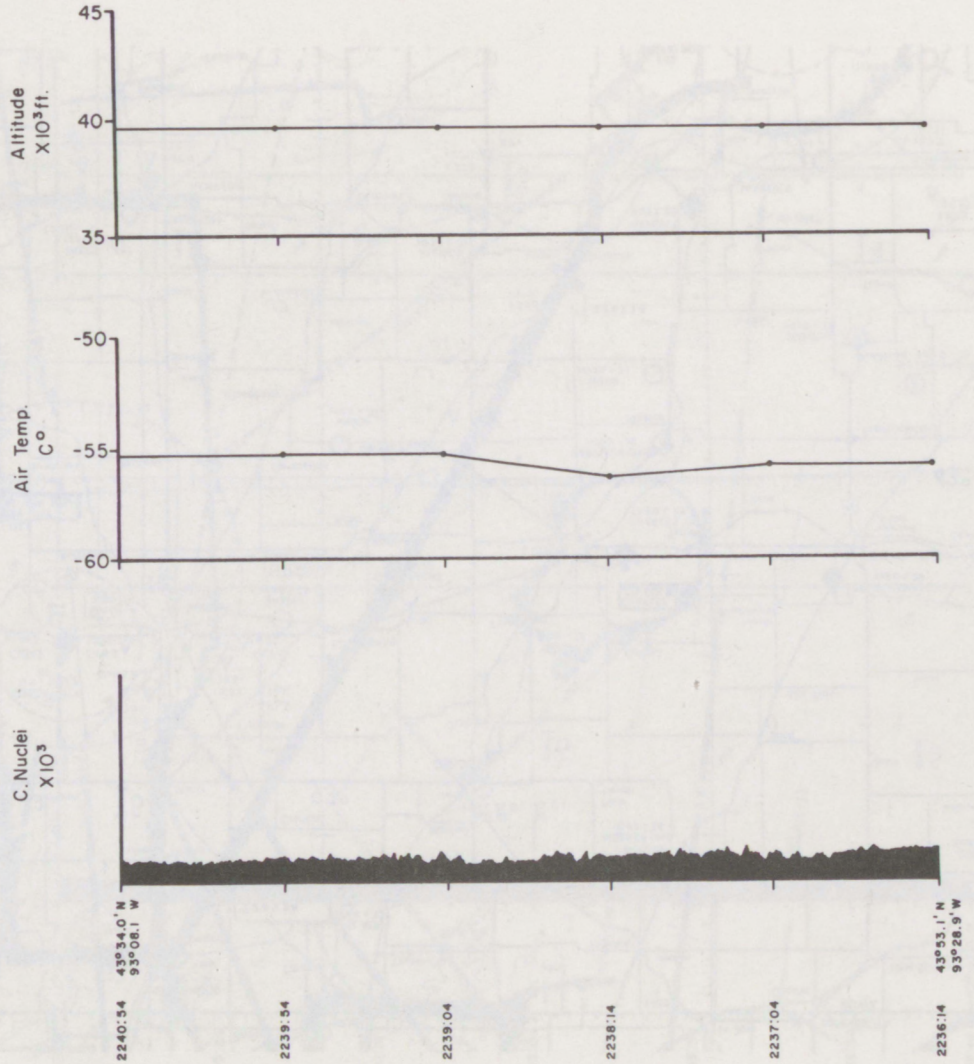

Figure 35A. Altitude, air temperature, and nuclei concentration along leg 11, flight 1, La Crosse, Wis., storm, July 12, 1971.

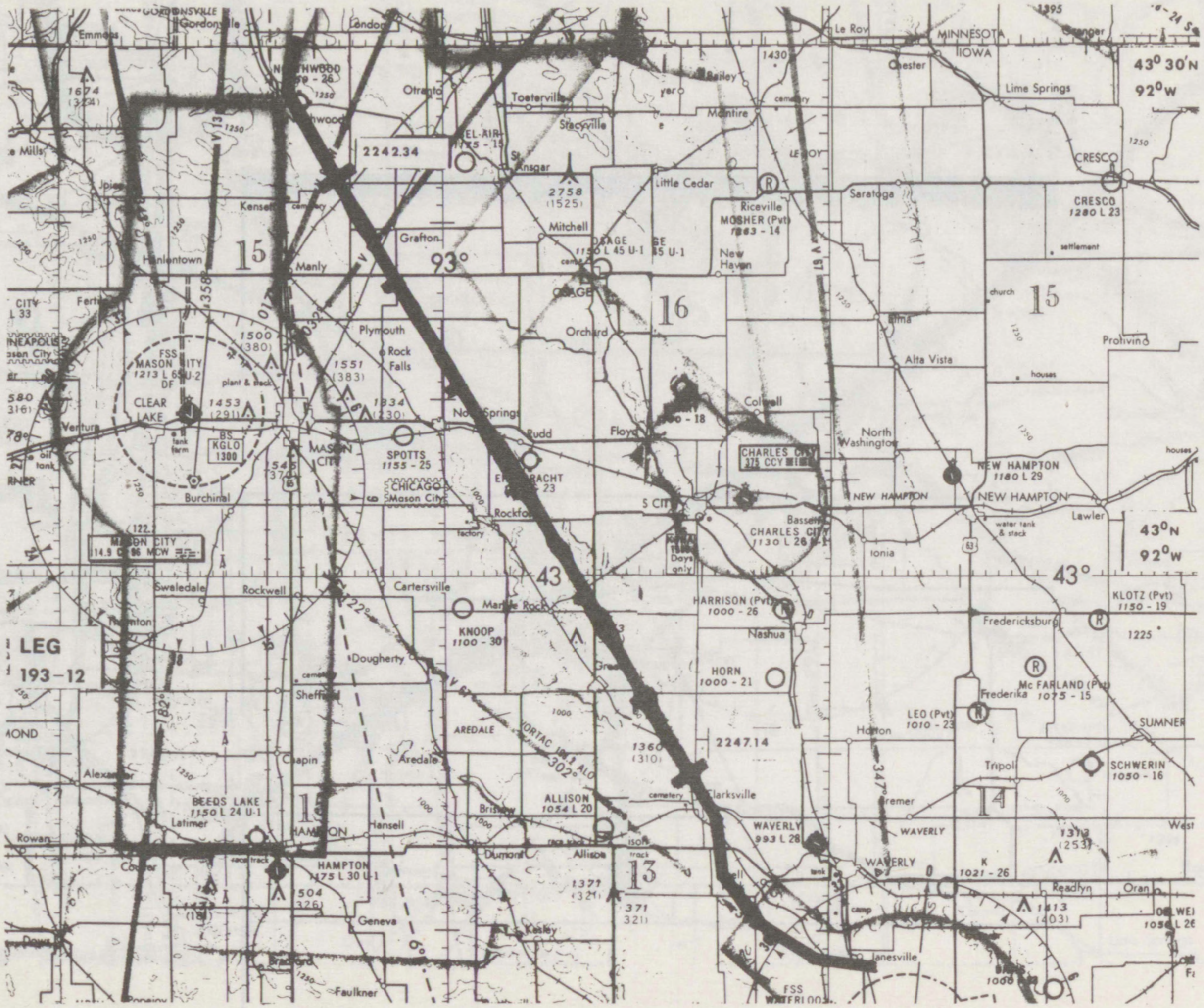

Figure 36. Flight path leg 12, flight 1, La Crosse, Wis., storm, July 12, 1971.

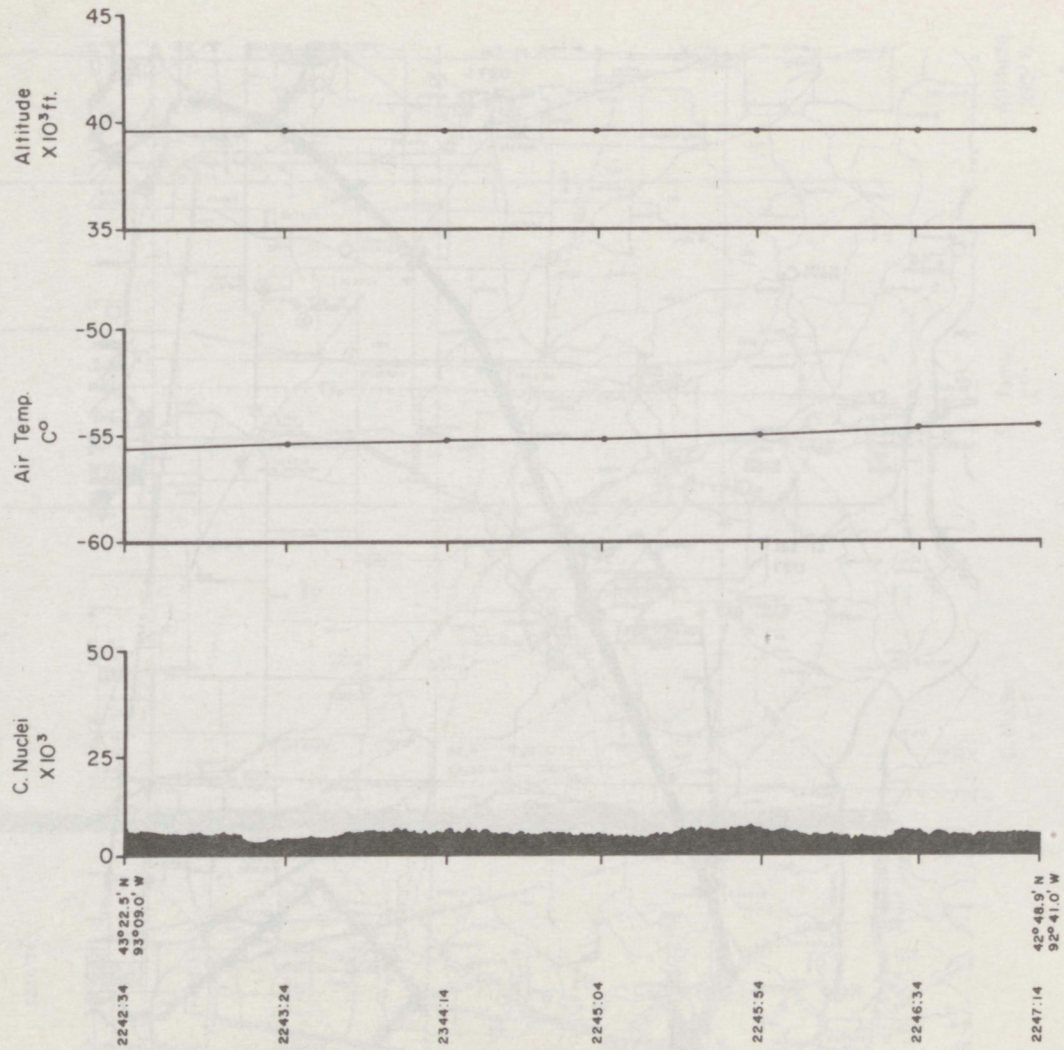

Figure 36A. Altitude, air temperature, and nuclei concentration along leg 12, flight 1, La Crosse, Wis., storm, July 12, 1971.

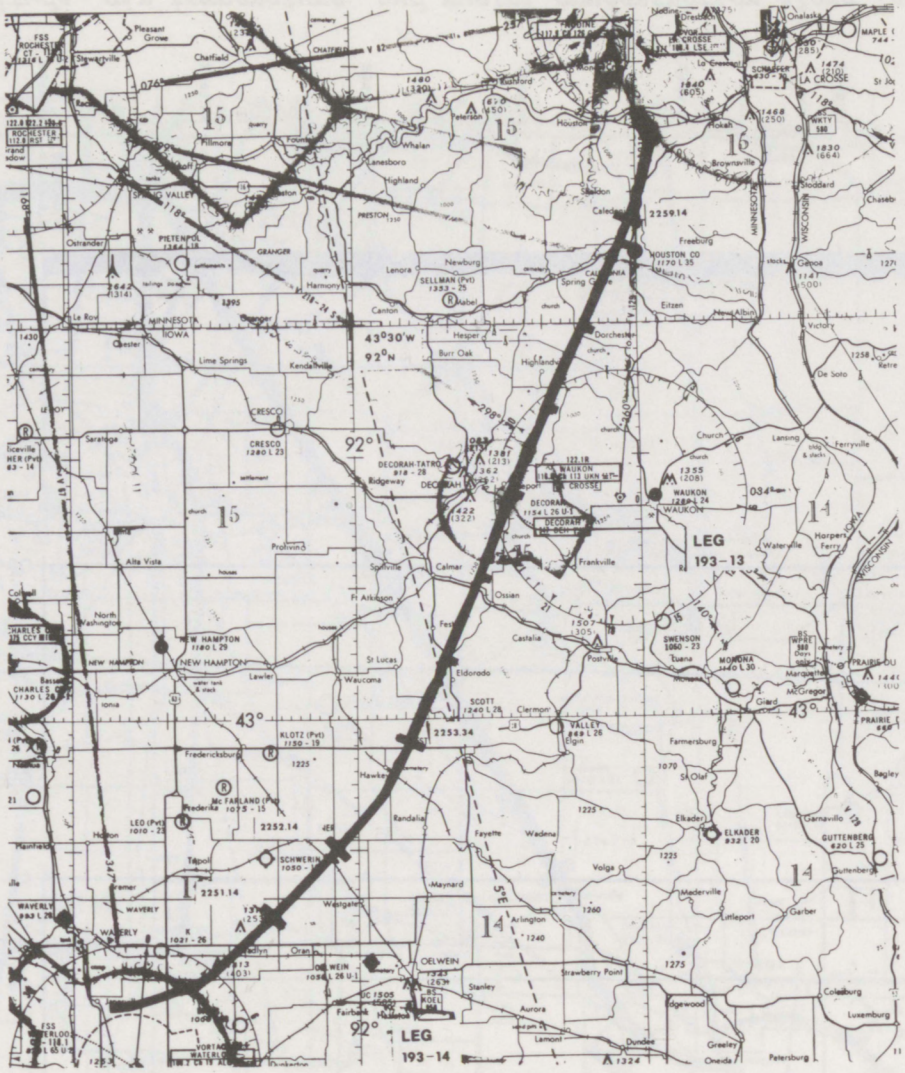

Figure 37. Flight path legs 13-14, flight 1, La Crosse, Wis., storm, July 12, 1971.

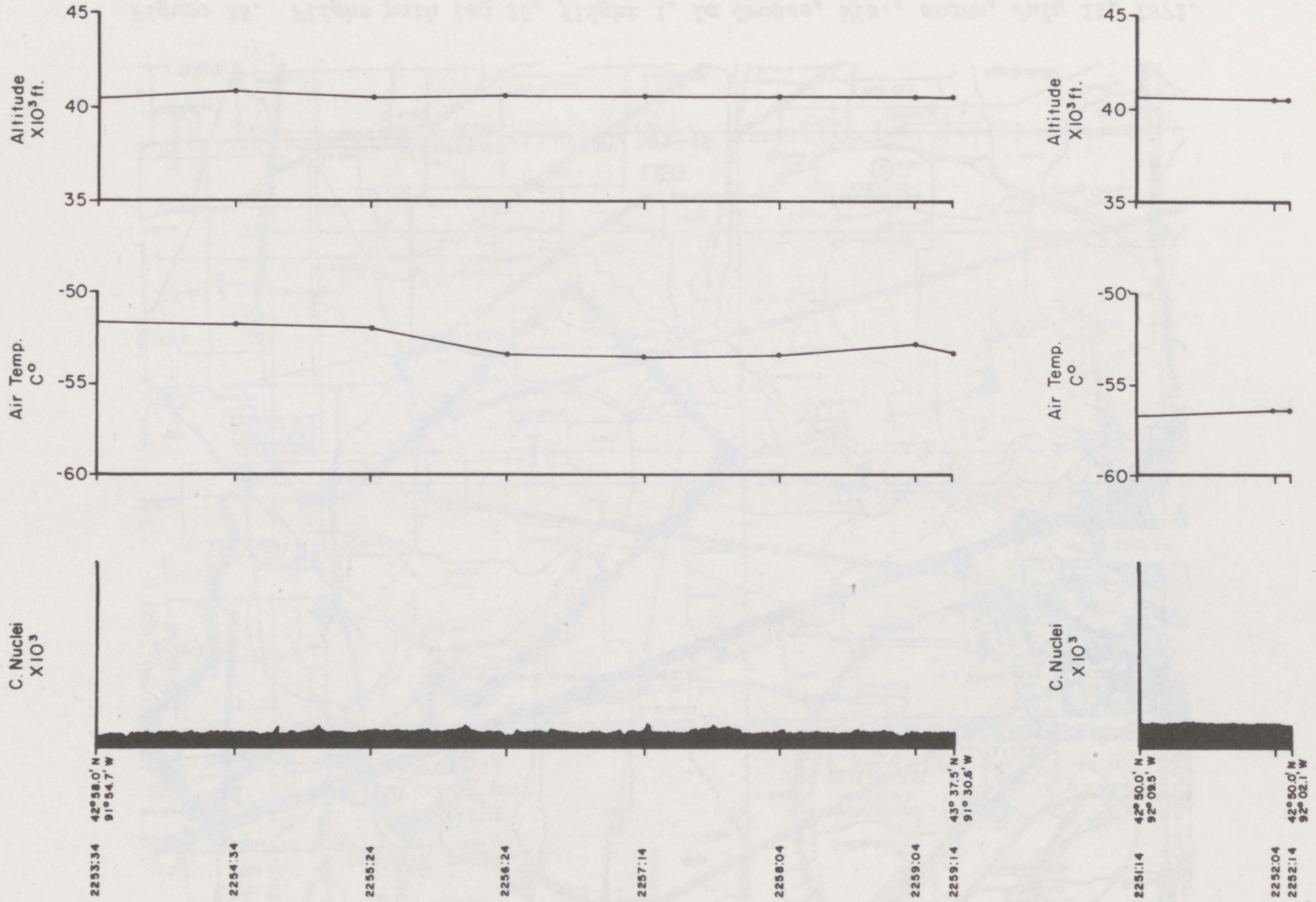

Figure 37A. Altitude, air temperature, and nuclei concentration along legs 13-14, flight 1, La Crosse, Wis., storm, July 12, 1971.

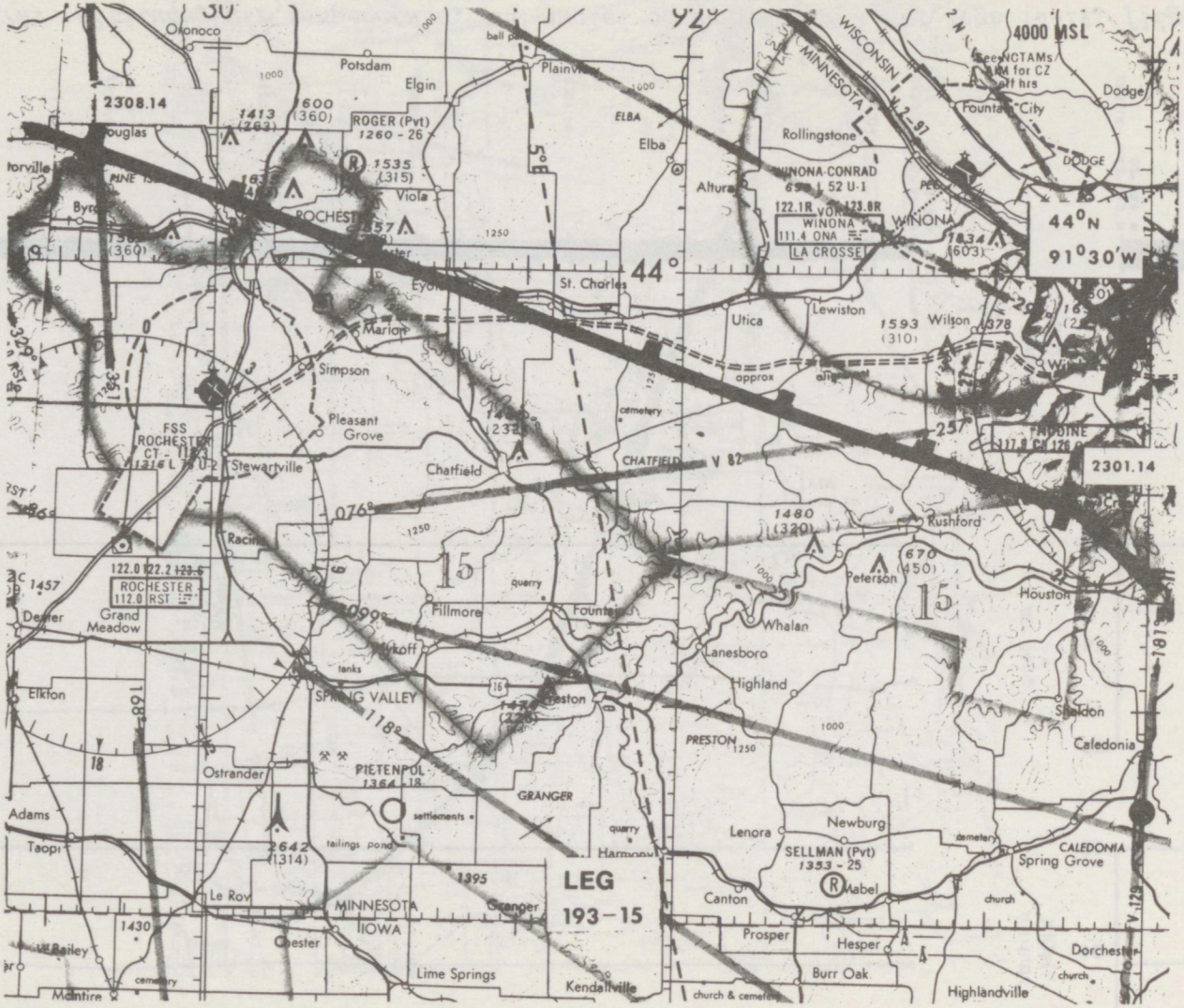

Figure 38. Flight path leg 15, flight 1, La Crosse, Wis., storm, July 12, 1971.

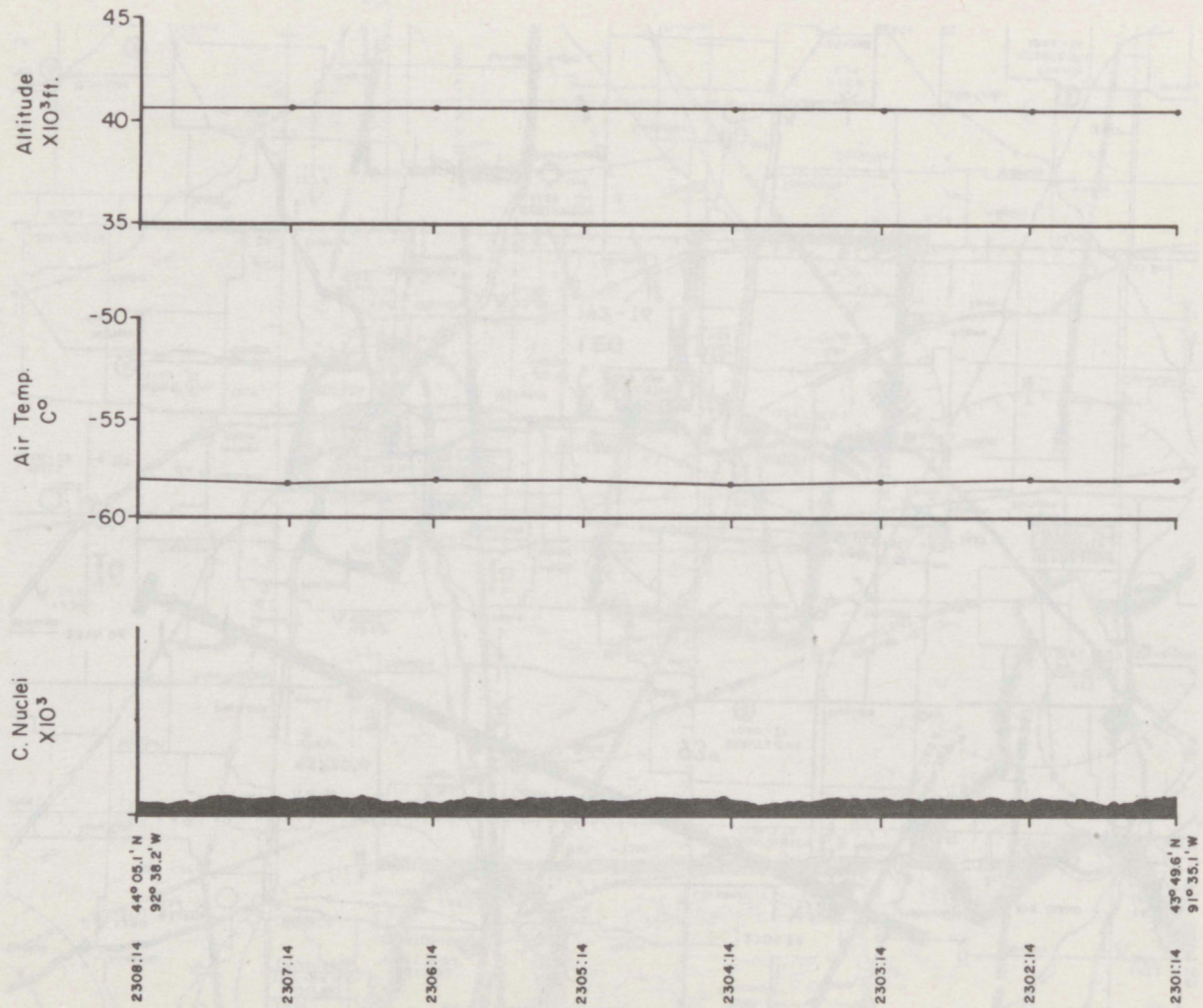

Figure 38A. Altitude, air temperature, and nuclei concentration along leg 15, flight 1, La Crosse, Wis., storm, July 12, 1971.

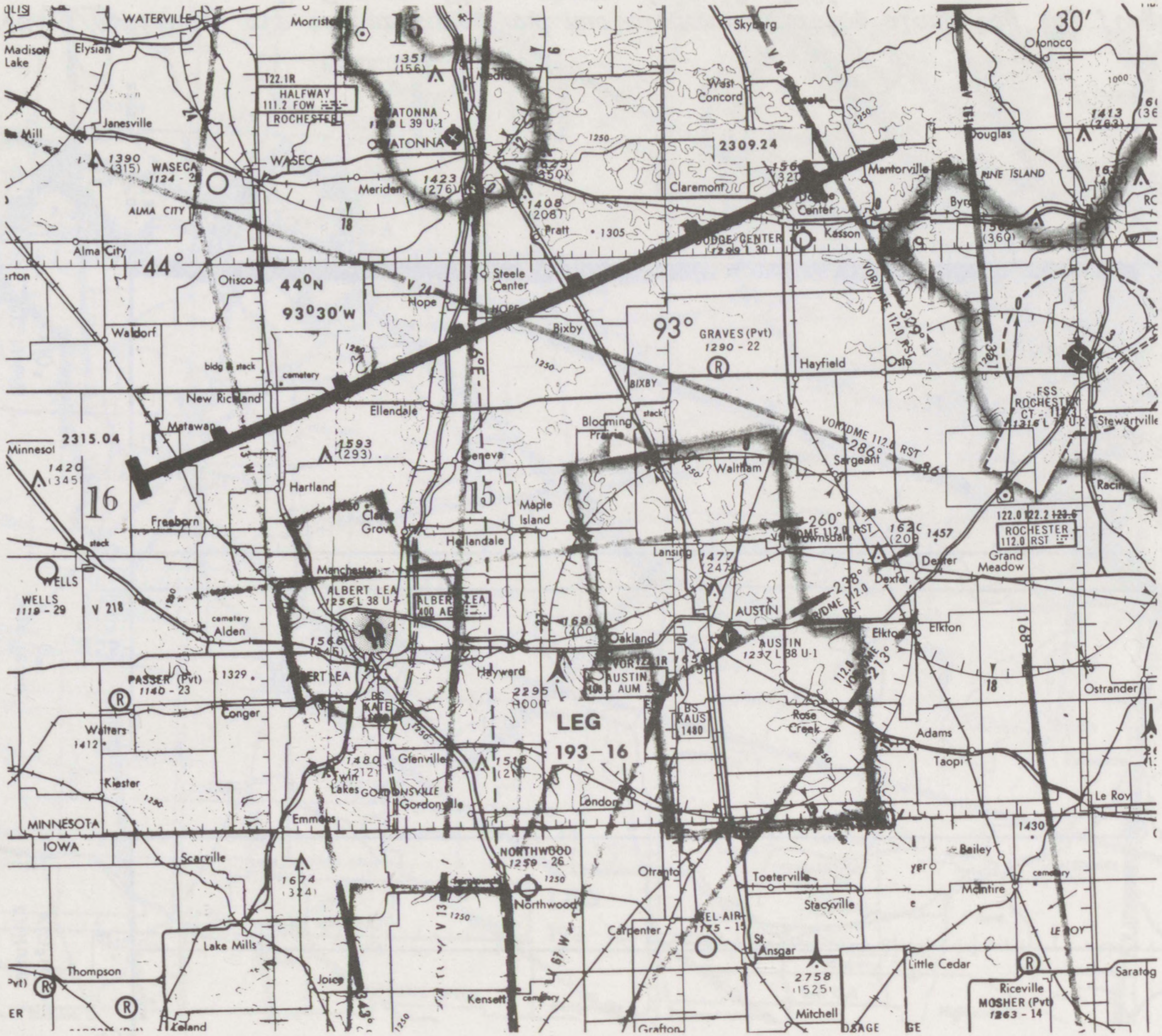

Figure 39. Flight path leg 16, flight 1, La Crosse, Wis., storm, July 12, 1971.

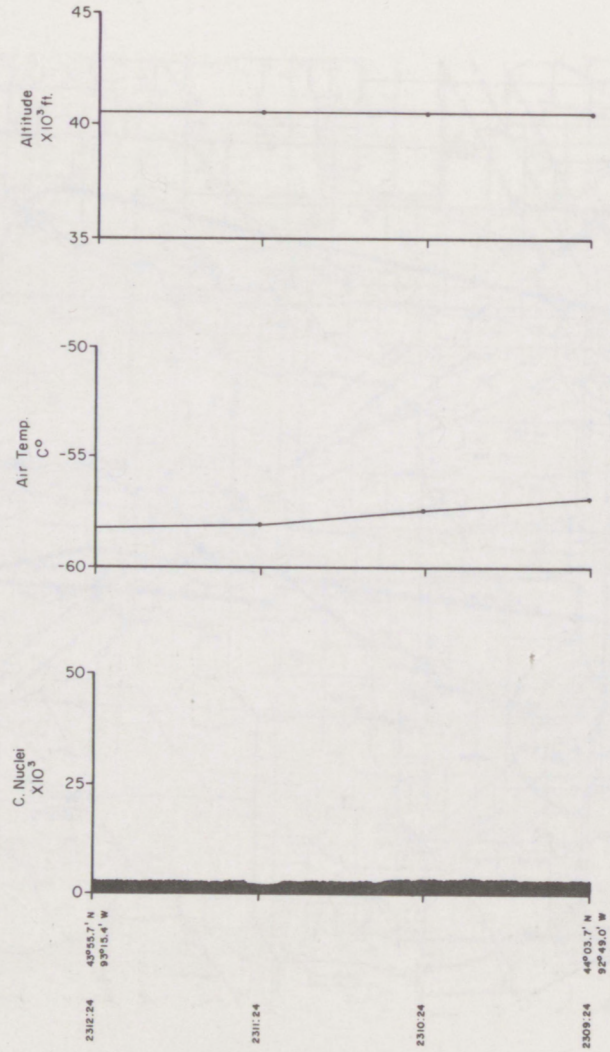

Figure 39A. Altitude, air temperature, and nuclei concentration along leg 16, flight 1, La Crosse, Wis., storm, July 12, 1971.

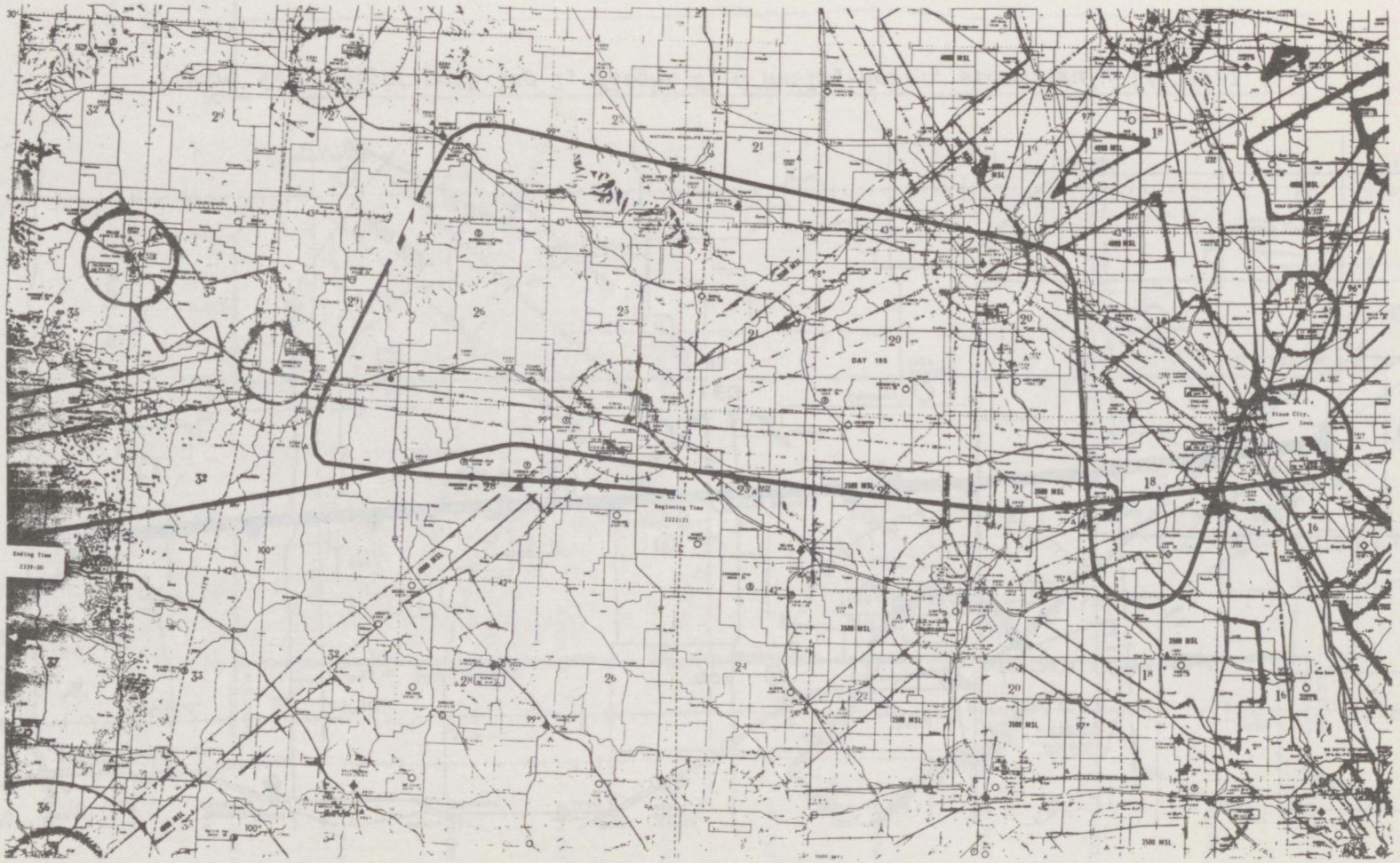

Figure 40. Flight path around the O'Neill, Nebr., storm.

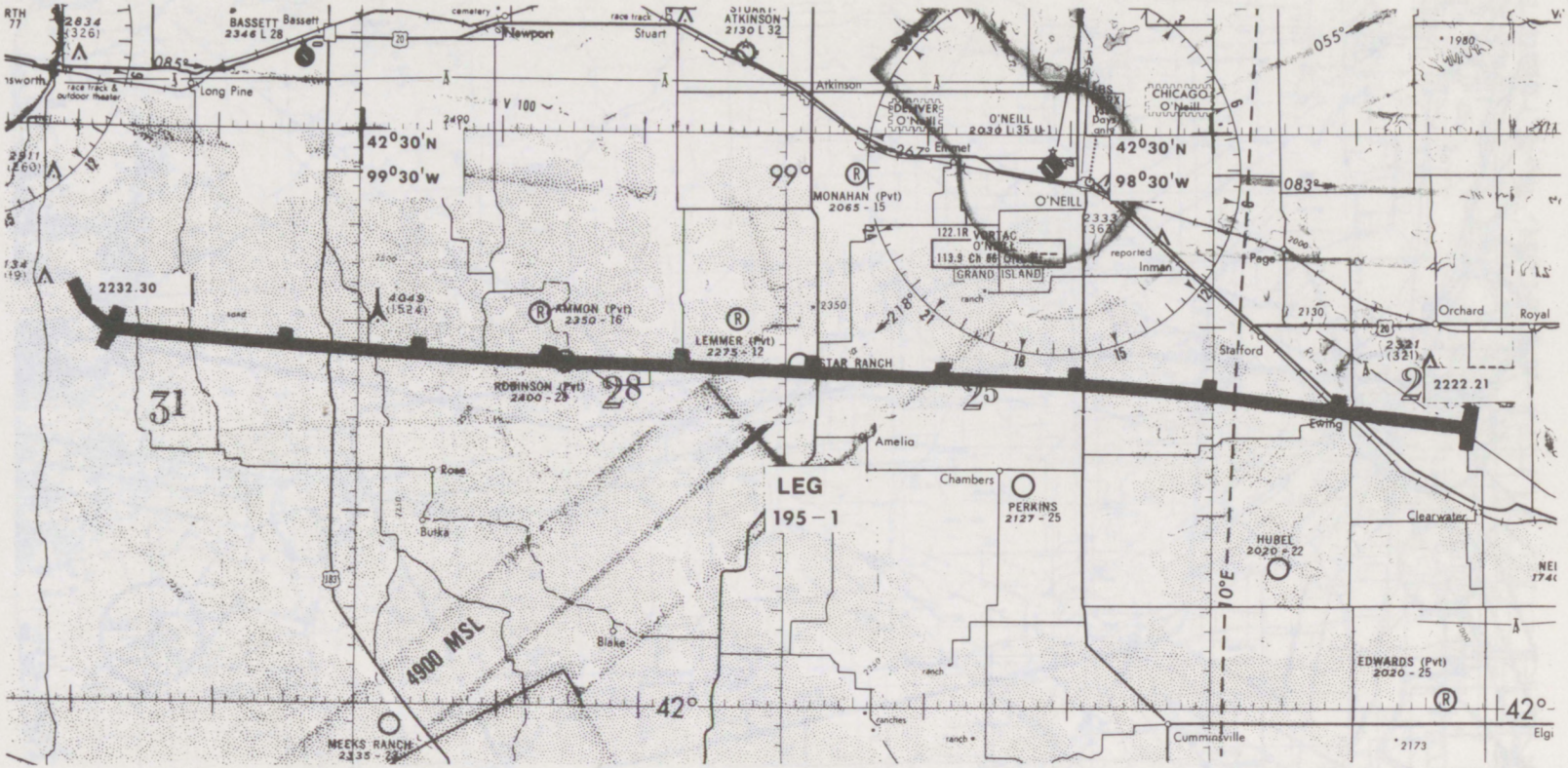

Figure 41. Flight path leg 1, flight 3, O'Neill, Nebr., storm, July 14, 1971.

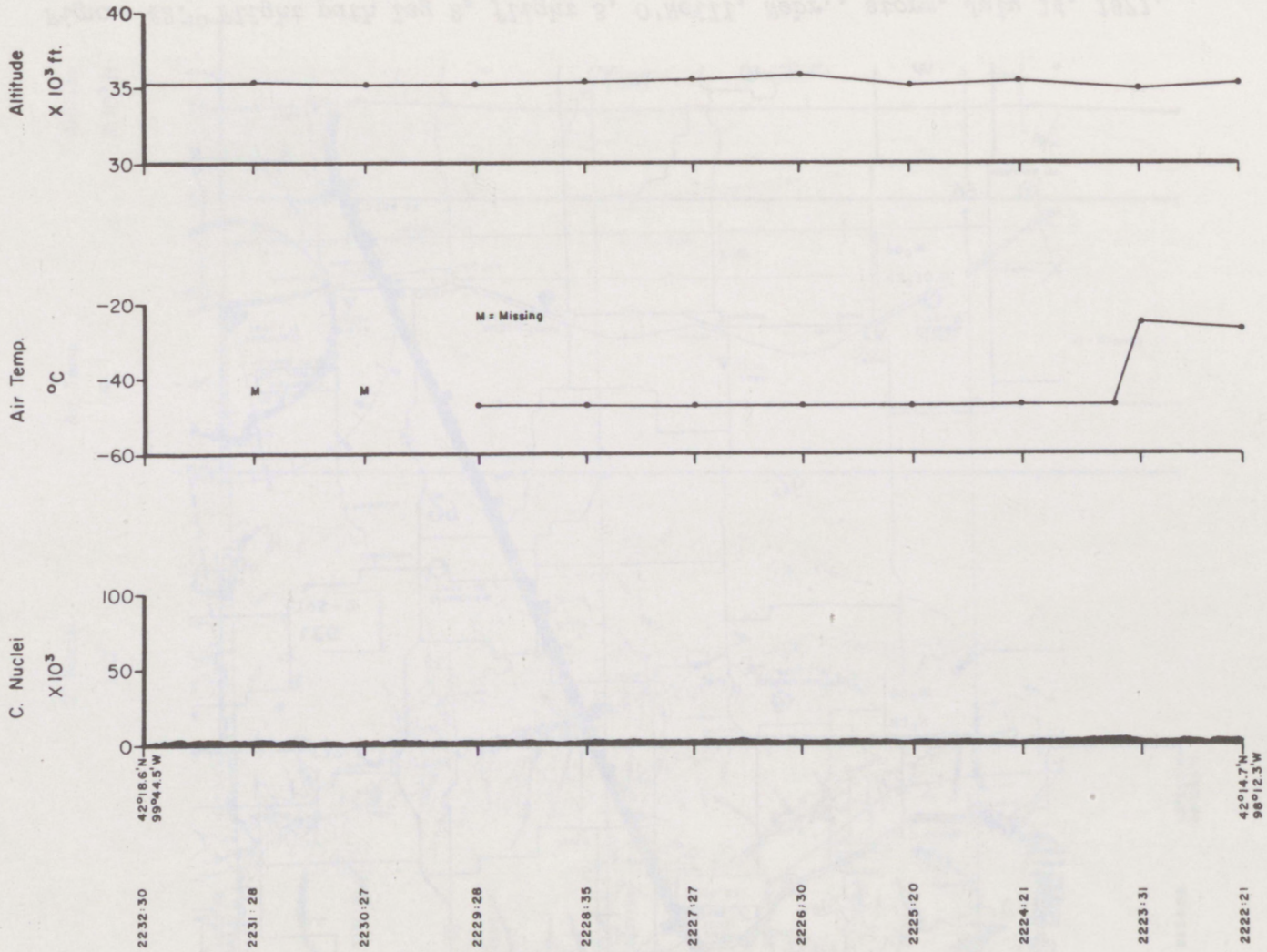

Figure 41A. Altitude, air temperature, and nuclei concentration along leg 1, flight 3, O'Neill, Nebr., storm, July 14, 1971.

Figure 42. Flight path leg 2, flight 3, O'Neill, Nebr., storm, July 14, 1971.

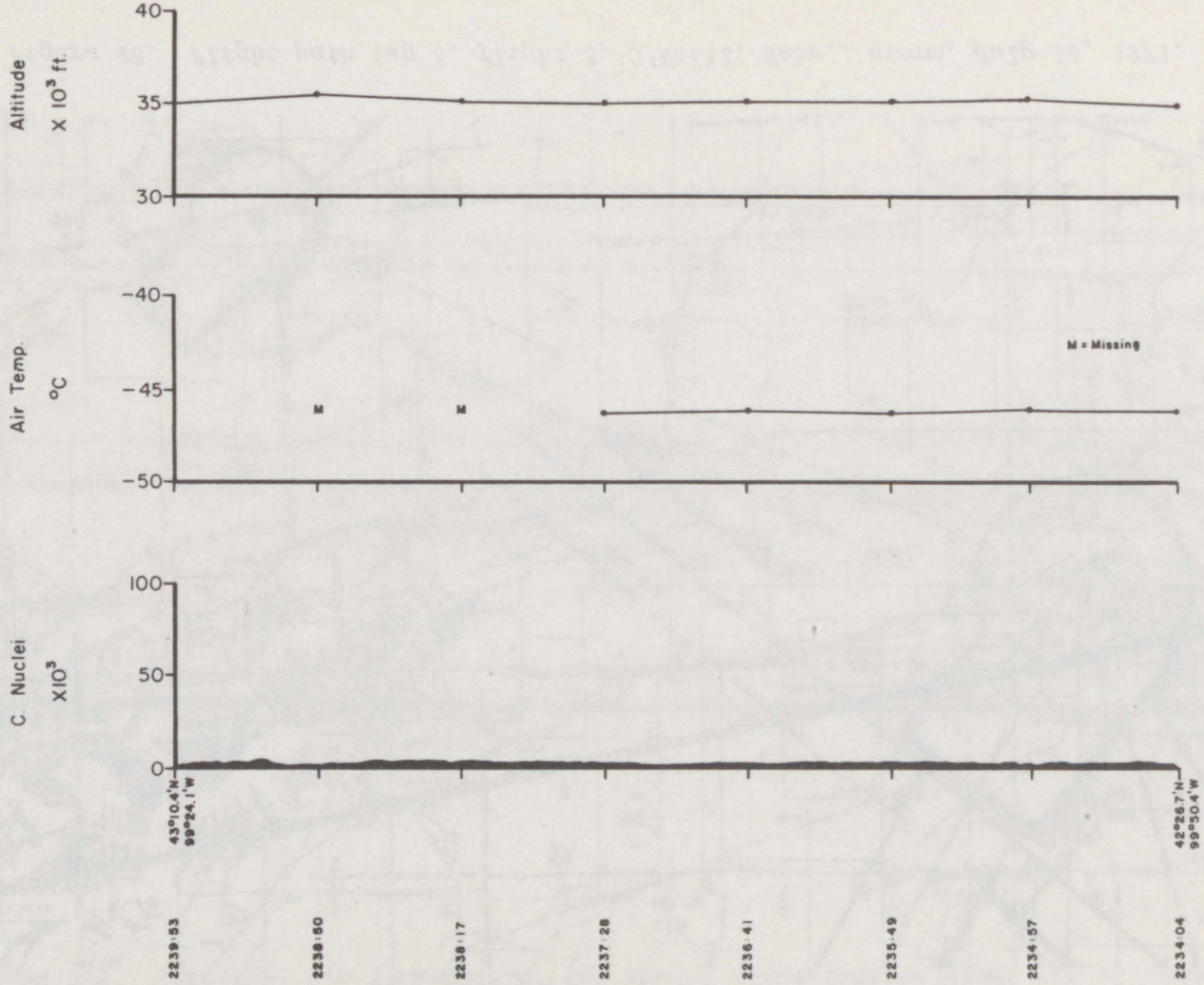

Figure 42A. Altitude, air temperature, and nuclei concentration along leg 2, flight 3, O'Neill, Nebr., storm, July 14, 1971.

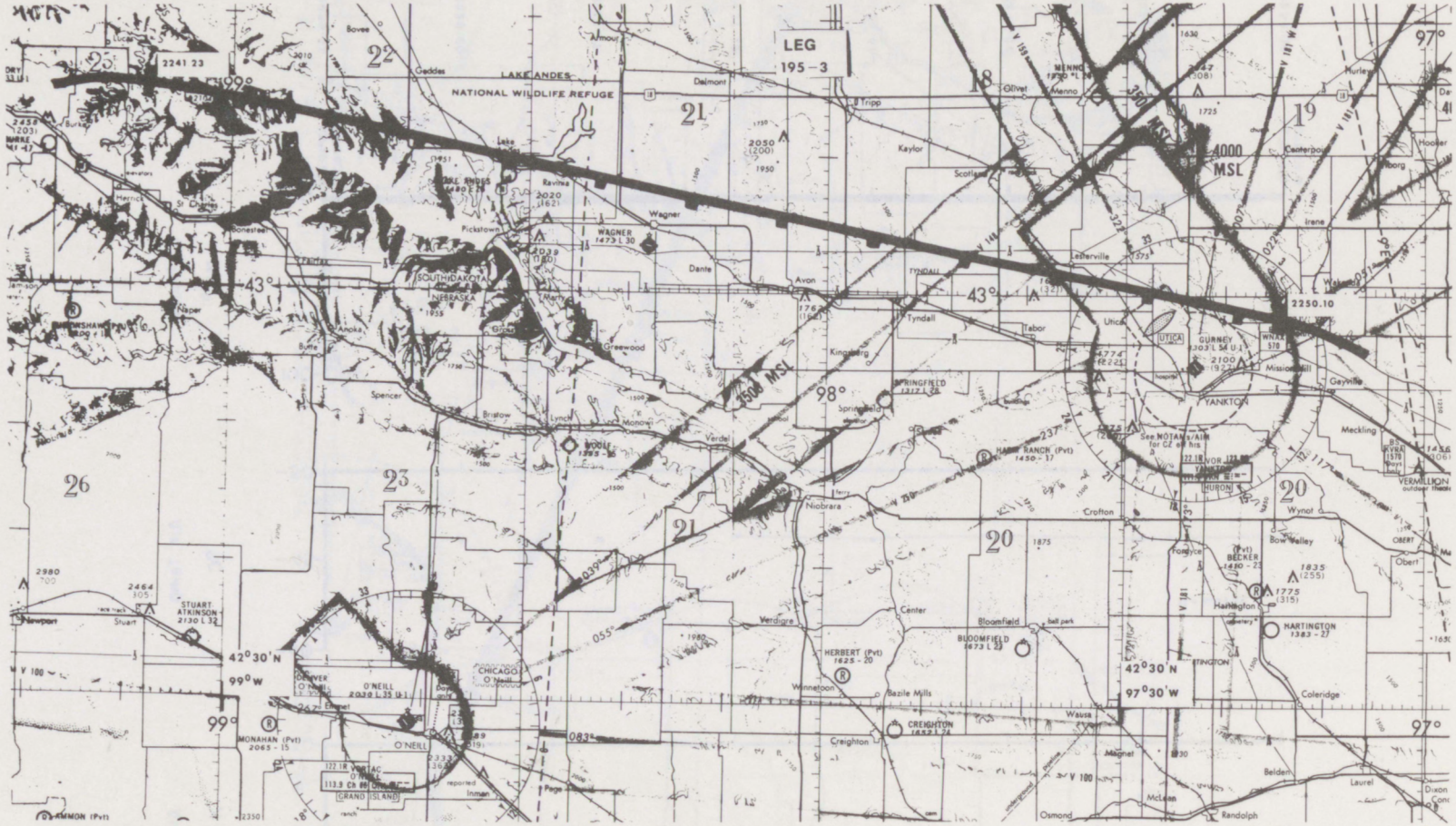

Figure 43. Flight path leg 3, flight 3, O'Neill, Nebr., storm, July 14, 1971.

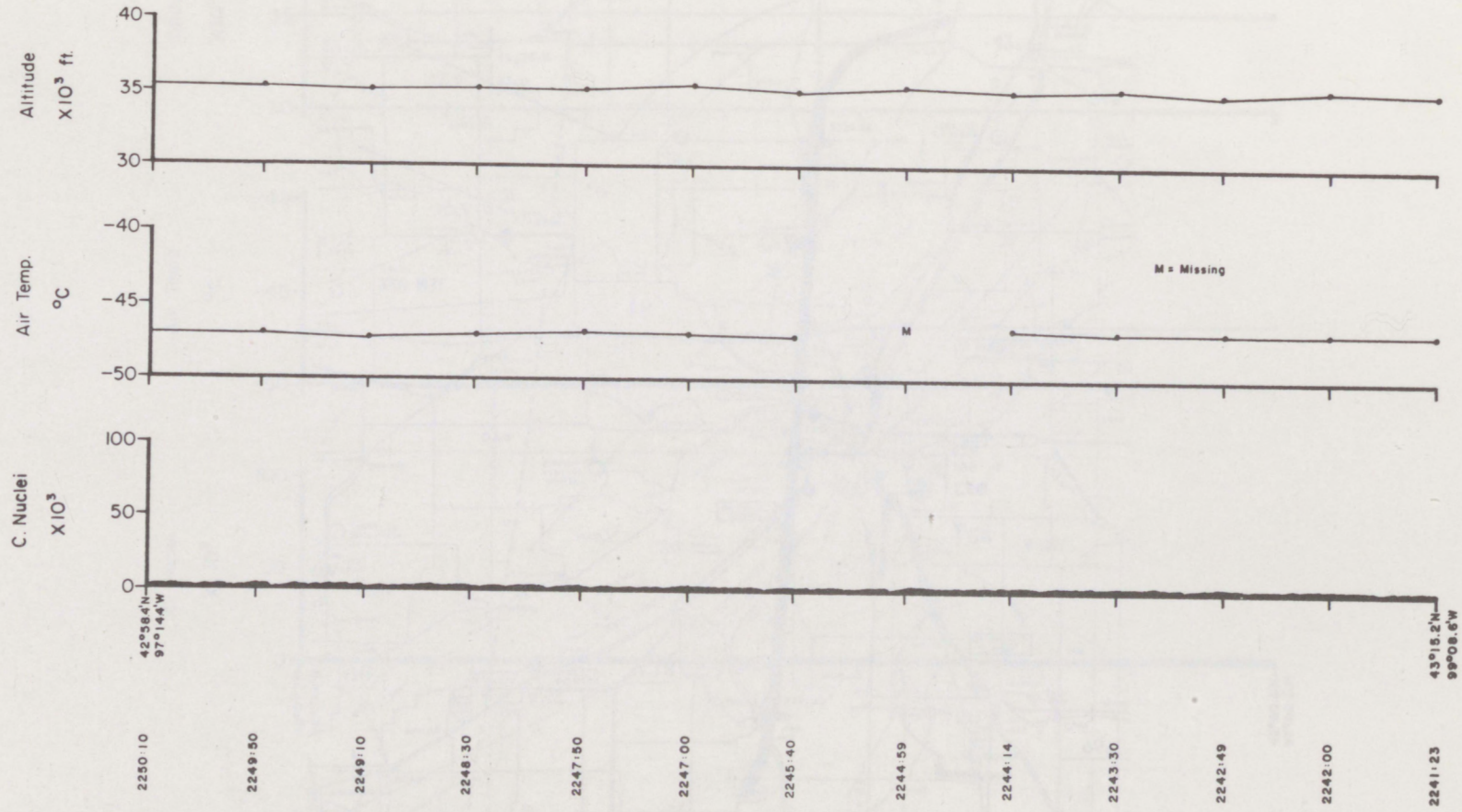

Figure 43A. Altitude, air temperature, and nuclei concentration along leg 3, flight 3, O'Neill, Nebr., storm, July 14, 1971.

Figure 44. Flight path leg 4, flight 3, O'Neill, Nebr., storm, July 14, 1971.

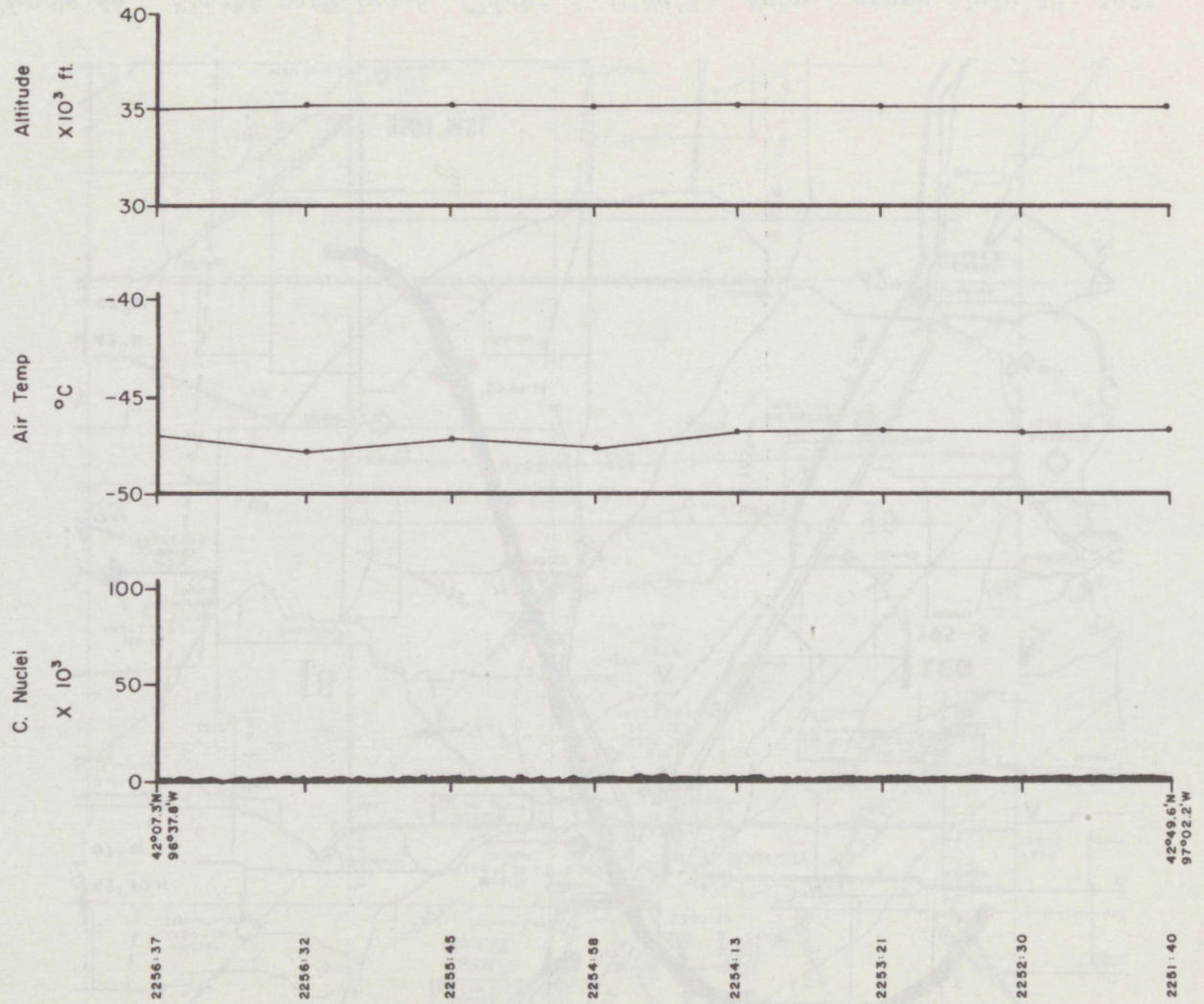

Figure 44A. Altitude, air temperature, and nuclei concentration along leg 4, flight 3, O'Neill, Nebr., storm, July 14, 1971.

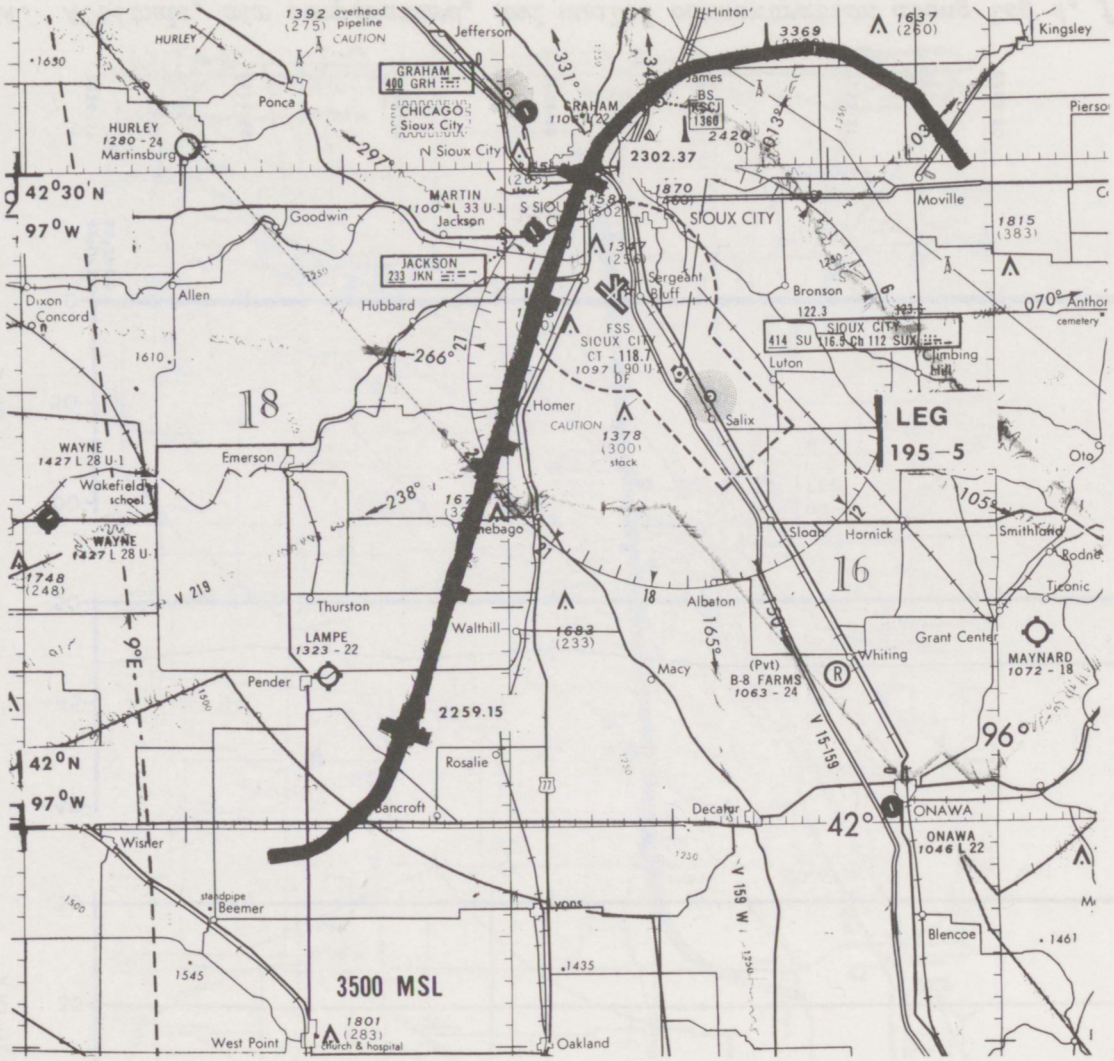

Figure 45. Flight path leg 5, flight 3, O'Neill, Nebr., storm, July 14, 1971.

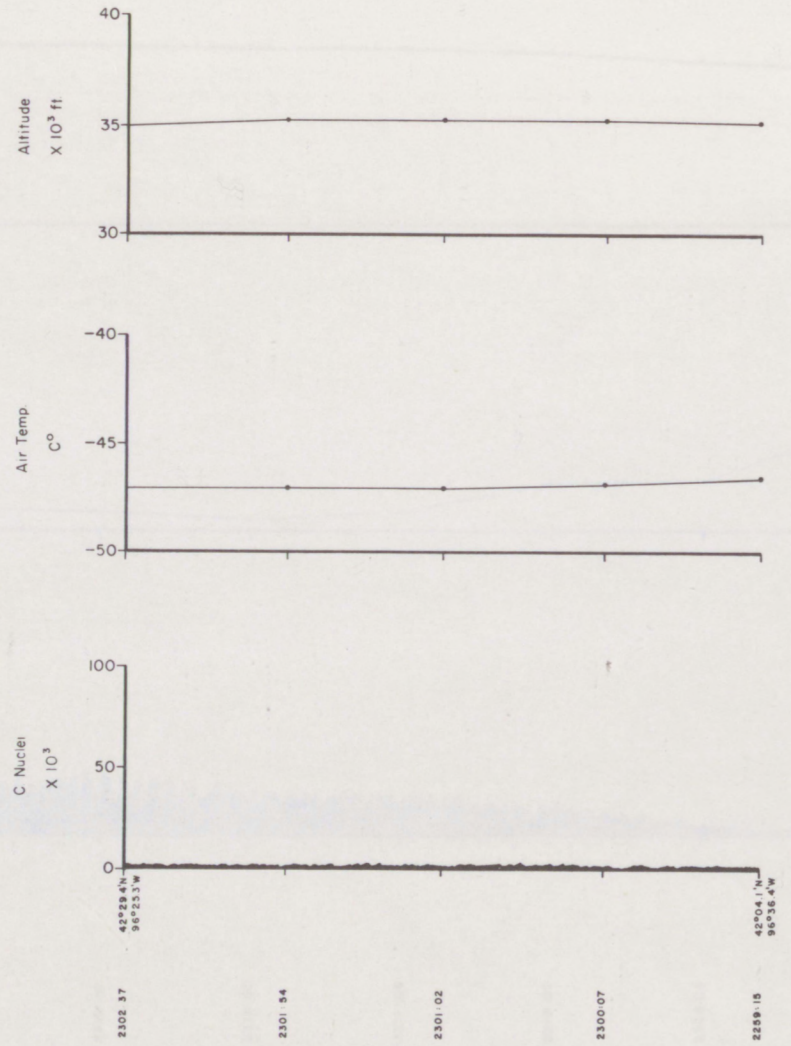

Figure 45A. Altitude, air temperature, and nuclei concentration along leg 5, flight 3, O'Neill, Nebr., storm, July 14, 1971.

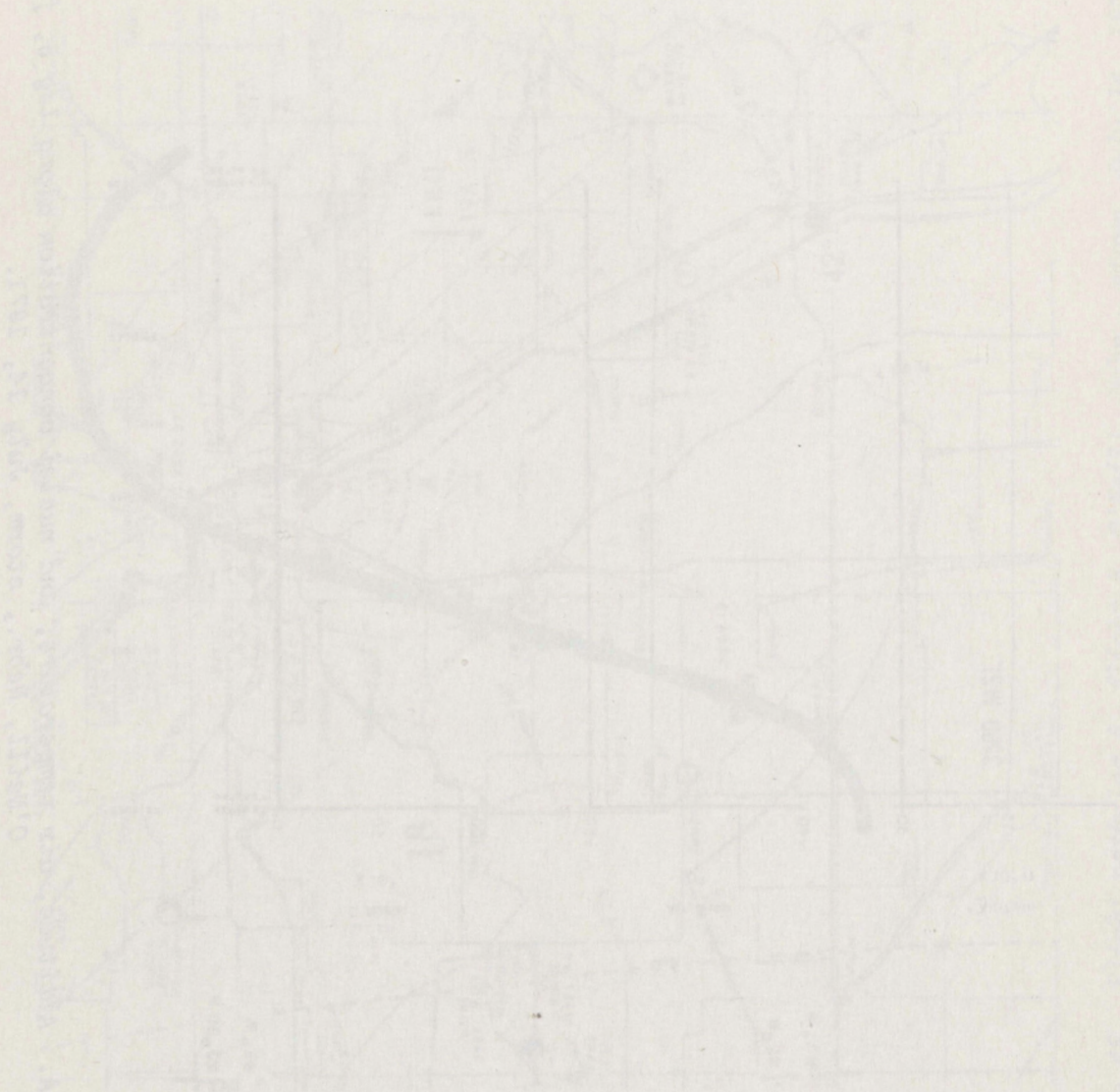

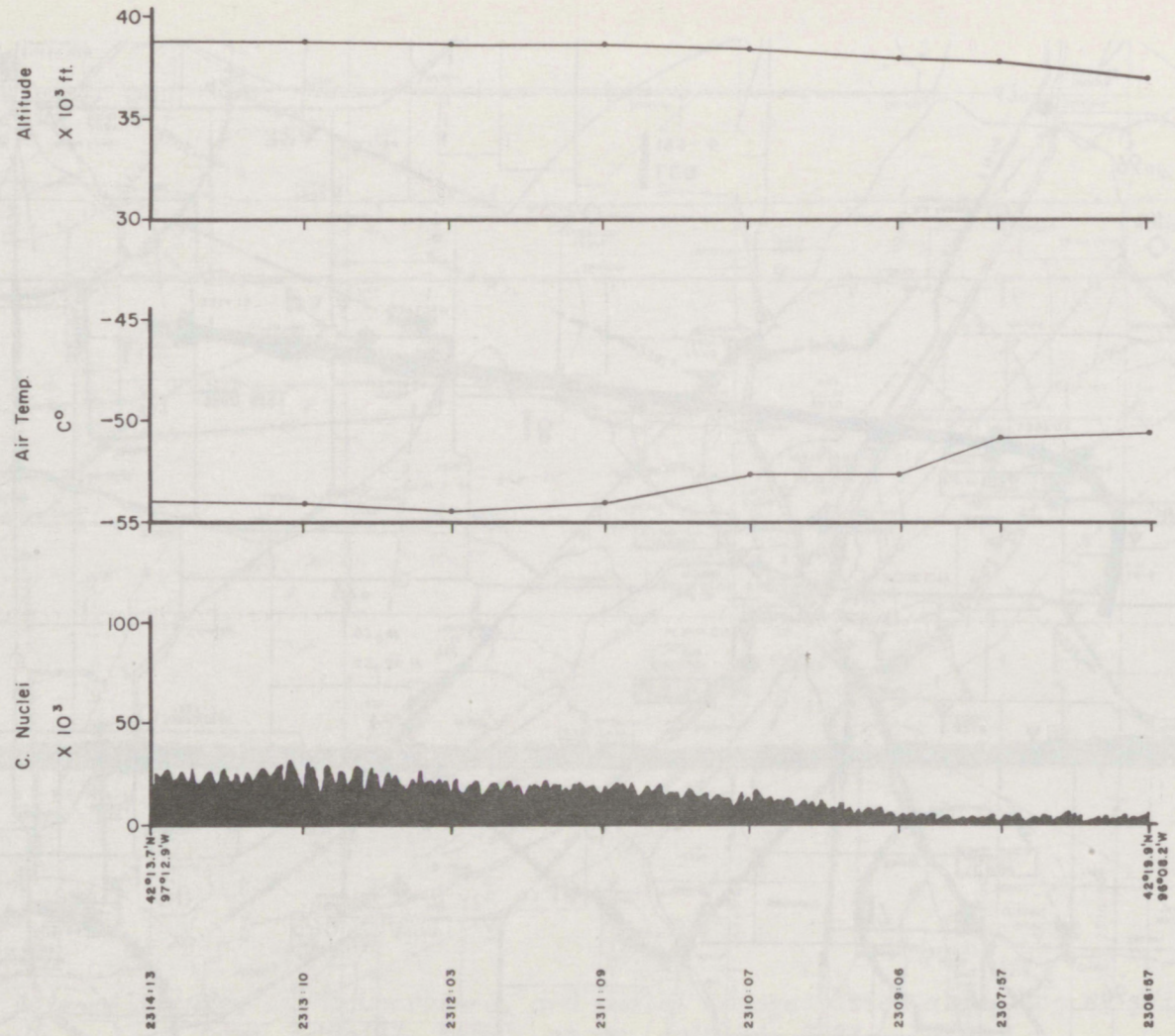

Figure 45B. Altitude, air temperature, and nuclei concentration along leg 5, flight 3, O'Neill, Nebr., storm, July 14, 1971 (continued).

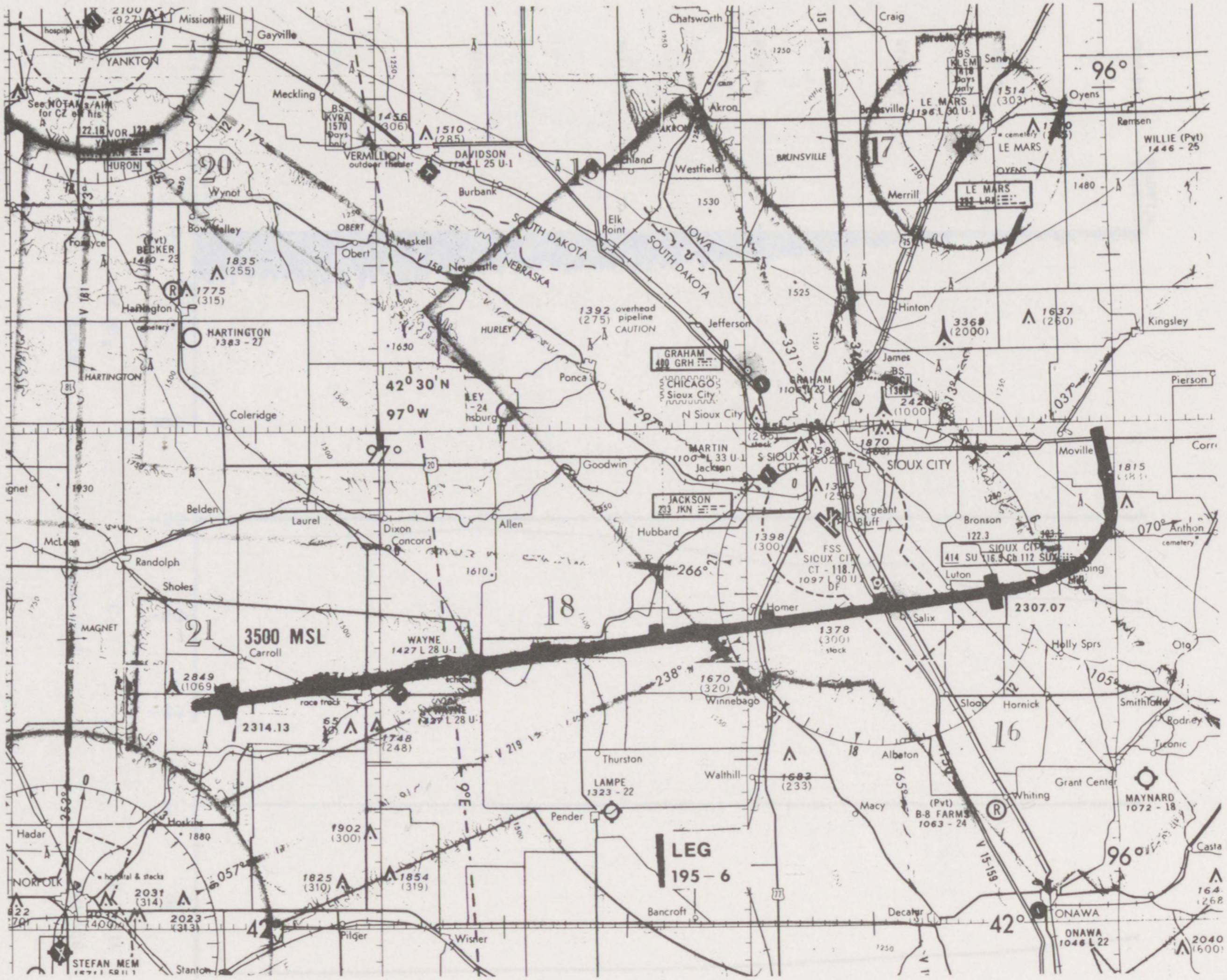

Figure 46. Flight path leg 6, flight 3, O'Neill, Nebr., storm, July 14, 1971.

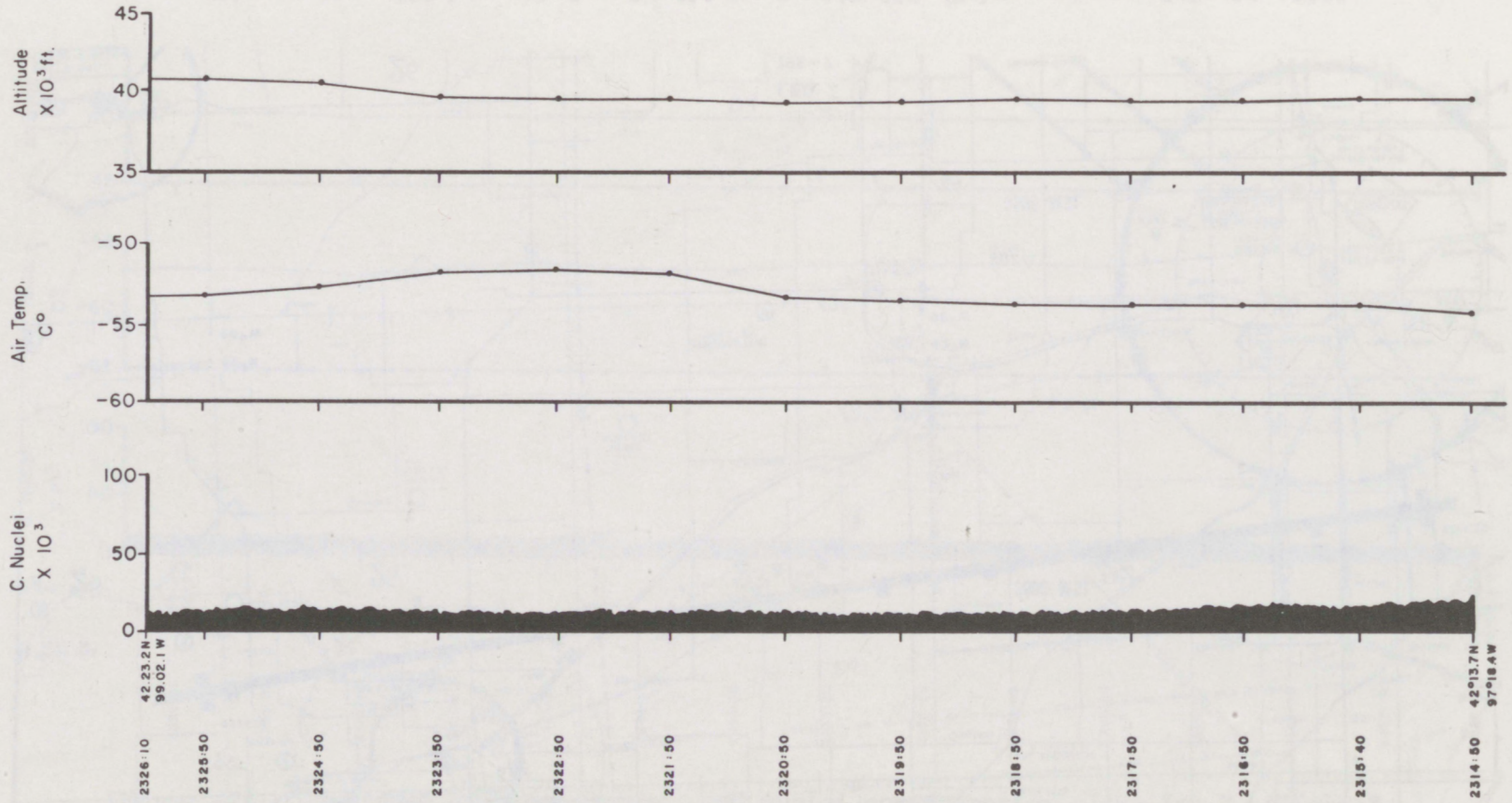

Figure 46A. Altitude, air temperature, and nuclei concentration along leg 6, flight 3, O'Neill, Nebr., storm, July 14, 1971.

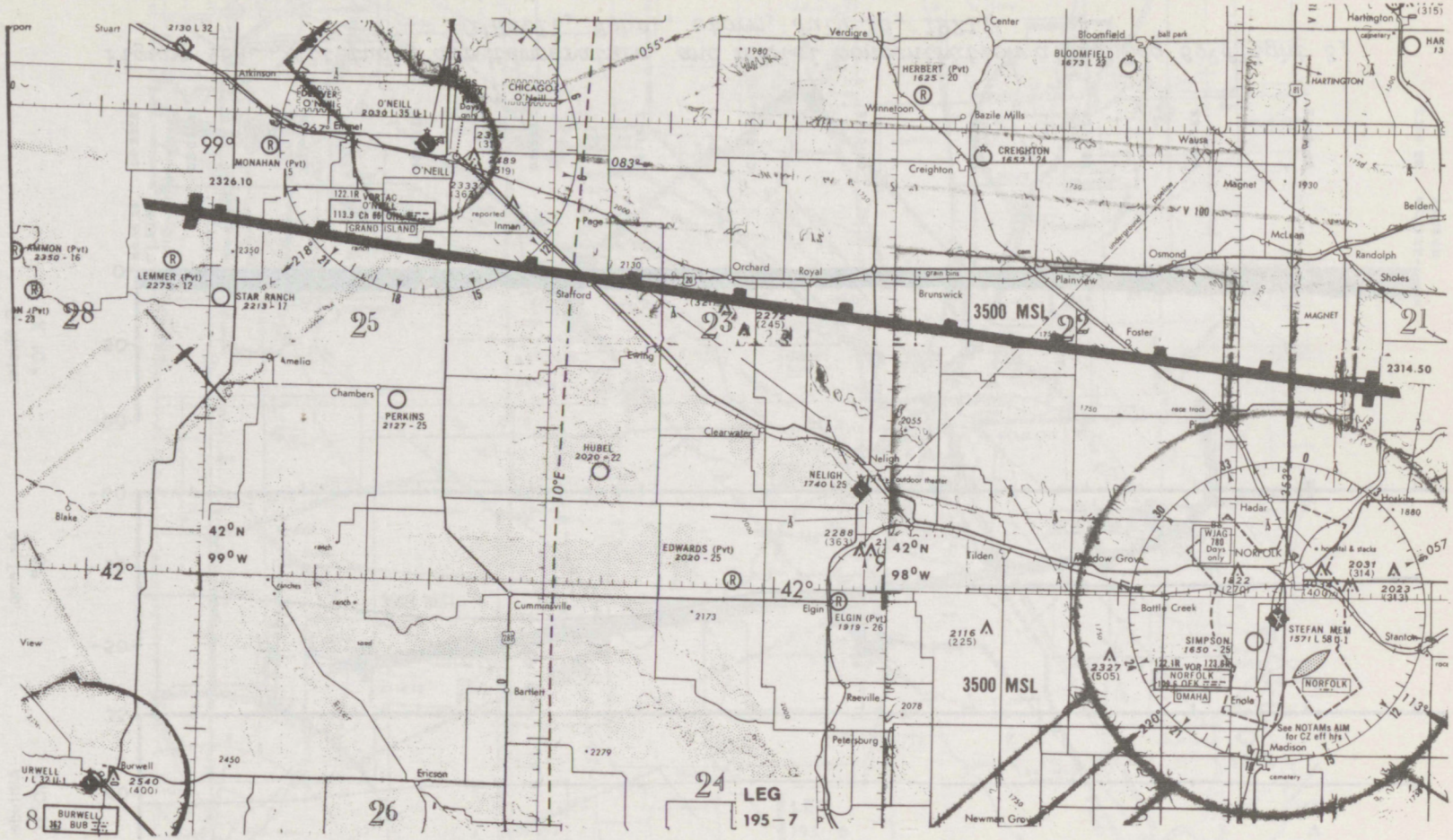

Figure 47. Flight path leg 7, flight 3, O'Neill, Nebr., storm, July 14, 1971.

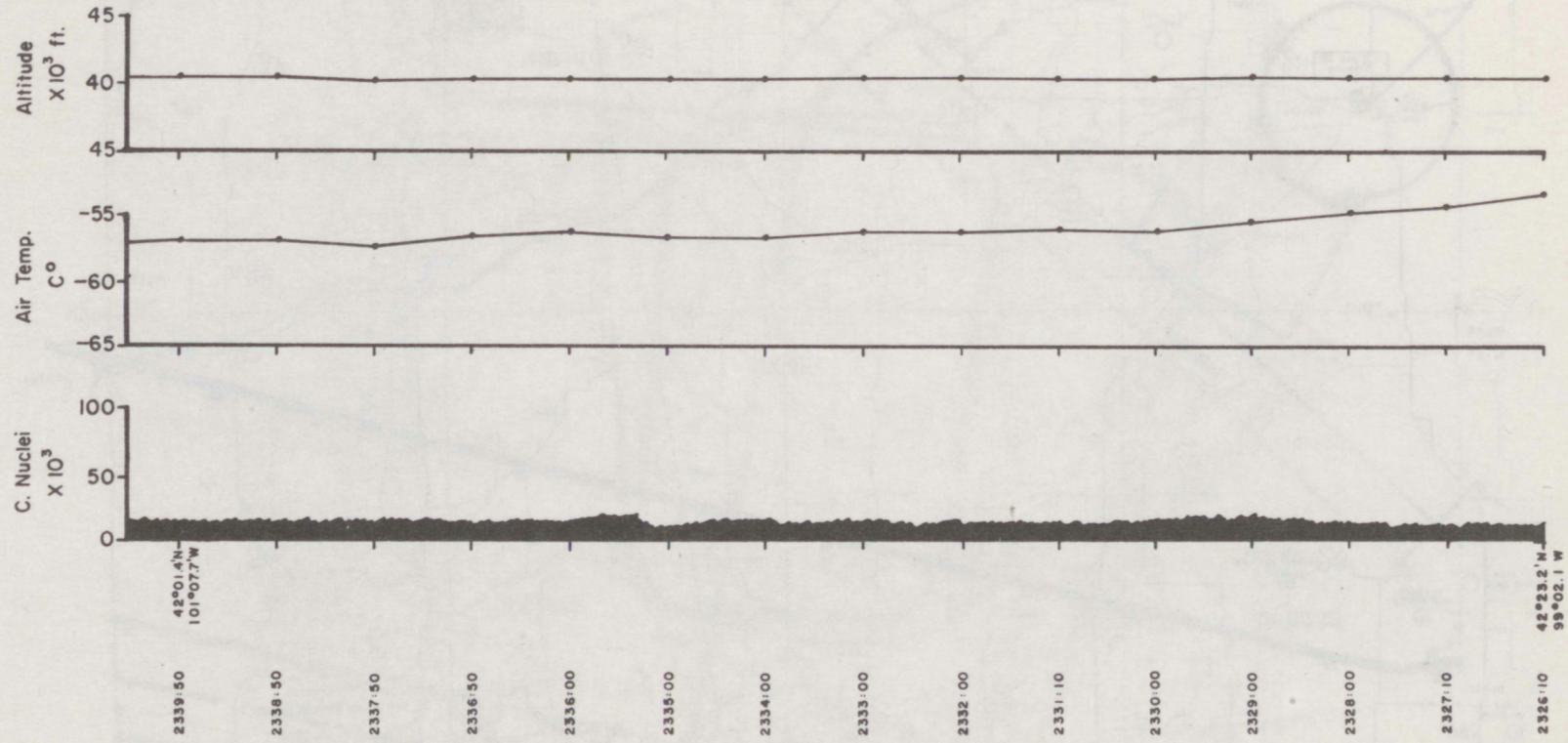

Figure 47A. Altitude, air temperature, and nuclei concentration along leg 7, flight 3, O'Neill, Nebr., storm, July 14, 1971.

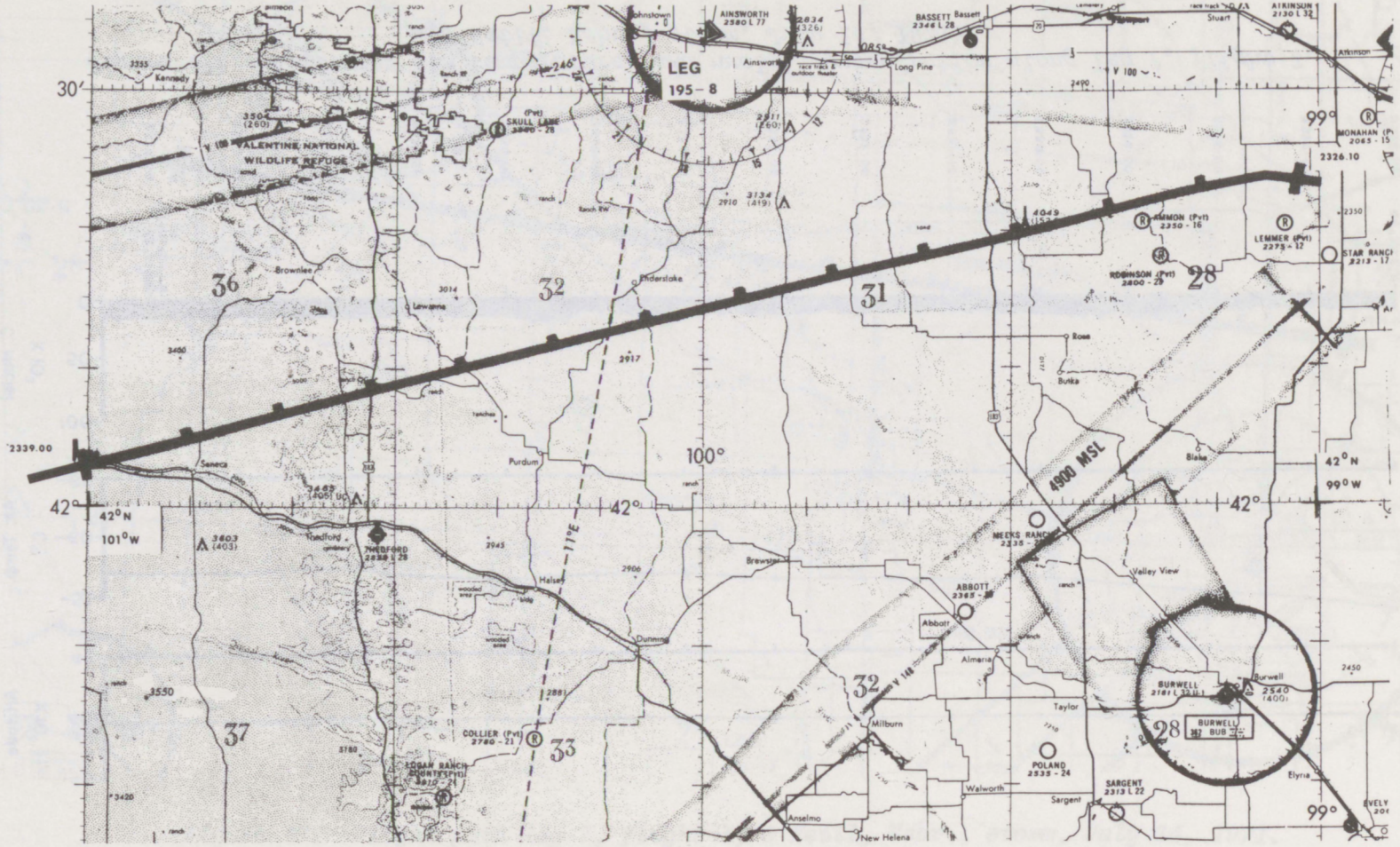

Figure 48. Flight path leg 8, flight 3, O'Neill, Nebr., storm, July 14, 1971. (Flight line between O'Neill storm and Grover, Colo., storm.)

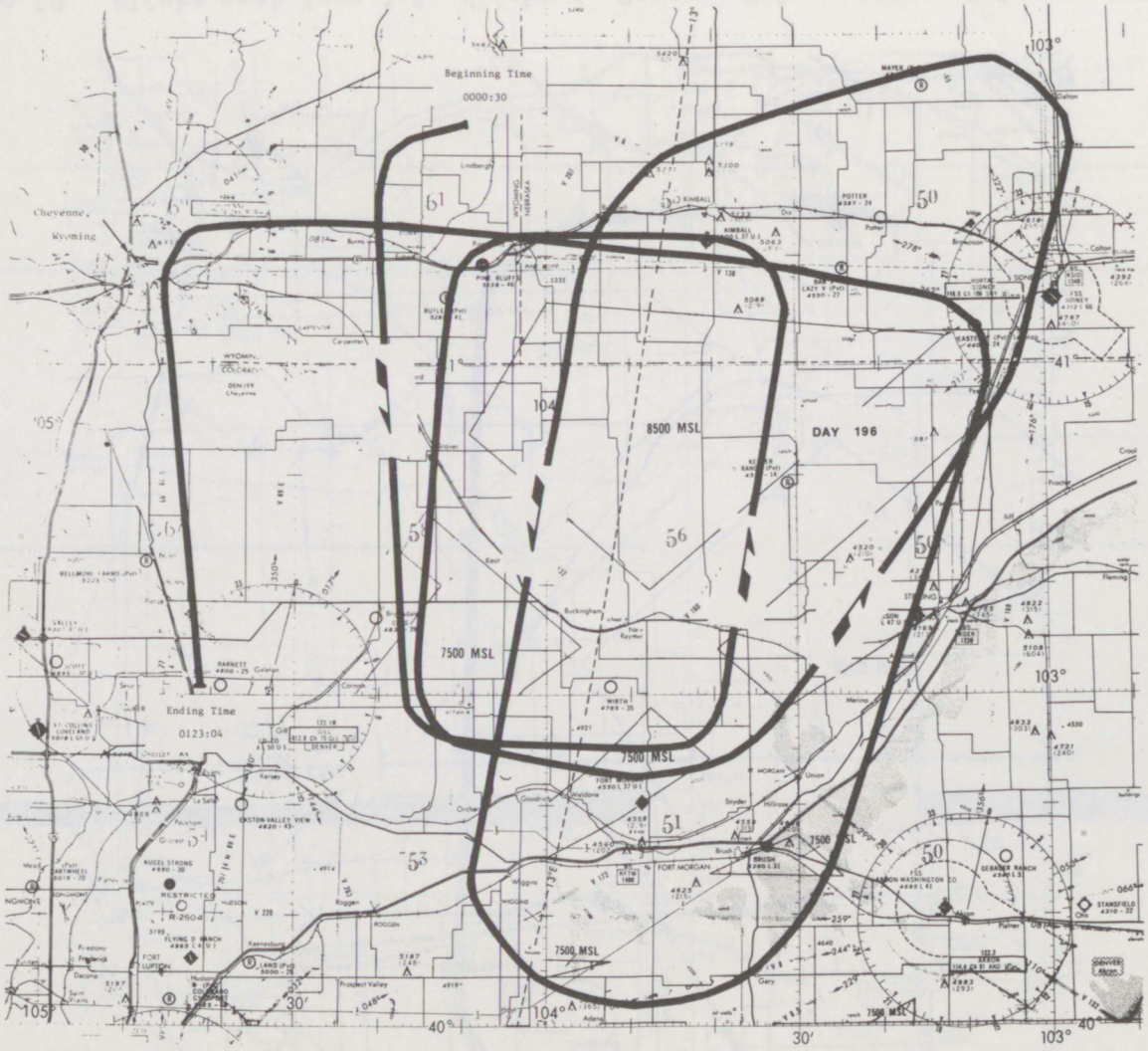

Figure 49. Flight path around the Grover, Colo., storm.

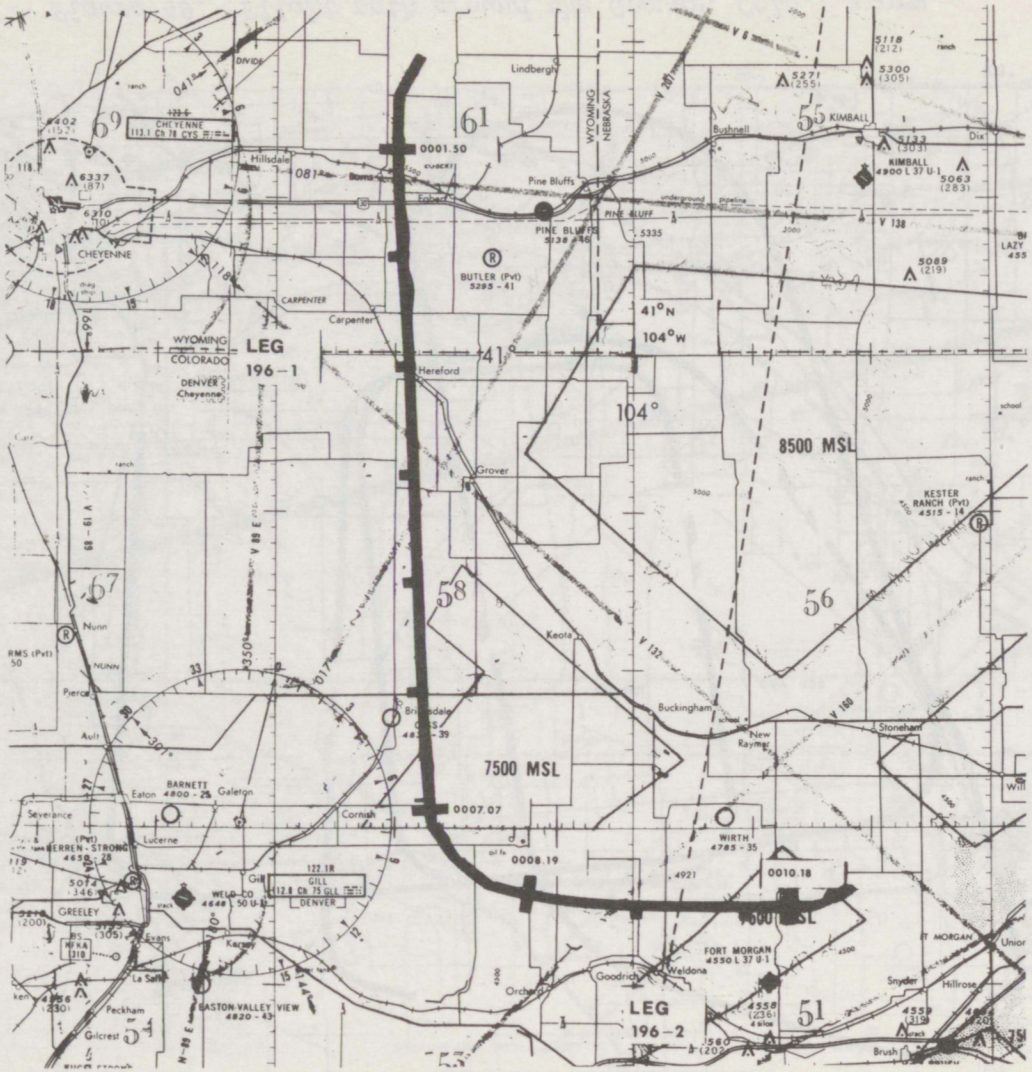

Figure 50. Flight path legs 1-2, flight 4, Grover, Colo., storm, July 15, 1971.

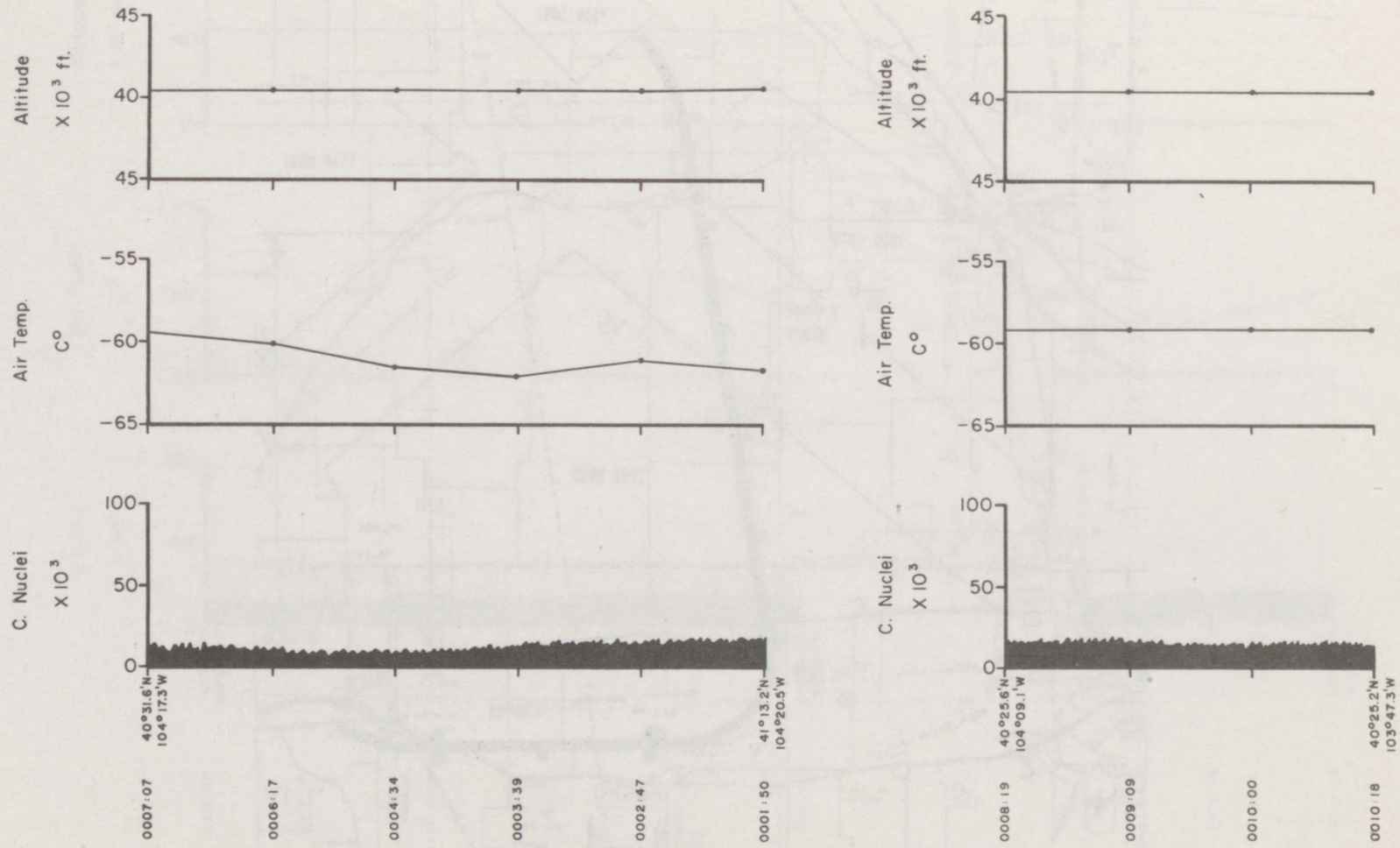

Figure 50A. Altitude, air temperature, and nuclei concentration along legs 1-2, flight 4, Grover, Colo., storm, July 15, 1971.

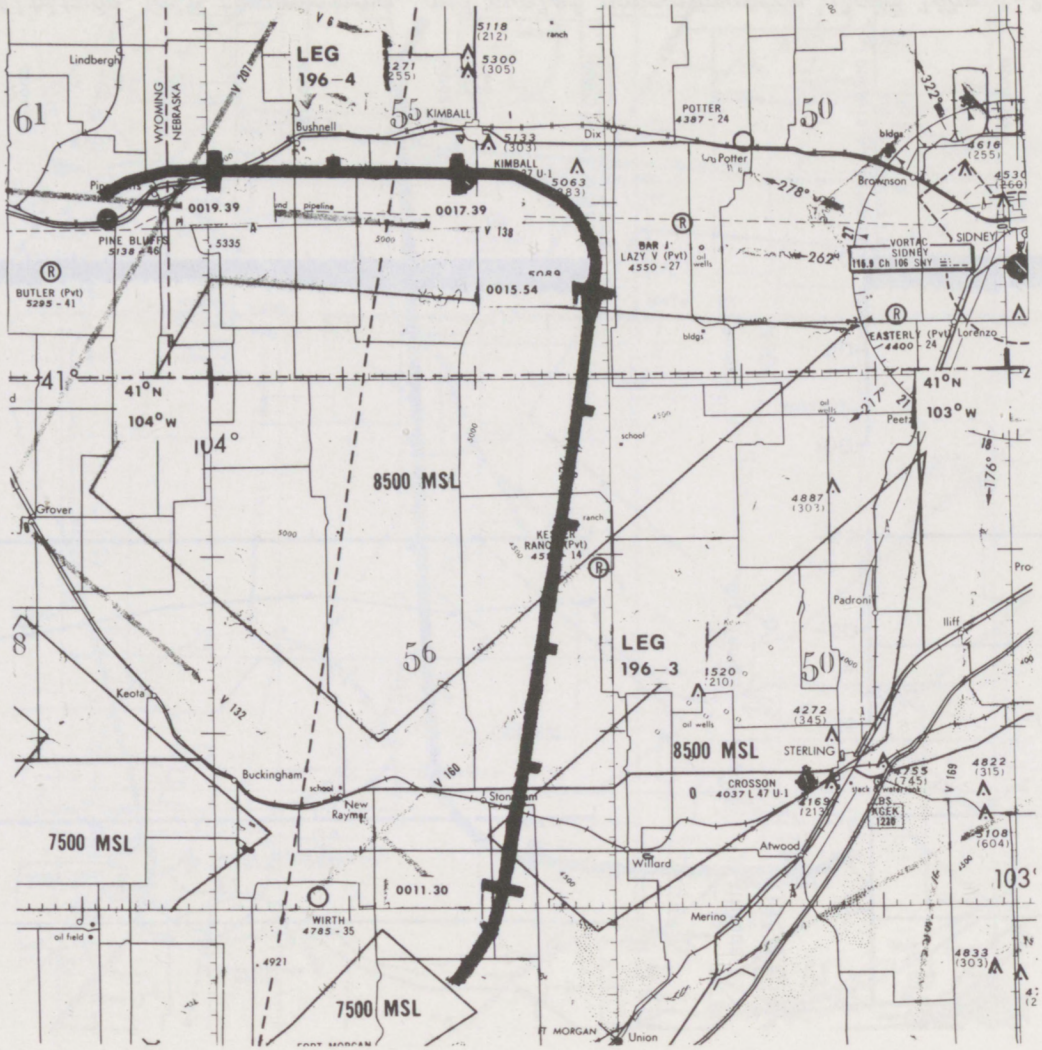

Figure 51. Flight path legs 3-4, flight 4, Grover, Colo., storm, July 15, 1971.

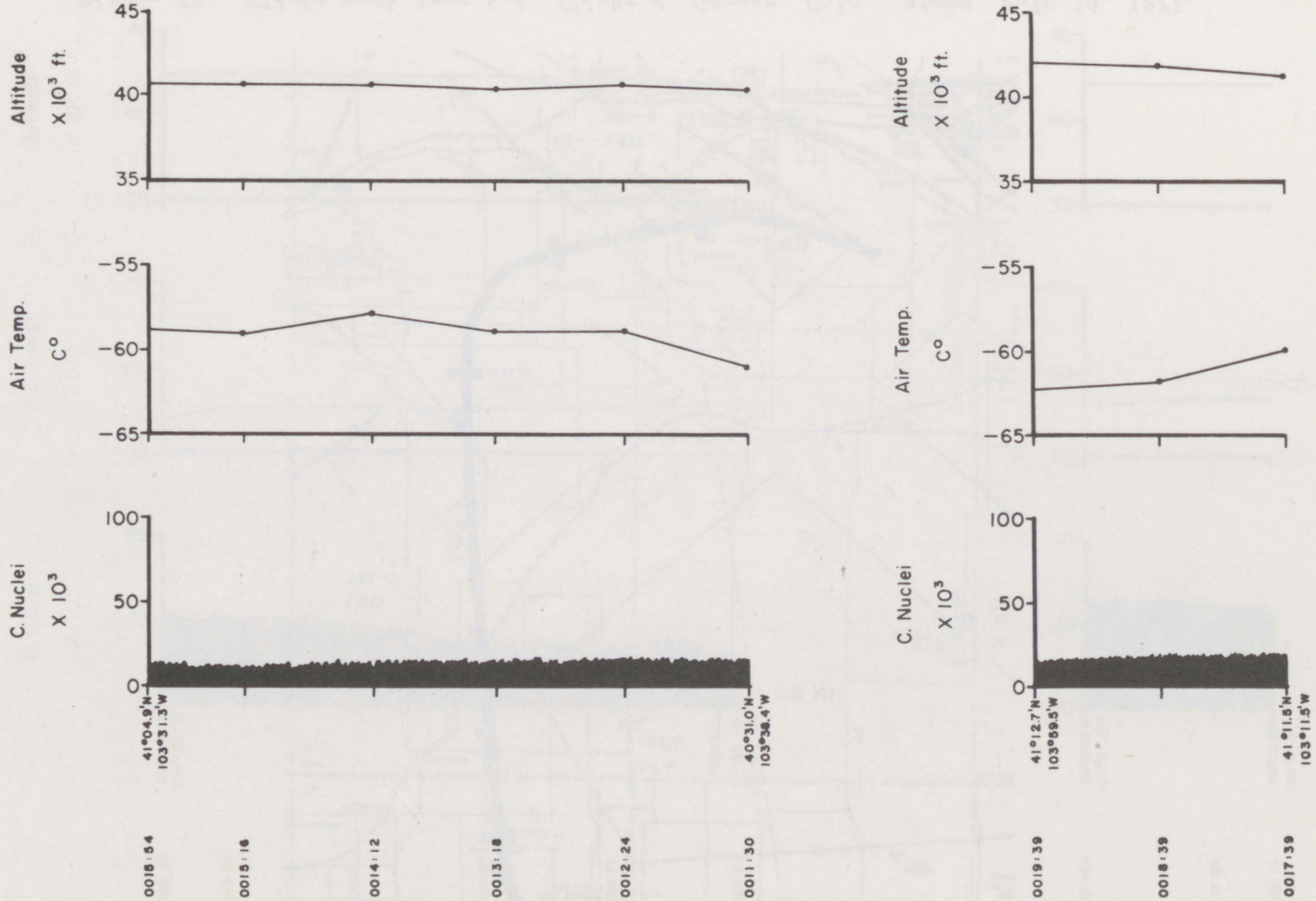

Figure 51A. Altitude, air temperature, and nuclei concentration along legs 3-4, flight 4, Grover, Colo., storm, July 15, 1971.

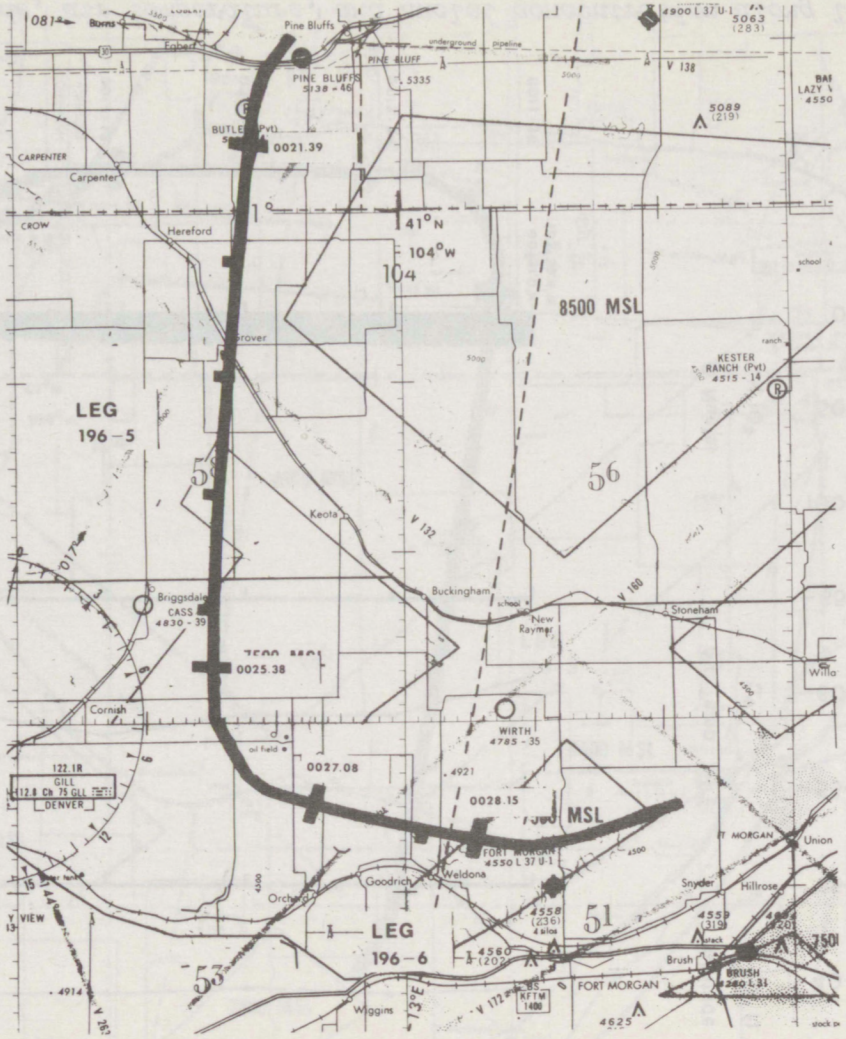

Figure 52. Flight path legs 5-6, flight 4, Grover, Colo., storm, July 15, 1971.

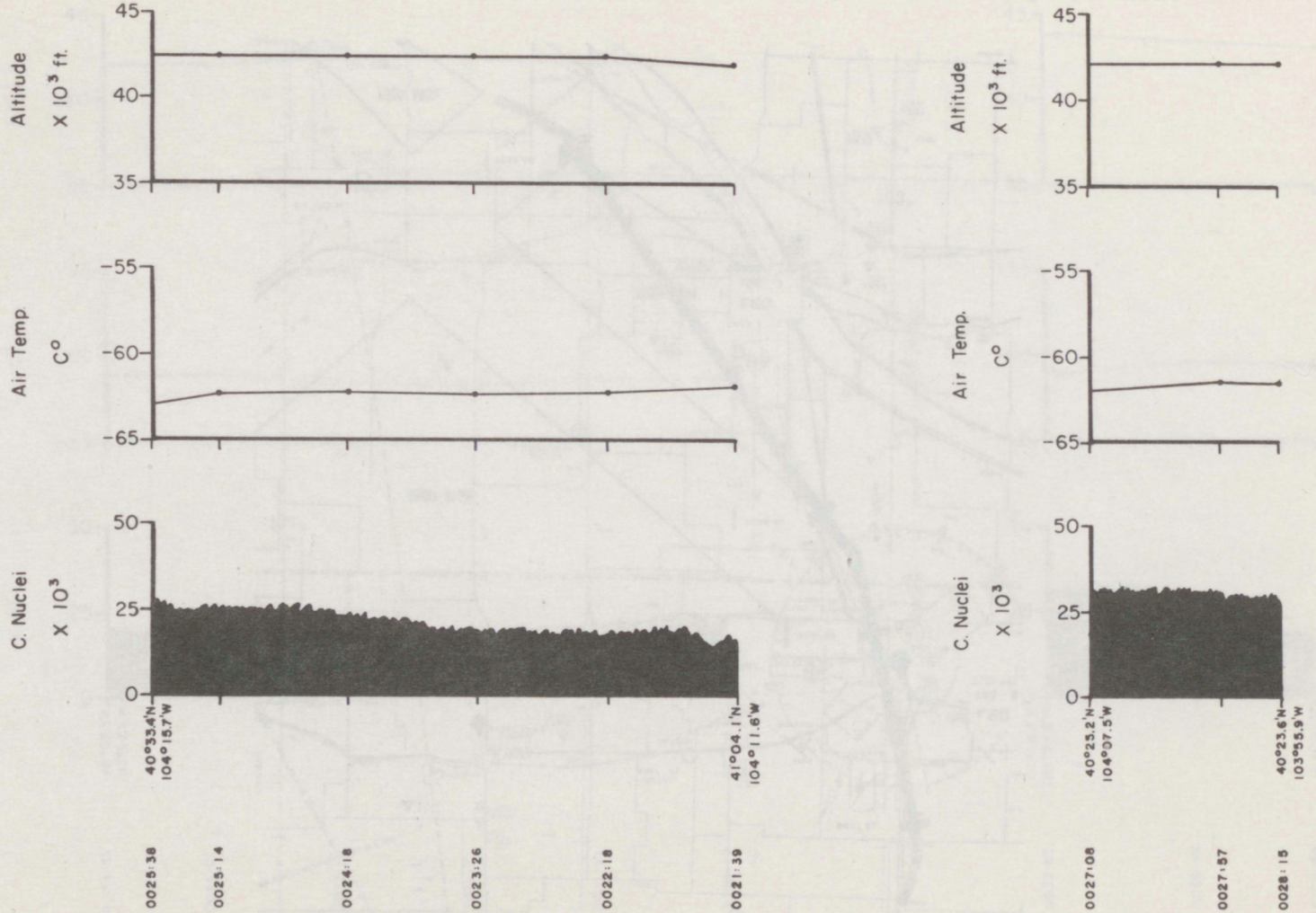

Figure 52A. Altitude, air temperature, and nuclei concentration along legs 5-6, flight 4, Grover, Colo., storm, July 15, 1971.

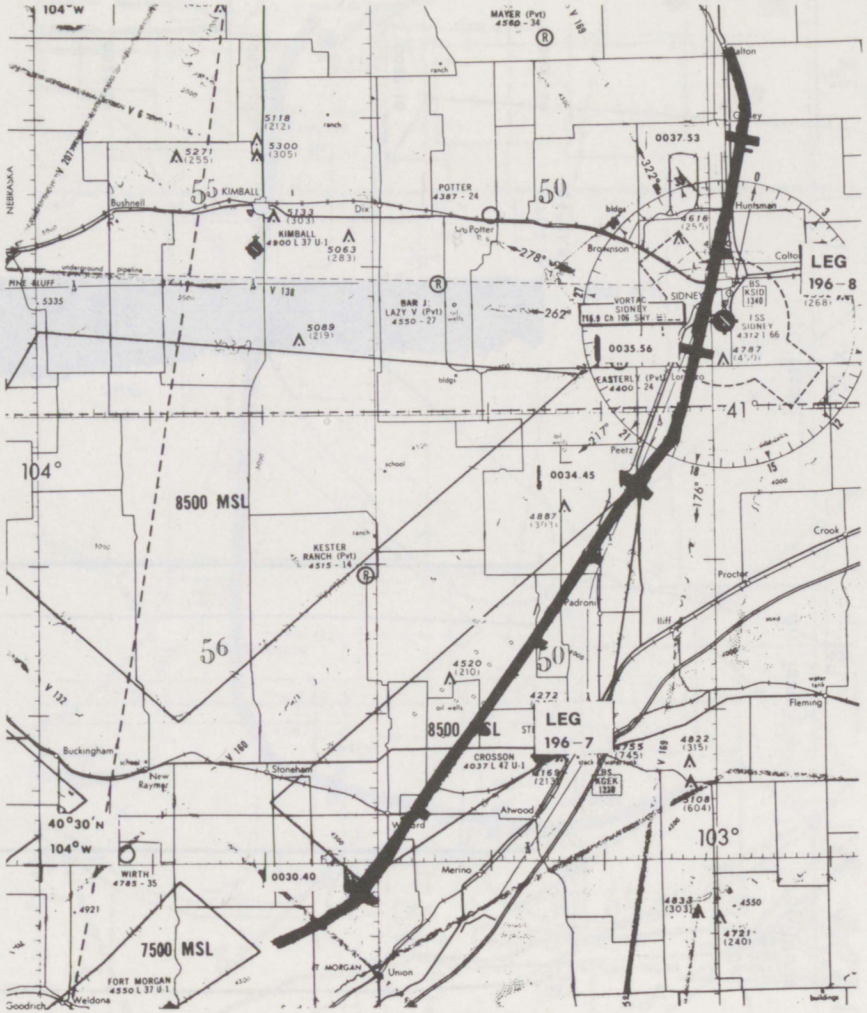

Figure 53. Flight path legs 7-8, flight 4, Grover, Colo., storm, July 15, 1971.

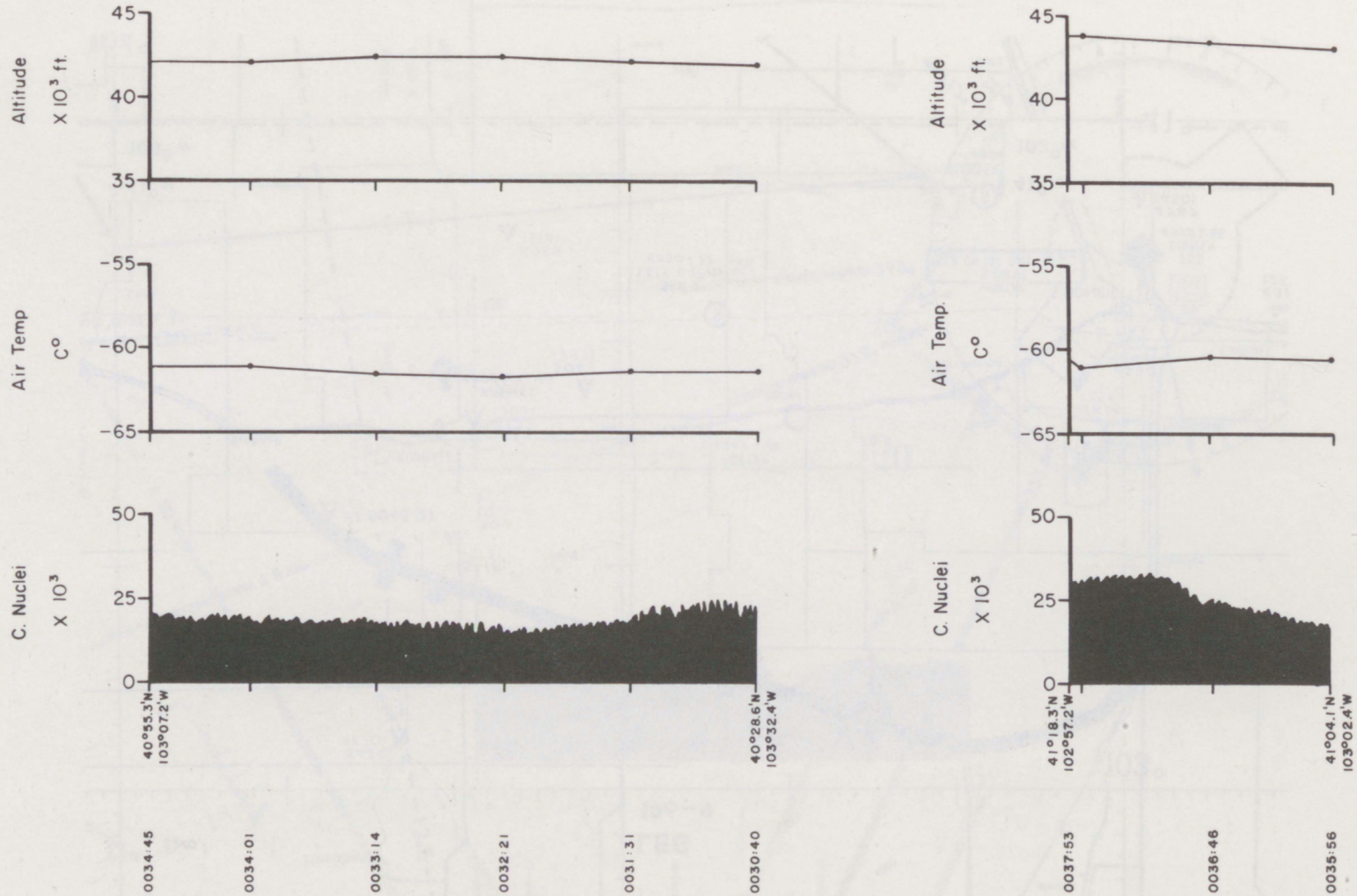

Figure 53A. Altitude, air temperature, and nuclei concentration along legs 7-8, flight 4, Grover, Colo., storm, July 15, 1971.

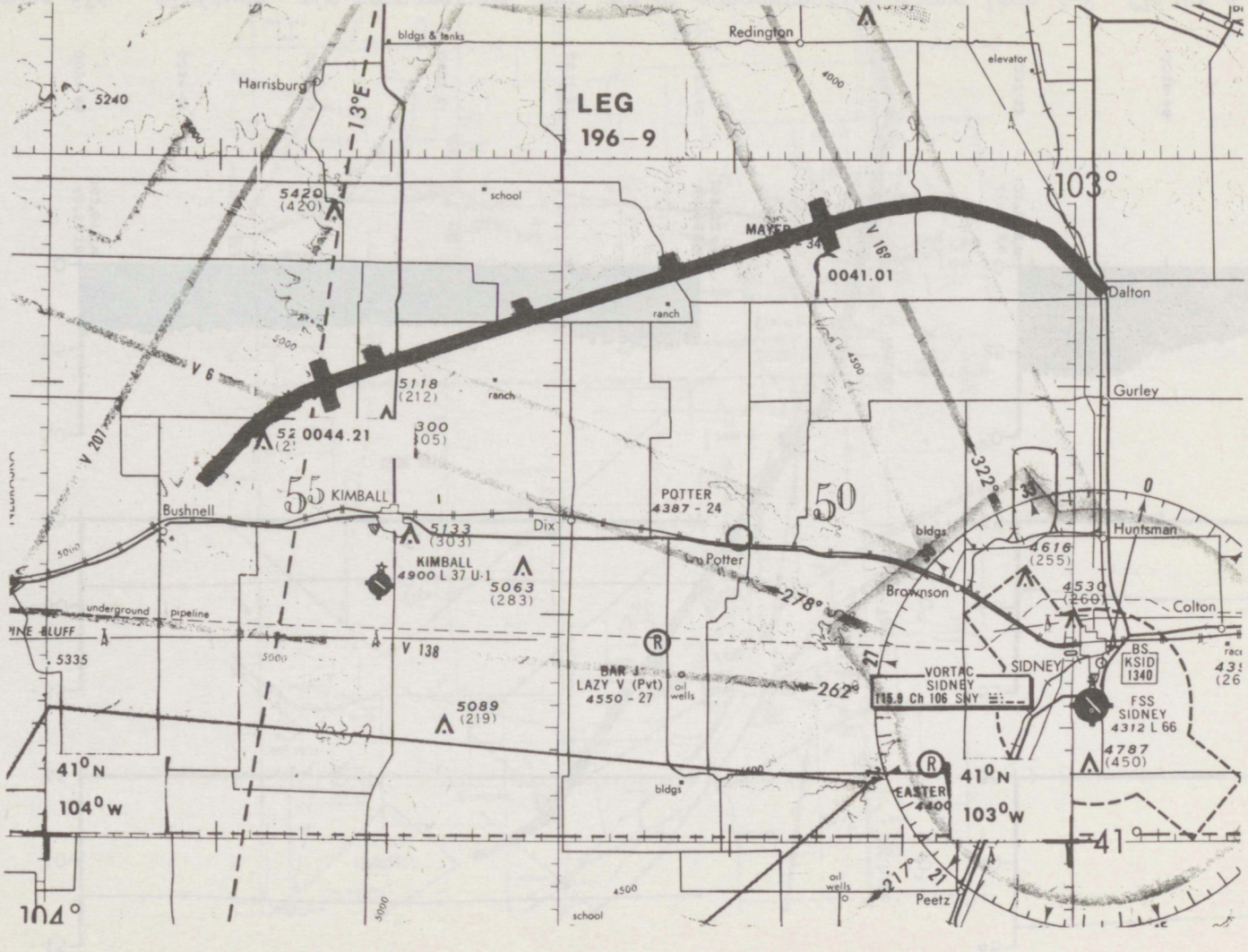

Figure 54. Flight path leg 9, flight 4, Grover, Colo., storm, July 15, 1971.

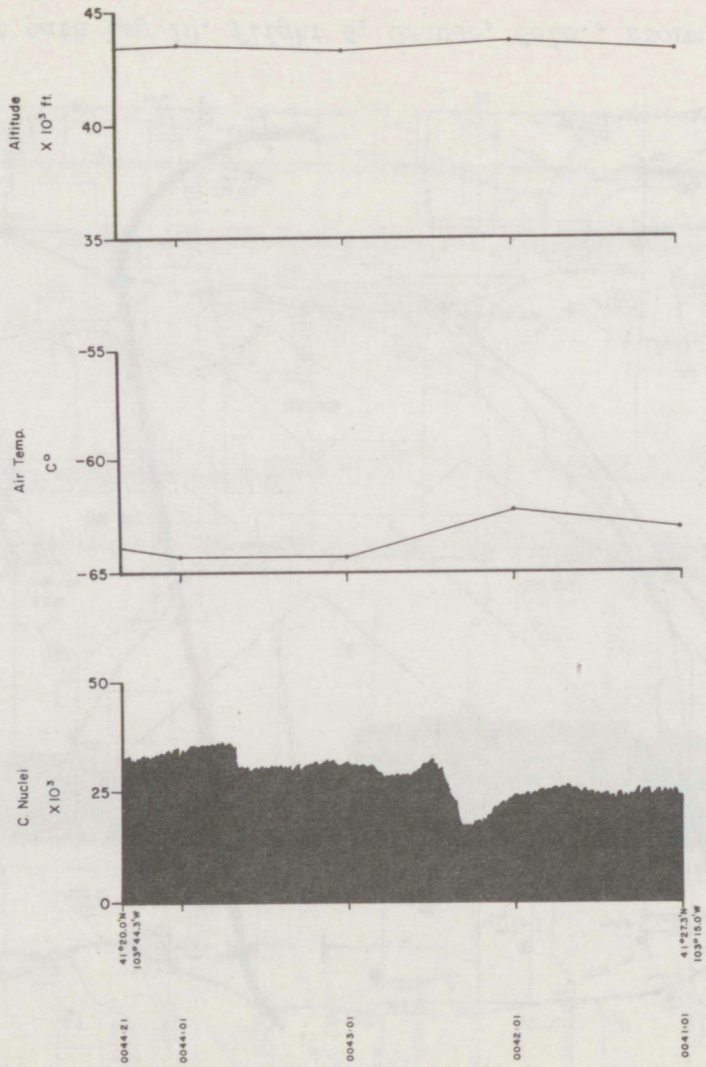

Figure 54A. Altitude, air temperature, and nuclei concentration along leg 9, flight 4, Grover, Colo., storm, July 15, 1971.

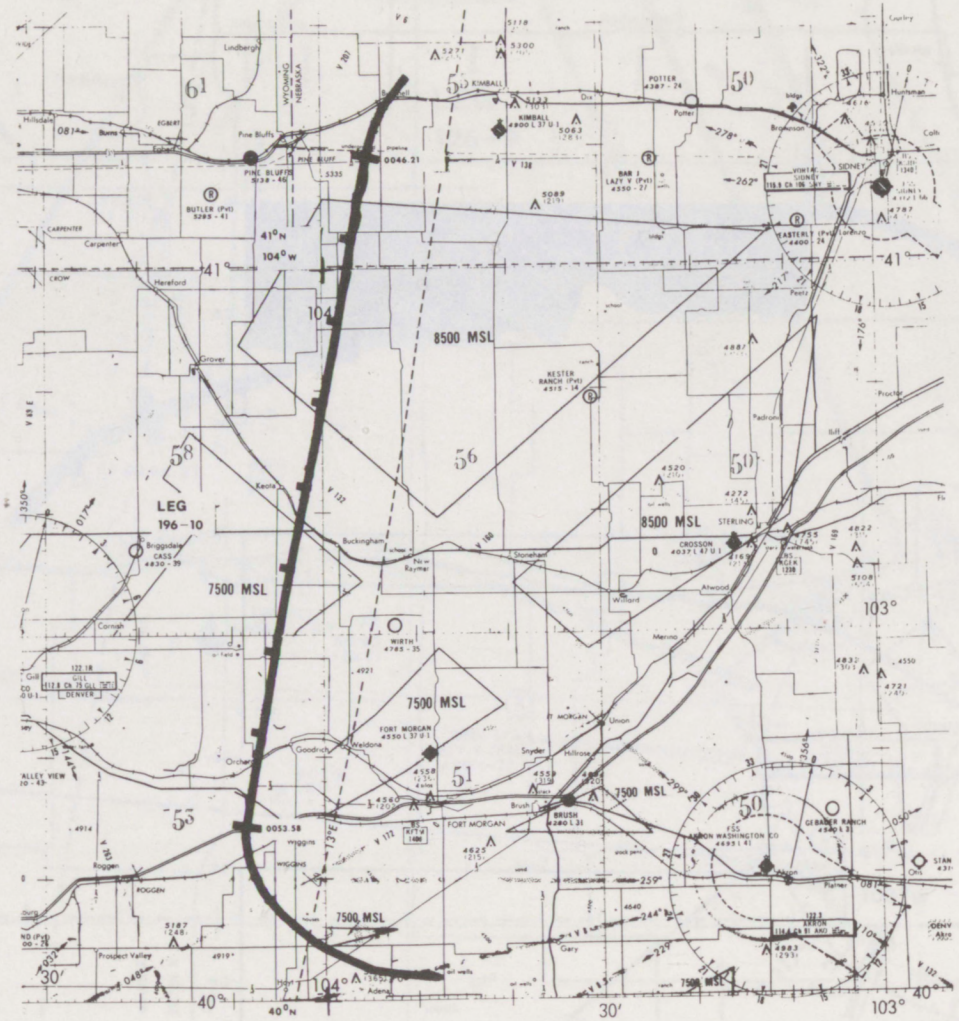

Figure 55. Flight path leg 10, flight 4, Grover, Colo., storm, July 15, 1971.

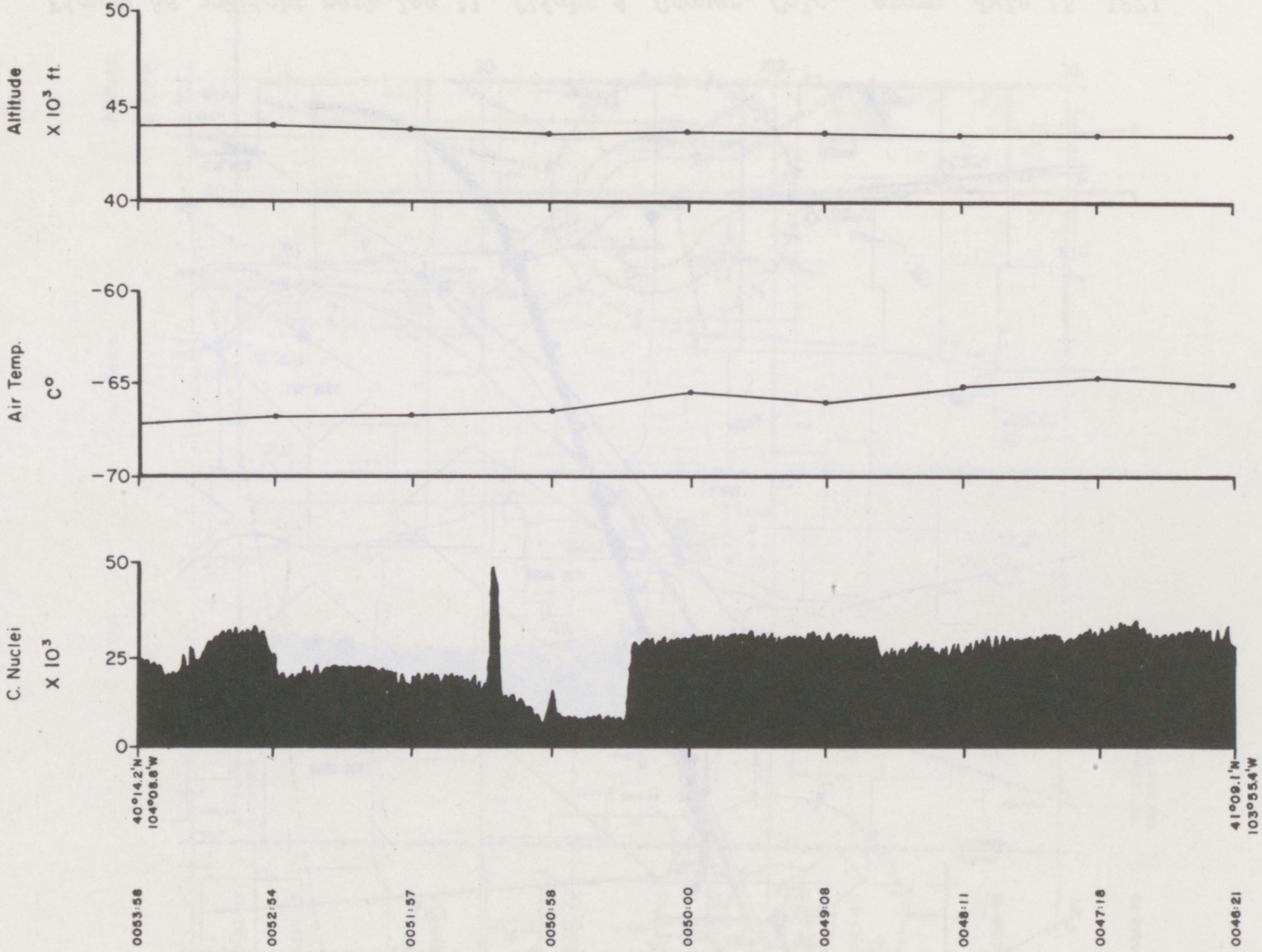

Figure 55A. Altitude, air temperature, and nuclei concentration along leg 10, flight 4, Grover, Colo., storm, July 15, 1971.

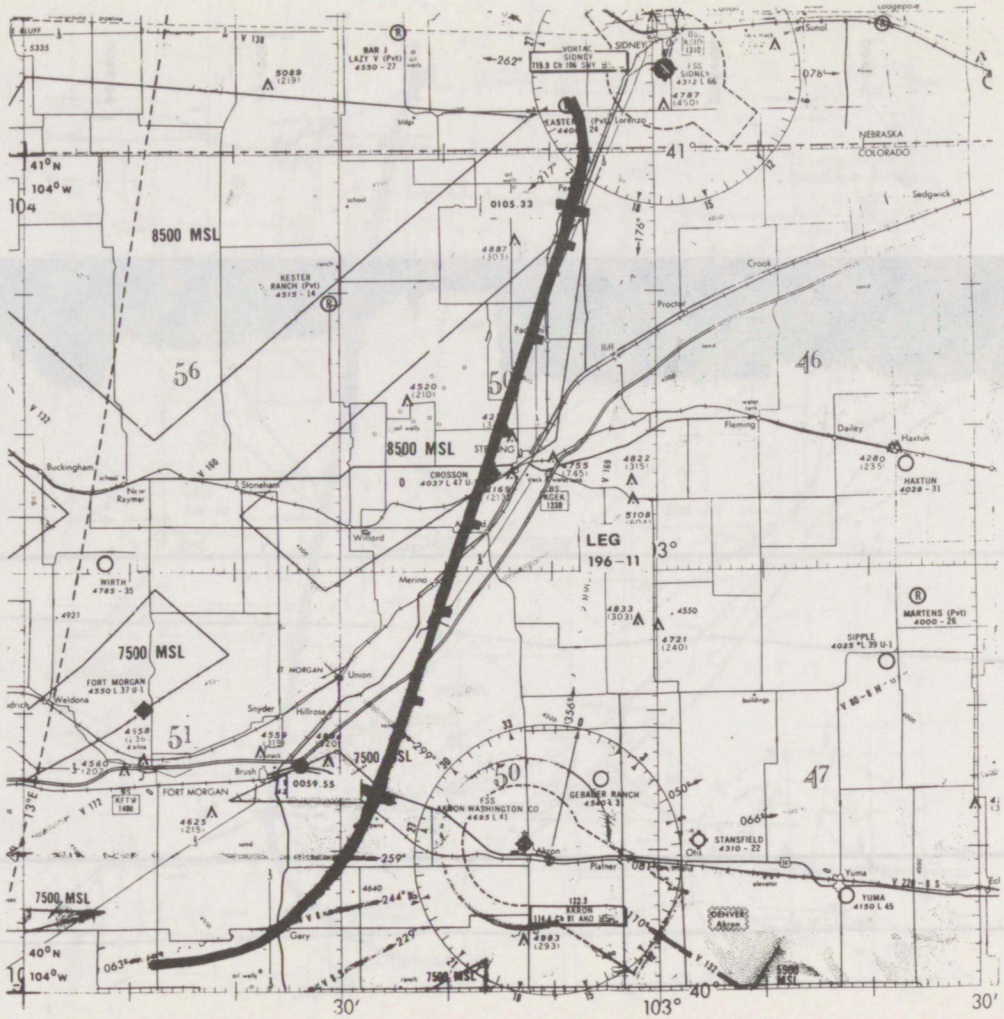

Figure 56. Flight path leg 11, flight 4, Grover, Colo., storm, July 15, 1971.

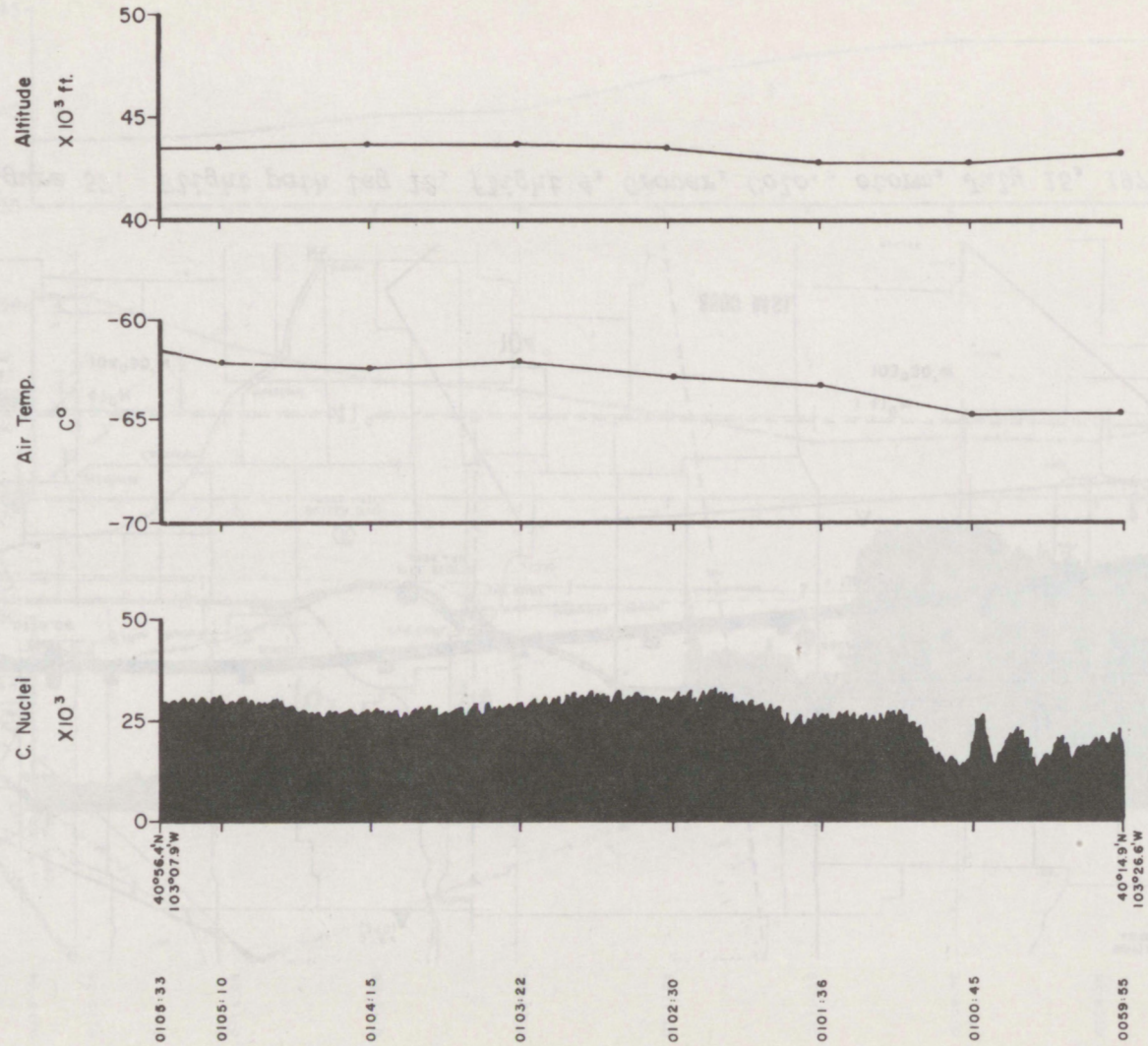

Figure 56A. Altitude, air temperature, and nuclei concentration along leg 11, flight 4, Grover, Colo., storm, July 15, 1971.

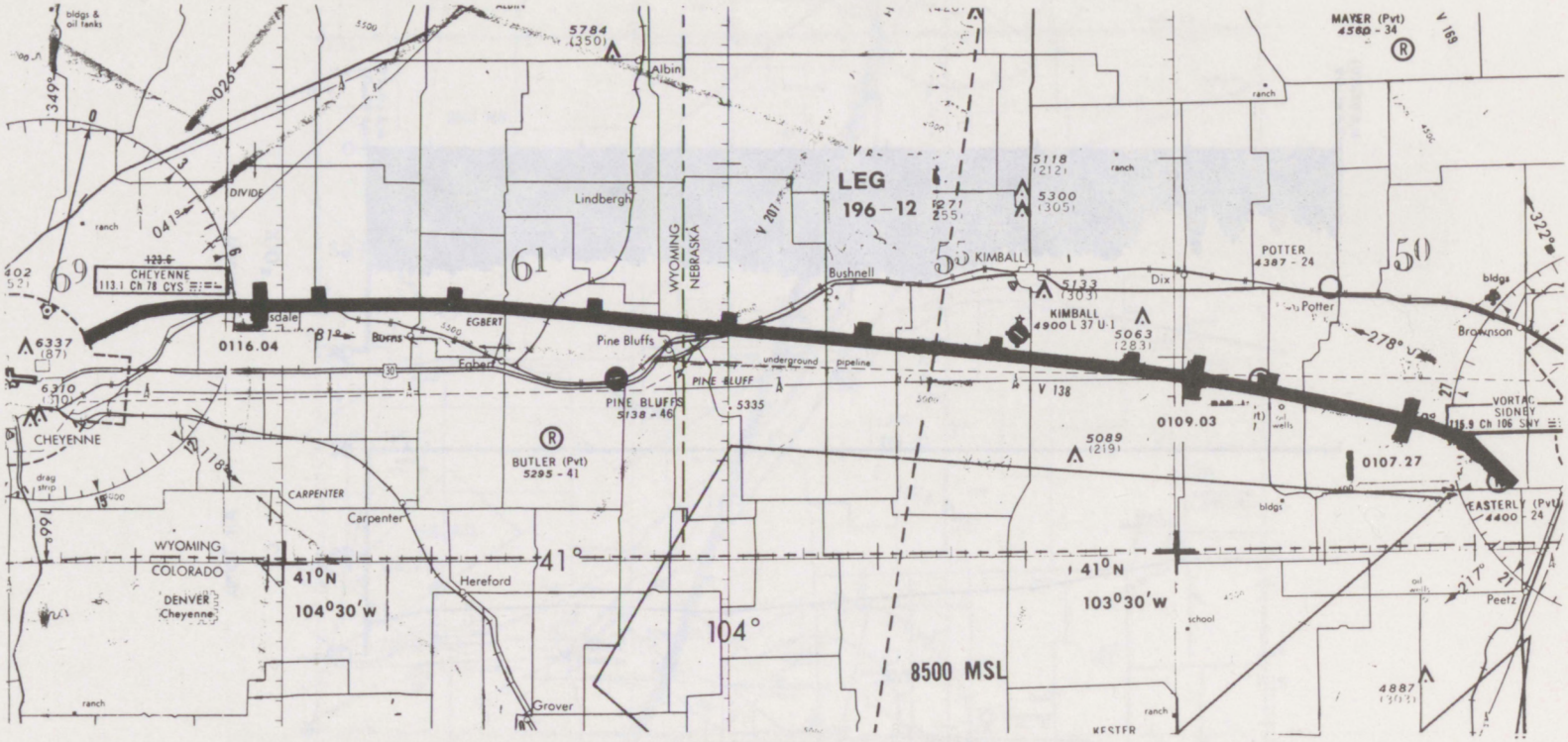

Figure 57. Flight path leg 12, flight 4, Grover, Colo., storm, July 15, 1971.

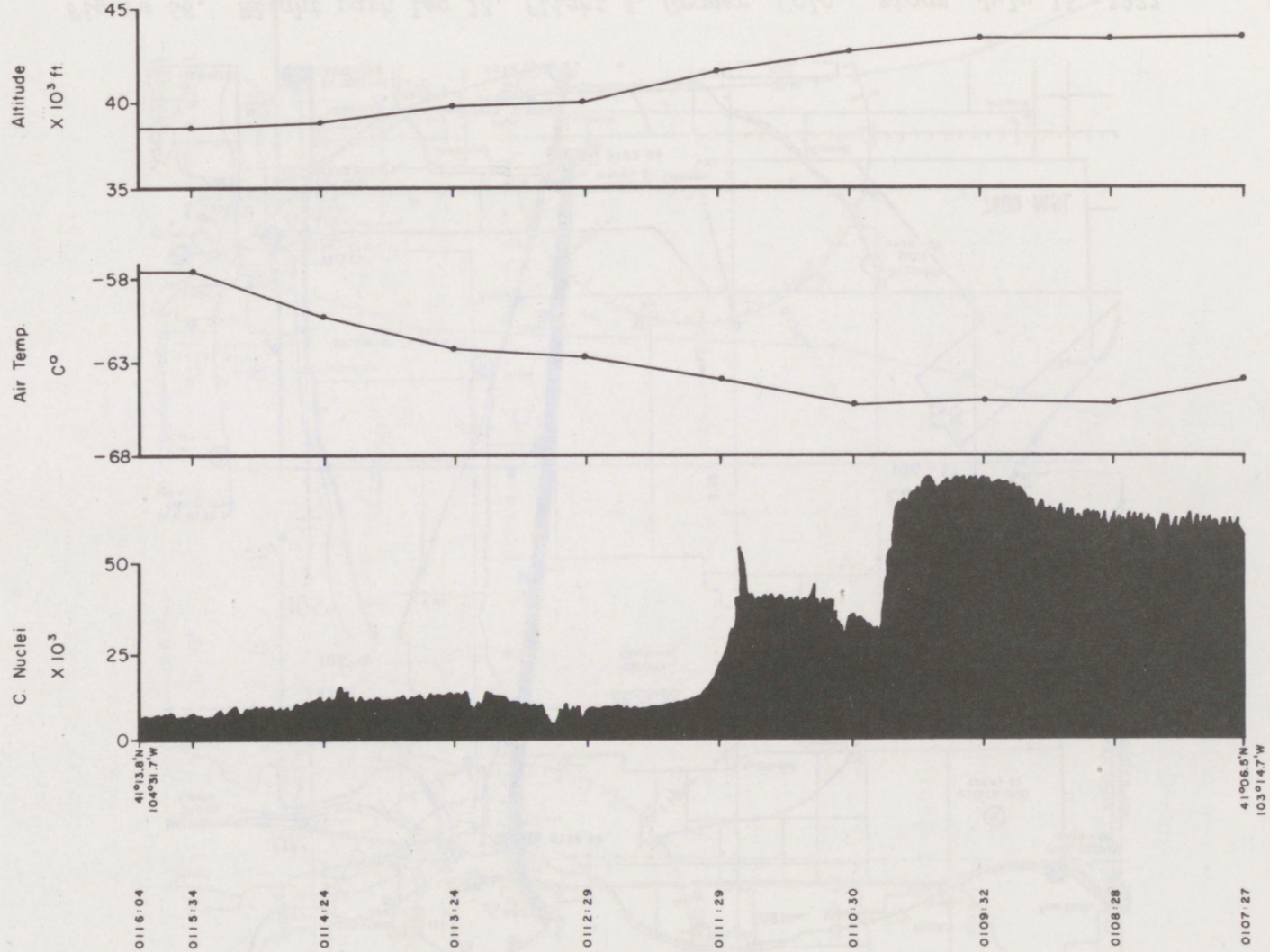

Figure 57A. Altitude, air temperature, and nuclei concentration along leg 12, flight 4, Grover, Colo., storm, July 15, 1971.

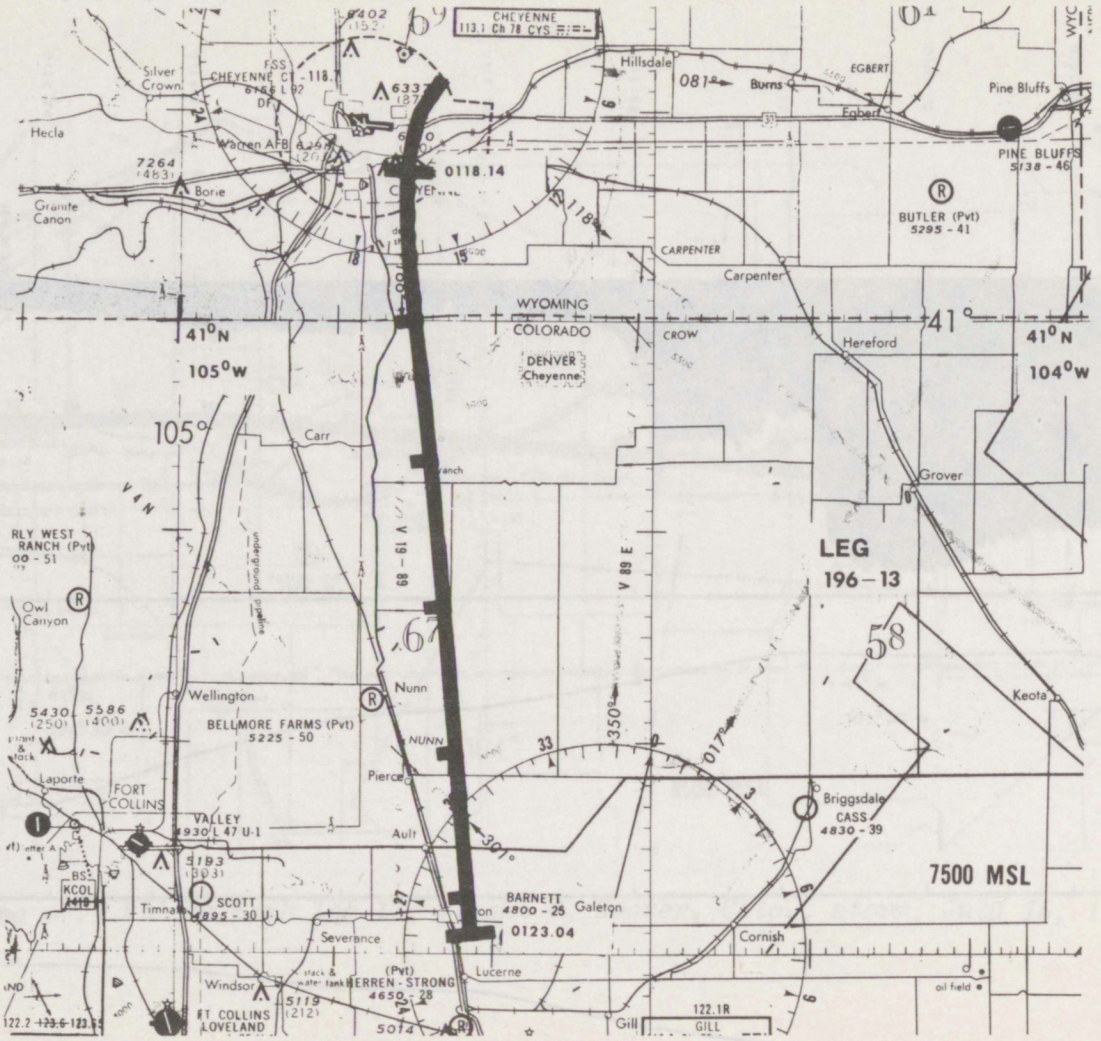

Figure 58. Flight path leg 13, flight 4, Grover, Colo., storm, July 15, 1971.

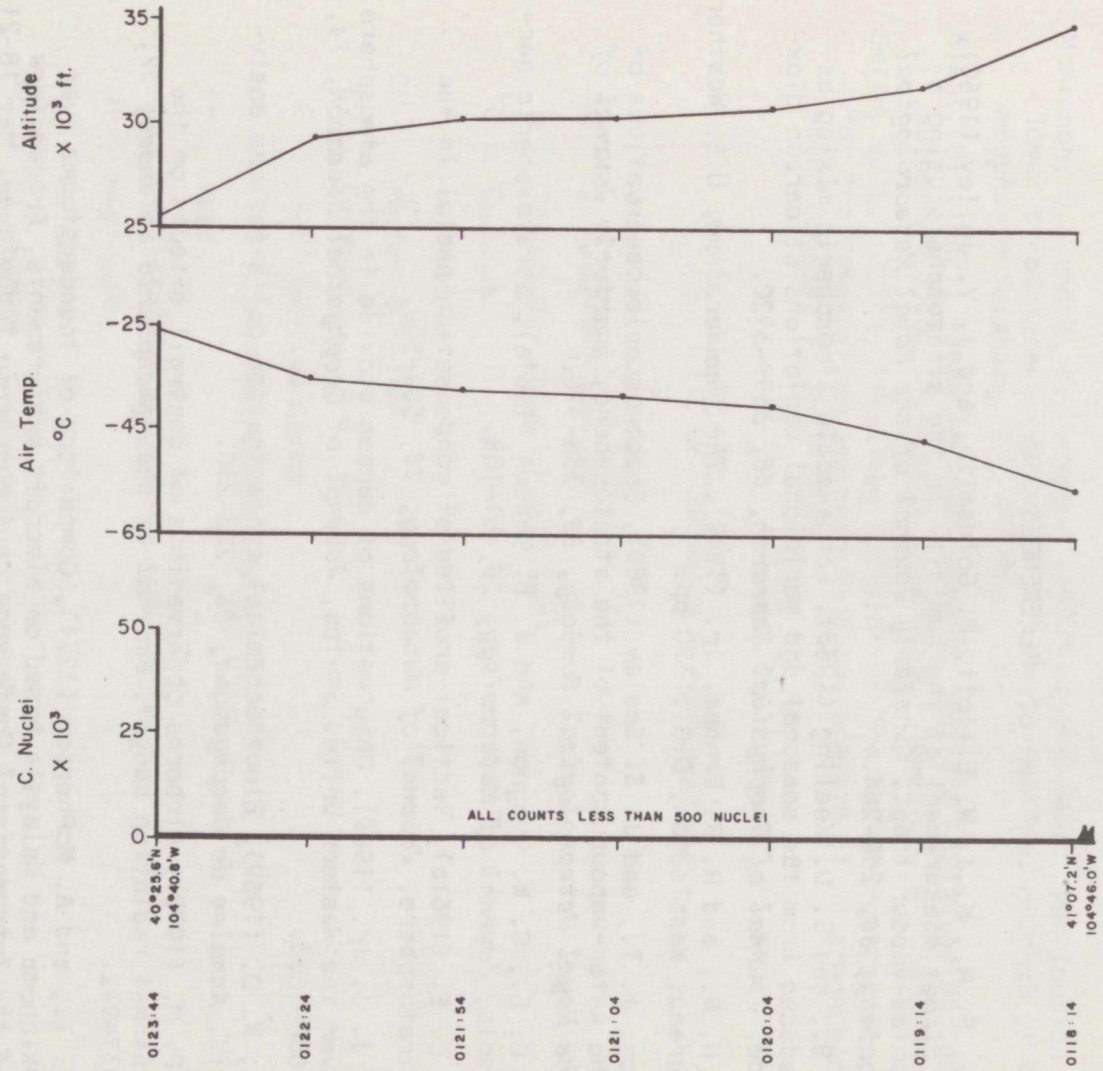

Figure 58A. Altitude, air temperature, and nuclei concentration along leg 13, flight 4, Grover, Colo., storm, July 15, 1971.

5. ACKNOWLEDGMENTS

The authors thank Lois P. Stearns for her professional efforts in assembling the manuscript for final publication and Mathew S. Lojko for his work in completing the computer plots and printout as well as the assembly of the "Total Water Vapor" Program.

6. REFERENCES

Barclay, F. R., M. J. W. Elliott, P. Goldsmith, and J. V. Jelley (1960), A direct measurement of the humidity in the stratosphere using a cooled-vapour trap., *Quarterly Journal of the Royal Meteorological Society, 86,* 259-264.

Bolin, B., and C. D. Keeling (1963), Large-scale atmospheric mixing as deduced from the seasonal and meridional variations of carbon dioxide, *Journal of Geophysical Research, 68,* 3899-3920.

Byers, H. R., and R. R. Braham, Jr. (1949), *The thunderstorm,* U.S. Weather Bureau, Washington, D.C., 320 pp.

Houghton, J. T., and J. S. Seeley (1960), Spectroscopic observations of the water-vapour content of the stratosphere, *Quarterly Journal of the Royal Meteorological Society, 86,* 358-370.

Junge, C. E., C. W. Chagnon, and J. E. Manson (1961a), Stratospheric aerosols, *Journal of Meteorology, 18,* 81-108.

Junge, C. E. (1961b), Vertical profiles of condensation nuclei in the stratosphere, *Journal of Meteorology, 18,* 501-509.

Kelly, J. J. Jr. (1969), Observations of carbon dioxide in the atmosphere over the Western United States, *Journal of Geophysical Research, 74,* 1688-1693.

Komhyr, W. D. (1969), Electrochemical concentration cells for gas analysis, *Annales de Geophysique, 25,* 203-210.

Kuhn, P. M. (1970), Airborne observations of contrail effects on the thermal radiation budget, *Journal of the Atmospheric Sciences, 27,* 937-942.

Lee, J. T., and A. McPherson (1971), Comparison of thunderstorms over Oklahoma and Malaysia based on aircraft measurements, *Proceedings of the International Conference on Atmospheric Turbulence,* May 18-21, 1971, B1, Royal Aeronautical Society, London, 13 pp.

Lovill, J. E. (1969), Transport processes in orographically induced gravity waves as indicated by atmospheric ozone, *Atmospheric Science Paper* No. 135, Dept. of Atmospheric Science, Colorado State University, Fort Collins, 87 pp.

Mastenbrook, H. J. (1971a), The variability of water vapor in the stratosphere, *Journal of the Atmospheric Sciences, 28,* 1495-1501.

Mastenbrook, H. J. (1971b), Personal communication with author during review of manuscript by author.

Mastenbrook, H. J. (1968), Water vapor distribution in the stratosphere and high troposphere, *Journal of the Atmospheric Sciences, 25,* 299-311.

McKinnon, D., and H. W. Morewood (1970), Water vapor distribution in the lower stratosphere over North and South America, *Journal of the Atmospheric Sciences, 27,* 483-493.

Riehl, H. (1962), Radiation measurements over the Caribbean during the autumn of 1960, *Journal of Geophysical Research, 67,* 3935-3942.

Smith, W. L. (1970), Iterative solution of the radiative transfer equation for the temperature and absorbing gas profile of an atmosphere, *Applied Optics, 9,* 1993-1999.

7. LIST OF SYMBOLS AND ABBREVIATIONS

a	electrolyte activities
AC	alternating current
B	Planck function (w cm^{-2} sr^{-1})
^oC	Celcius
cm	centimeter
CO_2	carbon dioxide
CV	Convair
E	electromotive force
ECC	Electrochemical Concentration Cell
ft	feet
g	acceleration of gravity (cm sec^{-2})
H	Hydrogen
Hg	Mercury
hp	horsepower
Hz	Hertz
I	Iodine
i	sensor current due to ozone (microamperes)
I.D.	inside diameter
K	Potassium

^{o}K	Kelvin (^{o} absolute)
kg	kilogram
km	kilometer
kt	knots
l	liter
lpm l/min	liters per minute
m	meter
mb	millibar
ml	milliliter
mm	millimeter
msl	mean sea level
N	Nitrogen
NASA	National Aeronautics and Space Administration
$N_c\downarrow$	downward radiance calculated (w cm^{-2} sr^{-1})
N.E.ΔN	noise equivalent radiance
nm	nautical mile
$N_o\downarrow$	downward radiance observed (w cm^{-2} sr^{-1})
NOAA	National Oceanic and Atmospheric Administration
O	Oxygen
O_3	ozone
P	pressure
pphm	parts per hundred million
ppm	parts per million
ppmv	parts per million by volume
Pt	Platinum
RAOB	radiosonde observation
RHI	Range-Height Indicator
rms	root mean square
$\bar{s}$	mean water vapor mixing ratio (g g^{-1})
$\bar{s}(P)$	water vapor mixing ratio (g g^{-1})
sec	second
sr	steradian
t	time (seconds)

$T(P)$	temperature ^{o}Kelvin at pressure level (mb)
Tr	vertical transport (g cm^{-2}); ozone meter pump temperature (^{o}K)
u $u(H_2O)$	optical mass of water vapor (g cm^{-2})
UT	Universal Time
V	volt; volume
w	watt; vertical velocity (m sec^{-1})
$\bar{w}$	water vapor mixing ratio (g g^{-1})
w_0	assumed water vapor mixing ratio (cm g kg^{-1})
Z	Universal (Greenwich time)
$\Delta\nu$	frequency interval
ε	N.E.ΔN, noise equivalent radiance
μm	micron (= 10^{-6} meter); micrometer
ρ	air density (g cm^{-3})
τ	transmissivity (percent)
ν	wavenumber (cm^{-1})